

LA-14087-MS

Approved for public release;
distribution is unlimited.

Paleoseismic Trenching in the Guaje Mountain Fault Zone, Pajarito Fault System, Rio Grande Rift, New Mexico



This work was funded by the Office of Infrastructure, Facilities, and Construction of Los Alamos National Laboratory.

Edited by Roger Eckhardt

Cover Photo: Logging trench CHU-1, within the Guaje Mountain fault zone, with a total station.



Los Alamos National Laboratory, an affirmative action/equal opportunity employer, is operated by the University of California for the United States Department of Energy under contract W-7405-ENG-36.

This report was prepared as an account of work sponsored by an agency of the United States Government. Neither the Regents of the University of California, the United States Government nor any agency thereof, nor any of their employees make any warranty, express or implied, or assume any legal liability or responsibility for the accuracy, completeness, or usefulness of any information, apparatus, product, or process disclosed, or represent that its use would not infringe privately owned rights. Reference herein to any specific commercial product, process, or service by trade name, trademark, manufacturer, or otherwise, does not necessarily constitute or imply its endorsement, recommendation, or favoring by the Regents of the University of California, the United States Government, or any agency thereof. The views and opinions of authors expressed herein do not necessarily state or reflect those of the Regents of the University of California, the United States Government, or any agency thereof. Los Alamos National Laboratory strongly supports academic freedom and a researcher's right to publish; as an institution, however, the Laboratory does not endorse the viewpoint of a publication or guarantee its technical correctness.

LA-14087-MS

Issued: October 2003

Paleoseismic Trenching in the Guaje Mountain
Fault Zone, Pajarito Fault System, Rio Grande
Rift, New Mexico

Jamie N. Gardner

Steven L. Reneau

Alexis Lavine

Claudia J. Lewis

Danny Katzman

Eric V. McDonald*

Kenneth Lepper

Keith I. Kelson[†]

Cathy Wilson

*Earth and Ecosystems Science, Desert Research Institute, Reno, NV

[†]William Lettis & Associates, Walnut Creek, CA

TABLE OF CONTENTS

	Page
TABLE OF CONTENTS	v
LIST OF FIGURES AND PLATES	vii
LIST OF TABLES	viii
 ABSTRACT	 1
 I. INTRODUCTION	 3
 II. PREVIOUS WORK AND SETTING OF PALEOSEISMIC TRENCHES	 5
 III. METHODS	 10
A. Trench Excavation and Logging	10
B. Geochronology	10
C. Stratigraphic Unit Names, Symbols, and Descriptions	10
 IV. RESULTS	 11
A. Cabra Canyon Trench	11
1. Stratigraphy	11
2. Structure	11
3. Paleoseismic Implications	15
B. Chupaderos Canyon Trench 1	16
1. Stratigraphy	16
2. Structure	17
3. Paleoseismic Implications	20
C. Chupaderos Canyon Trench 2	24
1. Stratigraphy	24
2. Structure	24
3. Paleoseismic Implications	26
D. Chupaderos Canyon Trench 3	26
1. Stratigraphy	26
2. Structure	27
3. Paleoseismic Implications	28
 V. DISCUSSION AND CONCLUSIONS	 30
 VI. ACKNOWLEDGEMENTS	 30
 VII. REFERENCES	 31
 APPENDIX A. GEOCHRONOLOGY	 35
A-1. Radiocarbon Geochronology	35
A-2. Optically Stimulated Luminescence (OSL) Geochronology	35

TABLE OF CONTENTS CONTINUED

	Page
1. General OSL methods	37
2. Summary of Phase-One Results: Evaluation of Techniques	39
3. Phase Two: Single-Grain Laser Luminescence Dating	42
A-3. Soil Stratigraphy and Pedologic Age Estimates for Chupaderos Canyon Trenches	44
1. Methods	44
2. Quantification of Soil Morphology	45
3. Pedologic Age Estimates Using PDI Values	45
4. Confidence Interval for Pedologic Age Estimates	45
5. Stratigraphic-Age Relations for Soils	46
6. Description of Soil Stratigraphy Exposed in Trenches	46
7. Results	47
a. <i>Trench CHU-1 Profiles</i>	47
b. <i>Summary of Trench CHU-1 Soil Stratigraphy</i>	60
c. <i>Trench CHU-2 Profiles</i>	61
d. <i>Summary of Trench CHU-2 Soil Stratigraphy</i>	62
e. <i>Trench CHU-3 Profiles</i>	62
f. <i>Summary of Trench CHU-3 Soil Stratigraphy</i>	63
APPENDIX B. CHUPADEROS CANYON TRENCHES—UNIT DESCRIPTIONS64
B-1. Trench CHU-164
B-2. Trench CHU-266
B-3. Trench CHU-367

LIST OF FIGURES AND PLATES

	Page
FIGURES	
1. Map of the Rio Grande Rift in Northern New Mexico	3
2. Map of the Pajarito Fault System in the Vicinity of Los Alamos	4
3. Map of Paleoseismic Trenches in Chupaderos Canyon	7
4. Trench CHU-1 During Logging	7
5. Trench CHU-2	8
6. Trench CHU-3	8
7. Map of Paleoseismic Trench in Cabra Canyon	9
8. Lower Hemisphere Stereonet (Schmidt) Plots of Structures in the Cabra Canyon Trench	13
9. Age Constraints in Trench CHU-1	17
10. Structural Data from Trench CHU-1	19
11. Reconstruction of Late-Pleistocene and Younger Events from Trench CHU-1	22–23
12. Structural Data from Trench CHU-2	25
13. Structural Data from Trench CHU-3	28
14. Detailed Maps of the Chupaderos Canyon Trenches Showing Strikes of Faults	29
A-1. Dose Distributions for Sample CHU1OSL7	43
A-2. Deconvolved Probability Density Distribution for Sample CHU1OSL7	44
 PLATES	
1. Generalized Logs of the Cabra Canyon Trench	inside rear cover
2. Detailed Logs of Selected Zones in the Cabra Canyon Trench	inside rear cover
3. Log of Southwest Wall of Trench CHU-1	inside rear cover
4. Log of Southwest Wall of Trench CHU-2	inside rear cover
5. Log of South Wall of Trench CHU-3	inside rear cover

LIST OF TABLES

	Page
A-1. Radiocarbon Analyses	36
A-2. Evaluation of Data Collection Operations Used for the SAR and SGLL Procedures	38
A-3. Dosimetry-Related Data in Support of OSL Age Determinations	40
A-4. Alpha-Efficiency Values Measured in Past IRSL Dating Studies on the Pajarito Plateau	40
A-5. Tabulated Results from the Various OSL SAR and SGLL Methods Evaluated in Phase One	41
A-6. SGLL Ages Presented in Stratigraphic Approximation for Each Trench	42
A-7. Summary of Soil Morphology for Chupaderos Trench Excavations, 2001	48-56
A-8. PDI Age Estimates for Trenches CHU-1, CHU-2, and CHU-3	57

**PALEOSEISMIC TRENCHING IN THE GUAJE MOUNTAIN FAULT ZONE,
PAJARITO FAULT SYSTEM, RIO GRANDE RIFT, NEW MEXICO**

by

Jamie N. Gardner, Steven L. Reneau, Alexis Lavine, Claudia J. Lewis, Danny Katzman,
Eric V. McDonald, Kenneth Lepper, Keith I. Kelson, and Cathy Wilson

ABSTRACT

The Guaje Mountain fault zone is a significant structural element of the Pajarito fault system that is the active western boundary of the Rio Grande rift in the vicinity of Los Alamos. Faults constituting the active rift boundary pose potential seismic hazards to Los Alamos and, consequently, have been the focus of paleoseismic investigations to determine the frequency and nature of surface-rupturing prehistoric earthquakes to facilitate calculation of the probabilistic hazard. Results from four paleoseismic trenches in the Guaje Mountain fault zone, combined with previous studies of stream terraces flanking the fault, indicate the following paleoseismic events on the Guaje Mountain fault: 1) the most recent surface-rupturing event occurred between 4 and 6.5 ka with 1.5 to > 2 m of vertical displacement; 2) the penultimate surface-rupturing event occurred around 39 ka and was probably dominantly a strike-slip event with only a small vertical displacement of about 50 cm; and 3) an older event occurred between 144 and 300 ka with 1.5 to 2 m of vertical displacement. Generally, surface-rupturing earthquakes are magnitude 6 or larger, and the observed displacements indicate the paleoseismic events on the Guaje Mountain fault were in the range of magnitude 6.5 to 7. The trenches provide additional information for multiple, older events whose timing and magnitudes of displacement are not well constrained.

Paleoseismic Trenching in the Guaje Mountain Fault Zone

I. INTRODUCTION

Los Alamos National Laboratory (LANL) lies within a seismically active area and, as a result, investigations of various possible seismic hazards are on-going. The greatest potential seismic hazard for LANL results from the ground motion of a large earthquake on one of the local faults (Gardner and House 1987; Wong et al. 1995, 1996). Results of a number of studies indicate that the local faults are capable of generating earthquakes of approximate magnitude 7 and must be considered "active" in the definitions of Department of Energy (DOE) guides and standards (Gardner and House 1987; Wong et al. 1995, 1996; Olig et al. 1996; McCalpin 1998, 1999; Gardner et al. 1999; Reneau et al. 2002). Thus, the paleoseismic studies of the Los Alamos Seismic Hazards Program are focused on obtaining information on the nature and, especially, timing of surface-rupturing prehistoric earthquakes. These data are fundamental to calculation of the probabilistic seismic hazard.

Los Alamos is situated in the Rio Grande rift (Figure 1), an active continental rift and a major tectonic feature of the North American continent. The rift is a series of complex, asymmetric, fault-bounded basins extending from central Colorado, through New Mexico, to northern Mexico. Near Los Alamos, the local rift boundary is defined by the Pajarito fault system, a generally north-trending swath of normal to oblique slip faults,

which includes the Pajarito, Rendija Canyon, and Guaje Mountain fault zones (Figure 2). The Pajarito fault zone appears to be the master fault, thus lending its name to the larger fault system. It exhibits over 200 cumulative meters of dominantly normal, down-to-the-east displacement of the Tshirege Member of the Bandelier Tuff, erupted at 1.22 Ma (Ma = million years ago; age from Izett and Obradovich 1994) (Gardner and House 1987). The Rendija Canyon and Guaje Mountain faults

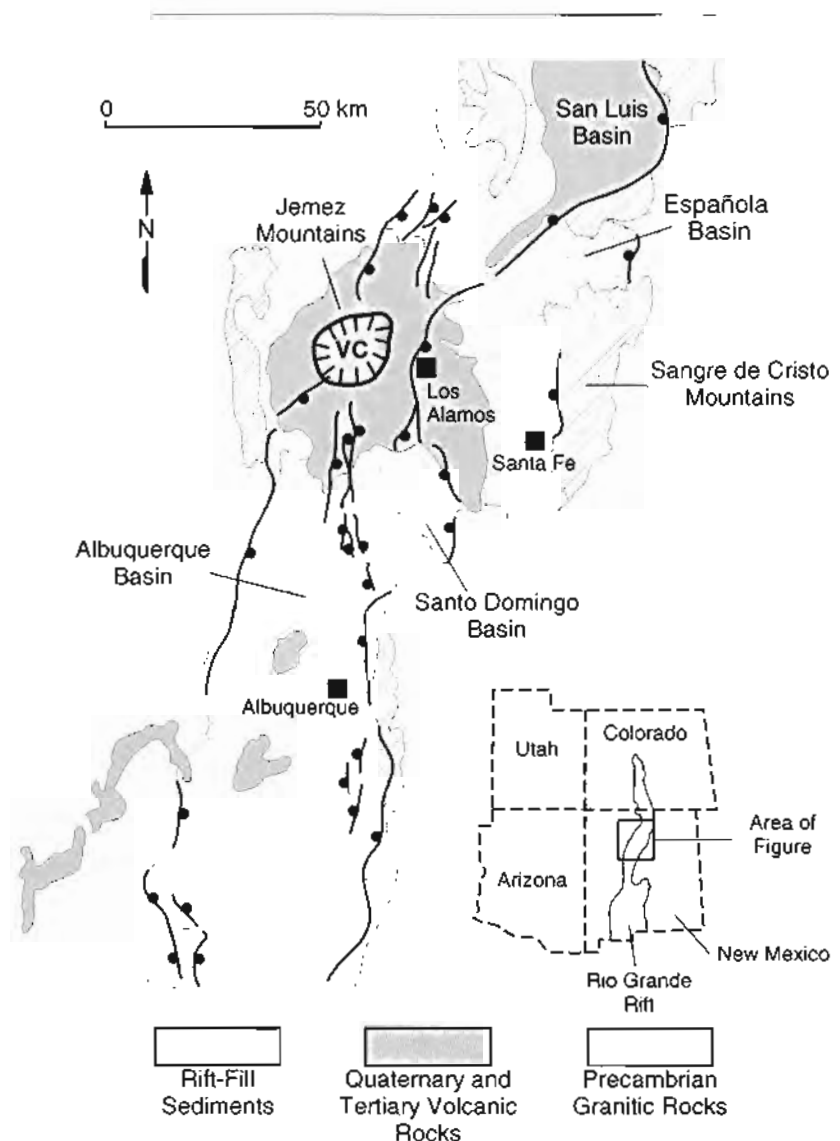


Figure 1. Map of the Rio Grande Rift in Northern New Mexico. Major fault systems are shown schematically (ball on downthrown side). VC is the Valles-Toledo caldera complex, the source of the Bandelier Tuff (modified from Gardner and Goff 1984).

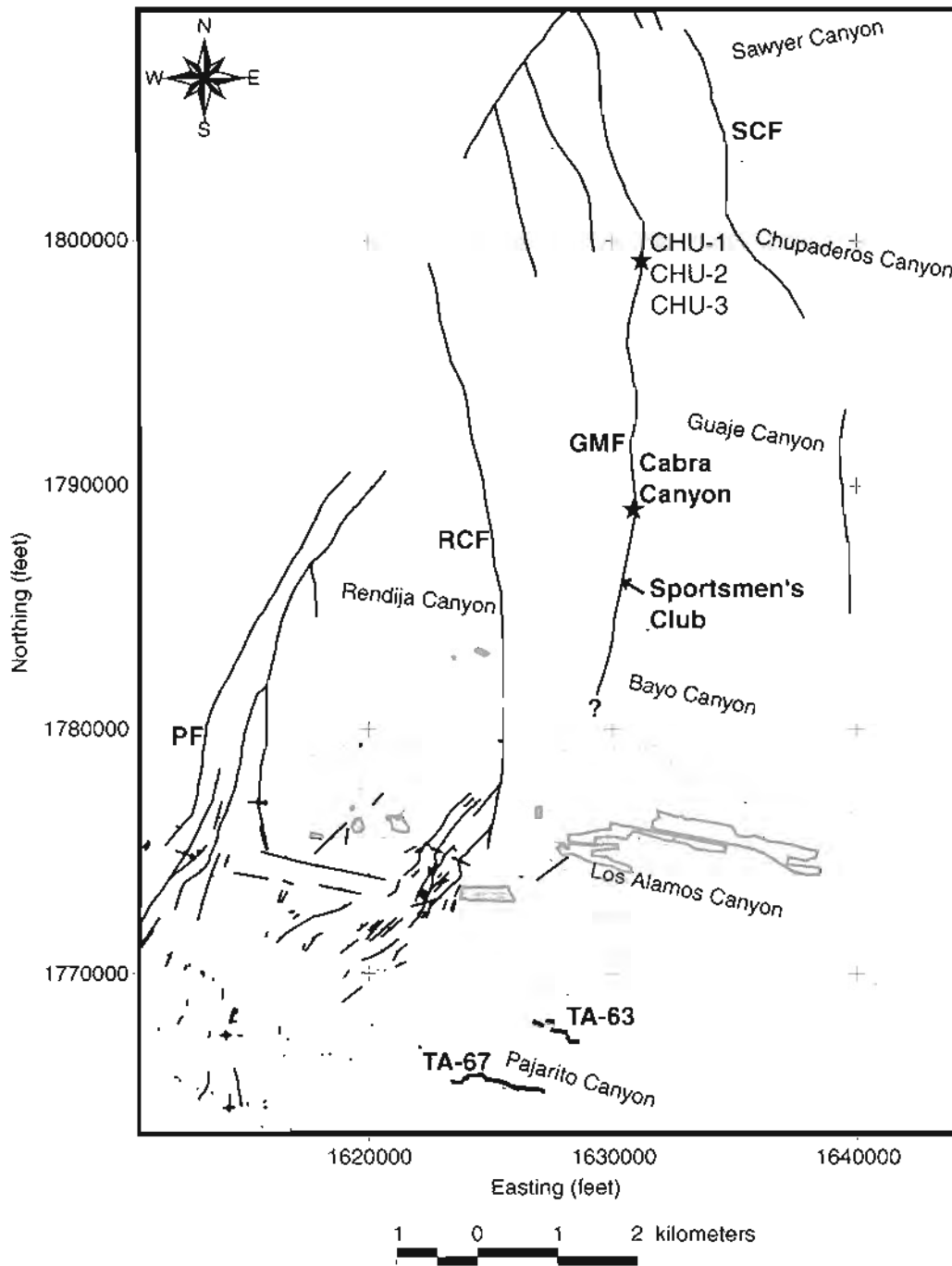


Figure 2. Map of the Pajarito Fault System in the Vicinity of Los Alamos. Abbreviations: PF = Pajarito fault; RCF = Rendija Canyon fault; GMF = Guaje Mountain fault; SCF = Sawyer Canyon fault. Red stars indicate locations of paleoseismic trenches of this report. Red lines at TA-63 and TA-67 indicate the trenches of Kolbe et al. (1994) and Kolbe et al. (1995), respectively. Major drainages are shown in blue. Urban culture and some political boundaries are shown in grey. Fault data are from Gardner and House (1987), Carter and Gardner (1995), Gardner et al. (1999), and Lewis et al. (2002). The grid on the borders of the figure is State Plane Coordinate System, New Mexico Central Zone, 1983 North American Datum.

appear to be antithetic to, and geometrically related to, the Pajarito fault zone. The Rendija Canyon and Guaje Mountain fault zones dip west and exhibit about 40 and 35 meters (m), respectively, of down-to-the-west displacements in the last 1.22 Ma (Olig et al. 1996; Carter and Gardner 1995). The issue of interdependence of the faults of the system is the subject of on-going studies, but it is likely that the timing of ruptures on the Guaje Mountain and Rendija Canyon faults reflects the occurrence of large paleoseismic events on the Pajarito fault.

In this report, we present results of paleoseismic studies in the Guaje Mountain fault zone (Figure 2), one of three potentially seismogenic faults in Los Alamos County. Paleoseismic studies of the other two faults of interest are the subjects of other reports (Wong et al. 1995, 1996; Kelson et al. 1996; Olig et al. 1996; McCalpin 1998, 1999; Reneau et al. 2002), and the faults are a focus for future work. In addition to results from three new trenches in the Guaje Mountain fault zone in the Chupaderos Canyon area, we summarize previously unpublished results from a trench in Cabra Canyon that was excavated and studied in 1987 to 1988 (Gardner et al. 1990).

II. PREVIOUS WORK AND SETTING OF PALEOSEISMIC TRENCHES

The Guaje Mountain fault zone trends generally north with a clear geomorphic expression of scarps and topographic linears that extends about 6 km; however, most workers have depicted the fault zone as being about 12 km in length (for example, Olig et al. 1996). The southern and northern ends of the fault zone are not well studied. On the south, Kolbe et al. (1994, 1995) trenched the along-strike, southern projections of the fault north and south of Pajarito Canyon (Figure 2) and found no evidence of surface faulting associated with the Guaje Mountain fault in the Bandelier Tuff and younger units. Wohletz (1995) inferred small displacements across zones of abundant

fractures in Los Alamos Canyon, along a projection of the fault's north-south strike. However, the southernmost positive evidence for surface faulting on the Guaje Mountain zone occurs around Bayo Canyon (Figure 2). Carter and Gardner (1995) report that the southern tail of the fault bends to the southwest; it is likely that the fault here merges with other faults of the Pajarito fault system in a fashion similar to the Rendija Canyon fault (Figure 2; see Gardner et al. 1999). On the northern end, north of Chupaderos Canyon, the fault evolves into a broad shear zone and several splays that bend to the northwest (Carter and Gardner 1995) until it apparently connects with the Pajarito fault zone on Santa Clara Pueblo lands. Along most of its strike, the fault is dominantly a zone of normal to normal-oblique faults that exhibit steep western dips of 60 degrees to vertical. Where the fault crosses Guaje Canyon, however, the surface trace with respect to topography indicates that it is locally a high-angle reverse fault (Gardner and House 1987).

In 1991, two small earthquakes occurred on the Guaje Mountain fault (Gardner and House 1994). Although each earthquake only had a local magnitude of about 2, they were felt by over 100 residents of the town of Los Alamos. Credible accounts by those having felt the earthquakes indicate highest Modified Mercalli Intensities of V to VI. The fact that these earthquakes were felt by large numbers of people, the surprisingly high resultant ground-motion intensities, and constraints provided by the closest operating seismograph indicate an extremely shallow focus for these earthquakes of certainly less than 5 km, perhaps as shallow as 2 km (Gardner and House 1994).

The Rendija Canyon fault zone lies generally about 2 km to the west of the Guaje Mountain fault zone (Figure 2). It exhibits similar trend, length, dip, and sense and magnitude of post-1.2-Ma displacements to the Guaje Mountain fault zone. The Rendija Canyon fault apparently dies out to the north just north of Guaje Canyon where it begins to bend to the northwest and displacements go to zero (Carter

and Gardner 1995; Olig et al. 1996). Kelson et al. (1996) report the most recent event (MRE) of surface rupturing for the Rendija Canyon fault as either 9 or 23 ka (thousands of years before present). About 1.5 km to the east of the Guaje Mountain fault is the northwest-trending, down-to-the-east Sawyer Canyon fault (Figure 2). The Sawyer Canyon fault has only been traced for about 5 km but has about 37 m of displacement of the Bandelier Tuff near its northern end (Carter and Gardner 1995). Outside of the brief treatment by Carter and Gardner (1995), the Sawyer Canyon fault is largely unstudied, but they report stream terraces that may be displaced by fault movements and warrant further study.

Generally, the Guaje Mountain fault juxtaposes Bandelier Tuff on the western side with older units such as the Tschicoma (locally about 5 Ma; Aldrich and Dethier 1990) and the Puye (generally, 7 to about 1.6 Ma; Gardner et al. 1986) formations on the eastern, upthrown block. Small pockets of post-Bandelier sediments have accumulated in the fault zone, particularly on the downthrown and upstream side of the fault, and these have constituted the main targets for paleoseismic trenching to date.

A series of stream terraces occurs on both the east and west sides of the Guaje Mountain fault zone near the Sportsmen's Club in Rendija Canyon (Figure 2). These terraces have been mapped in detail for paleoseismic constraints (Wong et al. 1995; Olig et al. 1996) and studied extensively for development of the local soils chronostratigraphy (for example, McDonald et al. 1996). Combined results of these studies are discussed in a later section.

Both Chupaderos and Cabra canyons are generally east-flowing drainages that intersect the Guaje Mountain fault zone at high angles. The Chupaderos drainage bends north and follows the approximate trace of the fault zone for about 0.5 km before turning east again (Figure 3). Small north-south trending side drainages are incised into the edges of mesas within the fault zone north and south of

Chupaderos Canyon. Homesteaders dammed the Chupaderos drainage where it crosses the fault, creating a pond that provides a normally perennial water source.

Three trenches were excavated in Chupaderos Canyon, designated from south to north CHU-1, CHU-2, and CHU-3 (Figure 3). CHU-1 (Figure 4) was excavated on a west-facing hillslope, formed at least in part by fault movements, that we originally interpreted to consist mainly of colluvial deposits shed from the fault scarp and higher slopes. Just west of and about at the same elevation as CHU-1, on the opposite side of the locally north-flowing drainage, is a prominent stream terrace. The target of CHU-1 was the main trace of the fault. The trench was excavated along the axis of a northwest-trending interfluvial, separating two gullies. CHU-1 was about 55 m long with the deepest part of the trench, about 5 m deep, within the main fault zone, which formed a subtle topographic bench on the hillslope. CHU-2 and CHU-3 revealed hanging-wall deformation, some of which appeared to be marked by topographic features, which is reported to be common and relatively intense in this area (Carter and Gardner 1995). Hanging-wall deformation has commonly provided some of the best paleoseismic information yet obtained in the Pajarito fault system (Gardner et al. 1990 and this report; McCalpin 1998; Reneau et al. 2002). CHU-2 (Figure 5) was a short (about 23 m long) trench that was sited to specifically examine a topographic swale that appears to have been cut along hanging-wall subsidiary faults. CHU-3 (Figure 6) was about 50 m long, with the eastern end about 10 m west of the projected main fault trace; CHU-3 appears to have captured most of the hanging-wall deformation west of the main fault trace. The Cabra Canyon trench (Figure 2) was about 75 m long (Figure 7) and was excavated in mostly Holocene sediments in the canyon bottom. The southeast end of the trench abutted dacite of the Tschicoma Formation, and the main trace of the fault zone and associated hanging-wall subsidiary faulting were exposed in the southeastern half of the trench.

continued on page 10

II. Previous Work and Setting of Paleoseismic Trenches

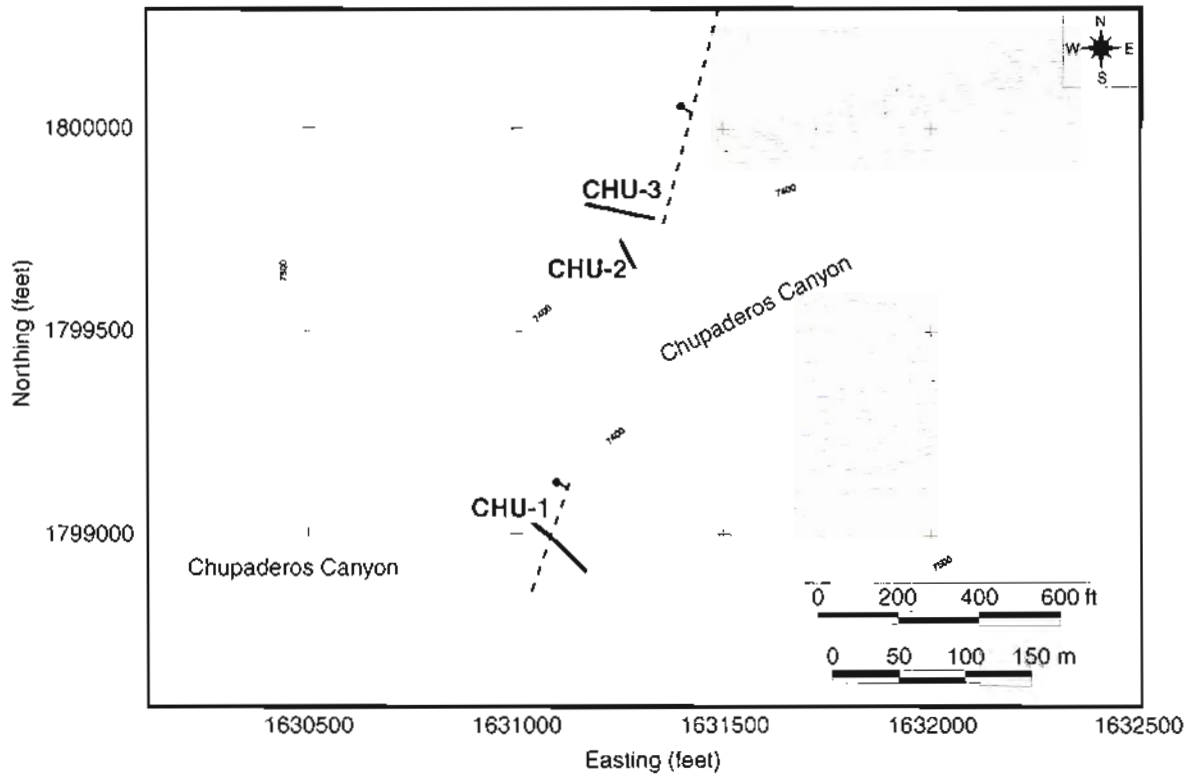


Figure 3. Map of Paleoseismic Trenches in Chupaderos Canyon. The location of the Guaje Mountain fault is shown only where it is certain at this scale. Note that the fault makes a small right step or bend between CHU-1 and CHU-3. The contour interval is 10 feet, and the grid on the borders of the figure is State Plane Coordinate System, New Mexico Central Zone, 1983 North American Datum.



Figure 4. Trench CHU-1 During Logging. The view in the photograph is to the southeast.

Paleoseismic Trenching in the Guaje Mountain Fault Zone



Figure 5. Trench CHU-2. The view in the photograph is to the northwest.



Figure 6. Trench CHU-3. The view in the photograph is looking west.

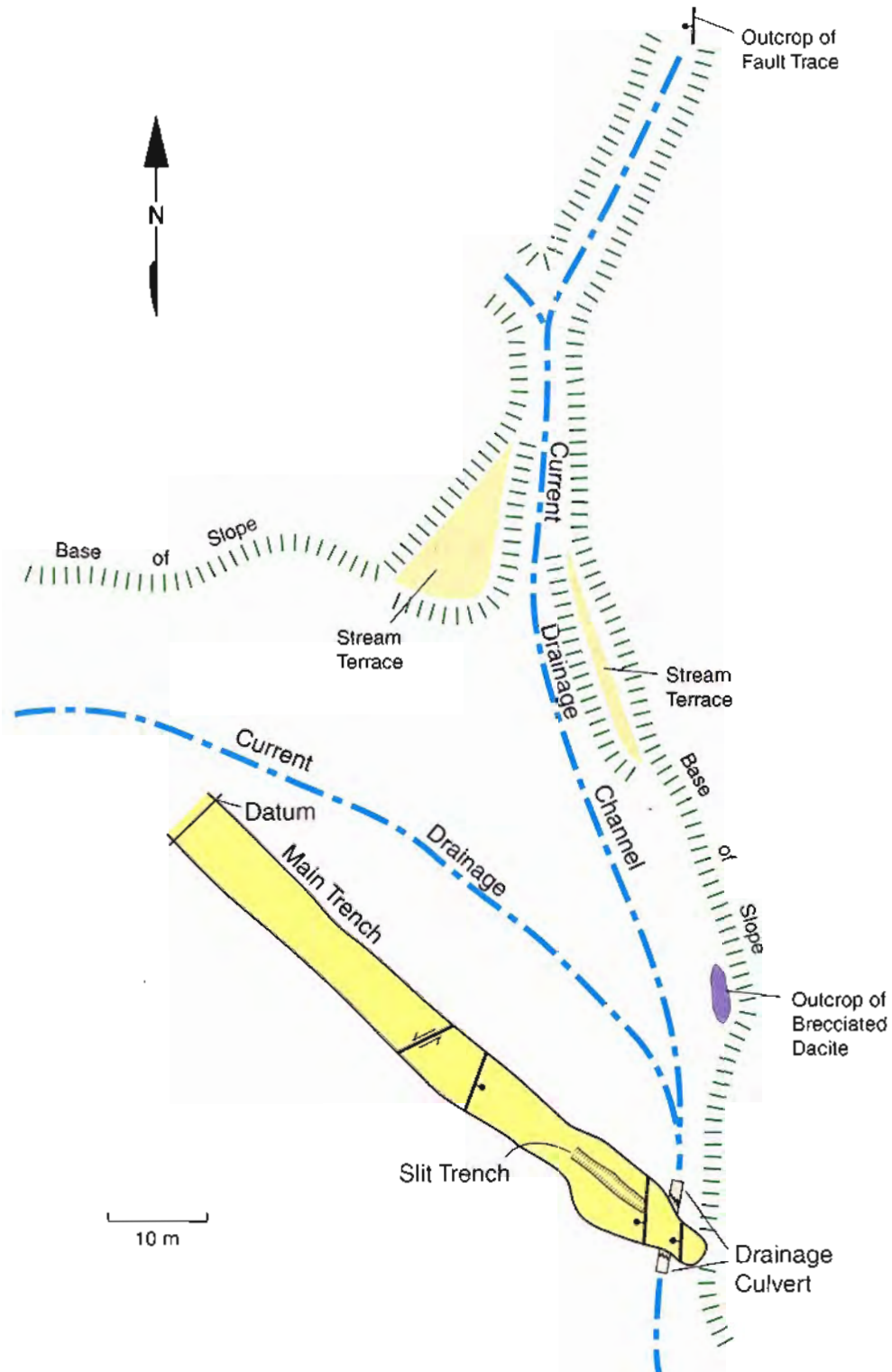


Figure 7. Map of Paleoseismic Trench in Cabra Canyon. The faults shown are, from northwest to southeast, the mid-trench strike-slip fault, the mid-trench low-angle fault, the main trace in the younger portion of the main fault zone, and the main trace in the older portion of the main fault zone (see text). The figure is modified from Gardner et al. (1990).

III. METHODS

A. Trench Excavation and Logging

The Chupaderos Canyon trenches were excavated with a trackhoe and were no deeper than about 5 m, typically about a meter wide with vertical walls, so as to enable use of a trench safety system of hydraulic aluminum shores (cover photo, Figures 4, 5, and 6). The Cabra Canyon trench, done in an era of different safety requirements, was mostly excavated with a front-end loader and was generally as wide as it was deep (about 4 to 5 m) with vertical walls and no shoring. The Cabra Canyon trench also featured a slit trench, about a meter wide and an additional 2 m deep, excavated with a small backhoe in the floor of the main trench (Figure 7). The slit trench afforded additional exposure of the main zone of faulting. Upon completion of in-trench studies, the trenches were backfilled, and native grass seed mixtures with straw mulch were spread over the sites. Small engineered barriers were constructed on slopes to help stem erosion.

Trench walls were scraped and cleaned with hand tools, and stratigraphic contacts and structural features were flagged with color-coded nails. In the Cabra Canyon trench, a grid of string lines was surveyed and spiked to the walls of the trench. Logging was done by measuring distances from the grid and plotting on graph paper. In the Chupaderos Canyon trenches, the colored-coded nails were surveyed with a total station (cover photo), plotted on graph paper, and used as control points for more detailed logging. All trenches were originally logged at a scale of 1:20, but structurally important zones in the Cahra Canyon trench were additionally logged at a scale of 1:10. Both northeast and southwest walls were logged in the Cabra Canyon trench. In the Chupaderos Canyon trenches, only the southwest walls were logged because of more uniform light over the course of a day and in the interests of expediency. The northeast walls in the Chupaderos trenches were examined in structurally important zones but not logged.

In all trenches, a reference datum of 0 m horizontal and 0 m vertical was established on the ground surface at an end of the trench. Locations in the trench are uniquely described by horizontal and vertical distances from the datum. For example, a location designated 55H, -3V is 55 m horizontally along the trench wall from the reference datum and 3 m vertically down from it. Addition of an N or S in front of the horizontal designator (eg. N55H) specifies a location on the north or south wall of the trench. Accuracy of logged features is within 10 cm by the string-grid method and within about 2 cm by the total-station method. For simplicity, however, we generally discuss locations within the closest half-meter.

B. Geochronology

Geochronologic controls on the ages of stratigraphic units are provided by several methods. In the Cabra Canyon trench, age controls were provided by stratigraphic relations and comparison of unit characteristics with those of previously dated deposits in nearby areas, radiocarbon analyses of detrital charcoal collected from various units, and natural remanent magnetism of certain units. In the Chupaderos Canyon trenches, ages were determined by stratigraphic relations and comparison of unit characteristics with those of previously dated deposits in nearby areas, radiocarbon analyses of charcoal, optically stimulated luminescence (OSL), and soil profile descriptions and profile development index (PDI) calculations (see Appendix A).

C. Stratigraphic Unit Names, Symbols, and Descriptions

Gardner et al. (1990) defined some 40 stratigraphic units in the Cabra Canyon trench based on visible contacts, composition, textures, and degree of induration. They used arbitrary letter designations as unit names or symbols with no sequential or stratigraphic significance for the letter designations. In the interests of simplification, we have generalized a great deal of the detailed stratigraphy of Gardner et al. (1990) but use some of their unit

symbols where necessary in discussions of structure. Detailed stratigraphy and unit descriptions can be found in the original, unpublished report (Gardner et al. 1990). In the Chupaderos Canyon trenches, units received symbols more typical of a geologic map. Explanations of these symbols and detailed descriptions of all logged units in the Chupaderos Canyon trenches are found in Appendix B. Structures in the Chupaderos trenches have received designators of the form I-B, indicating, in this example, a structure in trench CHU-1. In a given trench, structures that are discussed, or for which data are plotted in a figure, are lettered alphabetically from east to west. Faults are distinguished from fractures by observations of displacement of stratigraphic markers, shear fabrics, and/or cataclastic textures.

IV. RESULTS

A. Cabra Canyon Trench

For this section on the Cabra Canyon Trench, refer to Plate 1 and Plate 2. All discussions are modified from Gardner et al. (1990).

1. Stratigraphy

The oldest unit exposed in the Cabra Canyon trench is Tschicoma Formation dacite, which forms the hillslope on the upthrown block of the fault at the southeastern end of the trench and exhibits cataclastic brecciation in outcrops near the main fault trace (Figure 7). The dacite is part of a dome-and-flow complex that forms Guaje Mountain, dated at about 5 Ma (Aldrich and Dethier 1990). The oldest sedimentary unit in the trench is an interbedded sequence of moderately lithified, pumice-rich fluvial sands and lacustrine silts. Paleomagnetic studies of these deposits show they possess a reversed polarity. Stratigraphic relations indicate these deposits are younger than at least part of the Bandelier Tuff, so they are Pleistocene in age. An angular unconformity separates this Pleistocene lacustrine-fluvial sequence from overlying Holocene deposits. Most of the sediments exposed

in the Cabra Canyon trench are unconsolidated fluvial channel and overbank flood deposits. The channel deposits are mainly sands, gravelly sands, and sandy gravels that commonly exhibit bedding, crossbeds, and cut-and-fill structures. The overbank flood deposits are characterized by a dominantly fine sand matrix with sparse gravel clasts. These deposits lack induration and are largely devoid of sedimentary structures. Ten ^{14}C dates constrain the age of the exposed Holocene sequence from about 6.5 calibrated ^{14}C ka (cal ka) to modern (Plate 1 and Appendix A-1). The dates also imply three major episodes of Holocene sedimentation and aggradation from about 4 to 3 cal ka, around 1.6 cal ka, and during the last several centuries. Older periods of aggradation may be recorded in deposits not exposed, beneath the floor of the trench. The southeastern part of the trench exposed several colluvial units that have been shed across the fault scarps. Compositionally, these colluvial units vary little, and they consist of angular dacite clasts in a clay-rich, sandy matrix. Three colluvial units are distinguished on the basis of position, induration, and structural relations. Colluvium I, the oldest of the three, is well lithified and ubiquitously cataclastically brecciated. Colluvium II is weakly lithified and is partly draped across, but also partly faulted within, the main fault zone. Notable in the downfaulted portion of Colluvium II is a large block of nonwelded tuff; this tuff block is texturally identical to the basal portion of the Bandelier Tuff in surrounding natural exposures. Age relations of the colluvial units are otherwise poorly constrained. Colluvium III is not lithified and is overlain by deposits less than about 1.5 ka. Structural relations suggest that Colluvium II is younger than the lacustrine-fluvial sequence with reversed magnetic polarity.

2. Structure

For purposes of description, the three zones of deformation in the Cabra Canyon trench are called the main fault zone, the mid-trench low-angle fault, and the mid-trench strike-slip zone.

Main Fault Zone: The main fault zone (N51H to

N63H and S62H to S67H) is about 10 m wide and consists of younger and older portions, based on relative ages of displacements. Generally the main fault zone includes two major fault traces, highly fractured deposits, cataclastically brecciated and sheared deposits, and subsidiary faults. The older portion of the main fault zone (N58.5H to N63H, Plate 2-A) contains one of the two major traces, mentioned above, which is most obviously expressed as a 1- to 1.5-m, eroded scarp in dacite bedrock, above the fault that cuts across the trench with an attitude of N8W, 90. The face of the fault is plastered with brecciated dacite and brecciated Colluvium I. This fault and a highly sheared and brecciated zone of dacite and Colluvium I (from N58.5H to N63H) are overlain by Colluvium II that is mostly undeformed. On the southwest wall of the trench, this older portion of the main zone is expressed only as a patch of brecciated Colluvium I, which abuts the fault and is overlain by undeformed Colluvium II. In addition to the major fault trace, subsidiary faults and fractures that mostly predate Colluvium II occur in the older portion of the main fault zone. Most fractures are filled with amorphous silica, as indicated by x-ray diffraction analyses, and are parallel to subparallel to the faults (Figure 8a). Most slickensides in this area plunge south; however, one set of slickensides on a subsidiary fault between N60H and N61H plunges northeast but is nearly horizontal (Figure 8a). Displacements of these faulting events are difficult to estimate. The modification of the scarp above the major fault trace (Plate 2-A) indicates the scarp existed as a free face prior to burial by Colluvium II. The simplest explanation for these observed relations is net normal slip of greater than 1 to 1.5 m, the height of the scarp, in one event; however, multiple events to create the observed features cannot be refuted. We have no control on the magnitude of horizontal or oblique slip.

The younger portion of the main fault zone was best exposed from about N51H to N58.5H and, in the southwest wall, at about S62.5H. The major fault trace at about N57H to N58H and S62.5H is a band of gouge, generally 15 to 20 cm wide, surrounded

by dacite and Colluvium II that are sheared and cataclastically brecciated. As exposed in the northeast wall, the fault, with an attitude of N9W, 74W, juxtaposes at least 2 m of Colluvium II on the west against shattered dacite, overlain by about 1 m of Colluvium II, on the east (Plate 2-A). In the southwest wall of the trench, Colluvium II is on both sides of the fault. Net vertical displacement has been down to the west. Several subsidiary faults, between about N51H and N52H, exhibit bands of gouge and small displacements of sedimentary units. Where discernible, the sense of displacement on these small subsidiary faults is down to the east. Although relations are equivocal, these subsidiary faults may form the western edge of a small graben, with the downfaulted portion of Colluvium II within the graben between the major fault trace and the subsidiary faults. Faults and fractures in this younger portion of the main fault zone are nearly parallel, with most strikes between N-S and N10W (Figure 8b). Slickensides throughout this portion of the main fault zone show plunges that range from horizontal, to the south, to vertical (Figure 8b). Two sets of slickensides, however, have shallow plunges to the north (Figure 8b); one of these sets of slickensides is within the thick swath of gouge in the major fault trace. At the northwestern end of the younger portion of the main fault zone, the Pleistocene lacustrine-fluvial sequence is tilted about 20 to 30 degrees to the west with the strike of bedding parallel to the faults and fractures (Plate 1 and Plate 2-B). These relations suggest that the tilting has been caused by faulting. Overlying the entire younger portion of the main fault zone are undeformed sands and gravels of the Holocene sequence. Carbon-14 dates suggest that those units that directly overlie this portion of the main fault zone are about 4.2 cal ka.

The dominant sense of displacement across the main fault zone has been normal and down to the west based on the juxtaposition of stratigraphic units in the trench and nearby outcrops. Assuming entirely normal displacement, Colluvium II was faulted with greater than 2 m of vertical slip along the fault at N58H and S62H. Exposed relations in

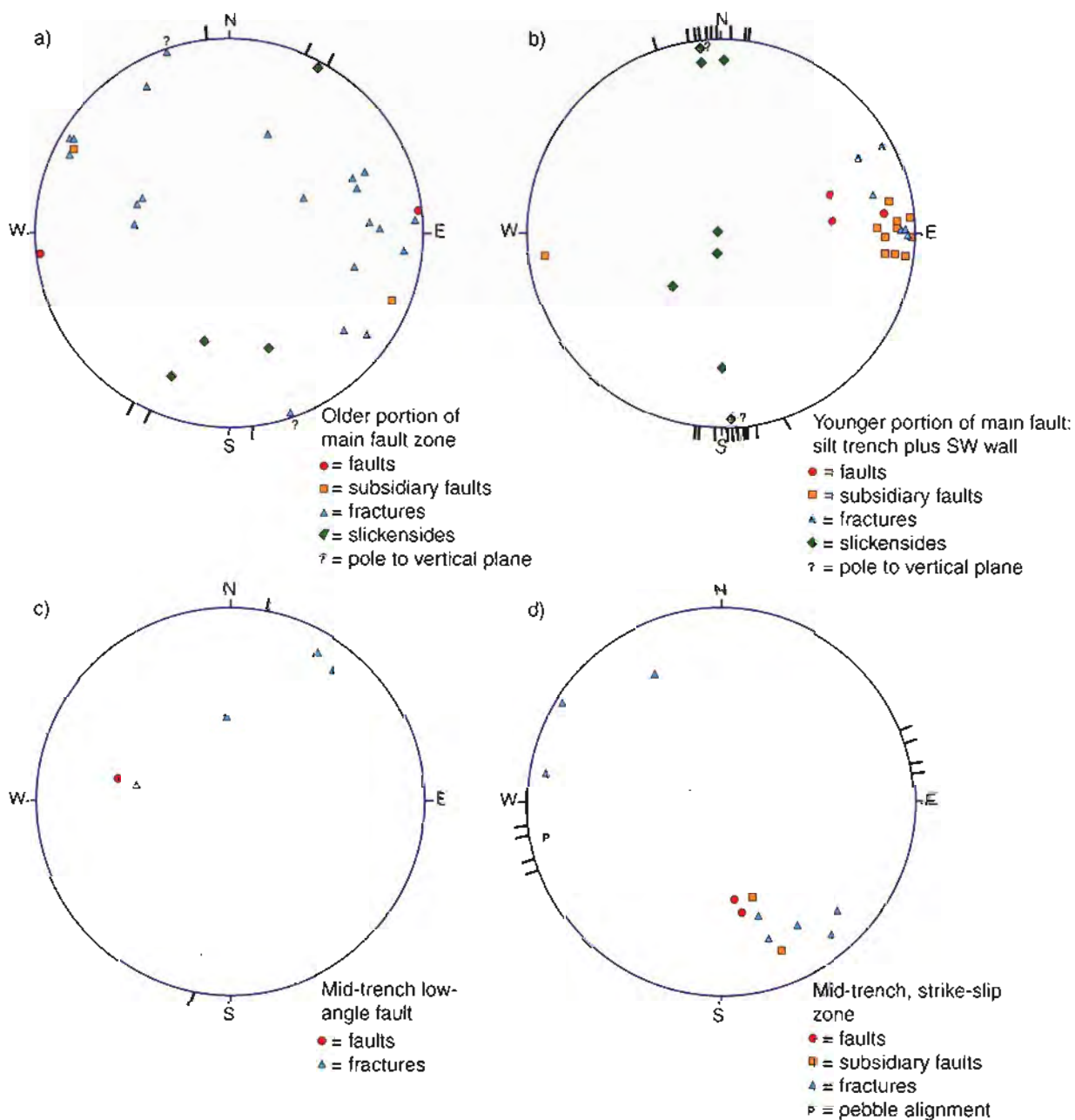


Figure 8. Lower Hemisphere Stereonet (Schmidt) Plots of Structures in the Cabra Canyon Trench. These lower-hemisphere stereonet plots show poles to planes of faults and fractures as well as strike lines of faults at the equator of the sphere. Lineations (slickensides and pebble alignments) are plotted as trend and plunge. a) is a plot of the older portion of the main fault zone; b) is the younger portion of the main fault zone; c) is the mid-trench low-angle fault; and d) is the mid-trench strike-slip zone. Figure is taken from Gardner et al. (1990).

this trench alone do not permit evaluation of this displacement as having been caused by one or multiple events. However, information from other trenches (see Section V, "Discussion and Conclusions") indicates that this vertical displacement of at least 2 m occurred in one paleoearthquake. Slickensides indicate an oblique to strike slip component is common during faulting. The orientations of most observed slickensides would require this oblique slip component to be left lateral. The northerly plunging slickensides, on the other hand, would require a right-lateral slip component. Again, the magnitude of these lateral or oblique components of slip cannot be estimated.

Mid-trench Low-Angle Fault: The mid-trench low-angle fault was exposed at about N37H to N38H and S39.5H. The fault is a sharp break with an attitude of N11E, 50E. The fault is 1.5 to 2 cm wide and is infilled with amorphous silica and roots. In contrast to the main fault at N57H to N58H, this fault exhibits no gouge and only has a weakly developed shear fabric. This fault is parallel to the main fault and dips into it, probably intersecting the younger portion of the main fault zone at about -15V to -17V. Fractures associated with the mid-trench low-angle fault have orientations similar to those of the main fault zone (Figure 8c). No slickensides were preserved in the low-angle fault. In the northeast wall of the trench, the Pleistocene lacustrine-fluvial sequence (Unit FF) is displaced about 1 m down to the east; here it is overlain by an undeformed Holocene fluvial unit (Unit S) that yielded a ^{14}C date on multiple charcoal fragments of about 3.8 cal ka. In the southwest wall, an Holocene overbank deposit (Unit yy), dated at about 6.5 cal ka, is faulted against the lower part of Unit FF of the Pleistocene sequence. Here the fault is overlain by an undeformed overbank deposit (Unit SS) that yielded a ^{14}C date on multiple charcoal fragments of 4.8 cal ka. Additionally, overlying Unit SS is another overbank deposit (Unit HH) that gave a date of about 4.2 cal ka on a single piece of charcoal. Based on correlations of subunits within Unit FF in the northeast wall of the trench, the mid-trench low-angle fault displays about 1 m of

normal slip on the Pleistocene sequence.

Mid-trench Strike-slip Zone: Deformation in the mid-trench strike-slip zone at N31H to N33H and S30H to S31H has involved Pleistocene units FF and GG and Holocene units V, G, and F. Foreset beds in unconsolidated Unit G on the northeast wall have been steepened and dragged into the failure surface by the deformation; on the southwest wall, well-defined bedding in a pebble gravel of the same unit is abruptly truncated. The upper part of fault has an attitude of N83E, 44N. On the northeast wall of the trench, a block of Unit FF, shattered with fractures and small faults that are all nearly parallel, sits above the sharp fault trace. The fault is about 0.5 to 1.5 cm wide and is infilled with roots and amorphous silica, as indicated by x-ray diffraction analyses. The dip of the fault is not constant and, in fact, decreases towards the base of the logged exposure. Additional manual excavation into the floor of the trench (not logged) revealed that the failure surface flattens out completely into an underlying, unconsolidated sand bed. A continuation of the fault was not found beneath the sand bed. Above the shattered block, elongate pebbles in Unit F exhibit a pronounced alignment of N78E, 0 to 10W. This pebble alignment, parallel to the faults and fractures of this zone (Figure 8d), is contrary to the paleocurrent flow directions of S68E measured in this unit away from the deformation. In the southwest wall of the trench, the fault is a zone of intense shearing and brecciation that has created a foliated mixture of components derived from a number of units. The zone of this melange is up to 20 cm wide and is oriented N80E, 50NW. Finger-like projections of Unit V have been squeezed up in the shear zone to intrude overlying Unit F (Plate 2-C). Undeformed Unit P, which yielded a ^{14}C date on multiple charcoal fragments of about 3.8 cal ka, overlies this zone in both trench walls.

The flattening of the dip of the fault surface and translation of deformation along and through the unconsolidated sand bed requires the deformation in this zone to be pure strike slip. Vertical to oblique movements would create a more vertically

continuous fault trace and obliterate large deviations of fault surface dip, such as those observed. The pebble alignment and plunge indicate that the shattered block, above the fault trace in the northeast wall of the trench, has been moved by left-lateral faulting. Lateral displacements of the shattered block, taken together with the abrupt facies changes of some units, also explains how some lithologies in the block are continuous and correlative across structures and some are not. The sense of the deformation of the foreset pebble beds in Unit G is also consistent with left slip, and the finger-like intrusions of Unit V into Unit F in the southwest wall are indicative of localized compression during the strike-slip deformation. Given that some subunits of FF correlate and some do not across the strike-slip fault and through the shattered block, we conclude the amount of net left slip in this zone must be up to, but no more than, a few tens of centimeters. This magnitude of net slip is consistent with the dragging and smearing of the foreset pebble beds of Unit G.

3. Paleoseismic Implications

The main fault zone exposed in the trench exhibits evidence for at least two episodes of faulting. Variable orientations of slickensides and the mature fabric and gouge in the fault at N57H to N58H argue for more. The scarp above the fault at N63H was created in the dacite and Colluvium I was deformed along with brecciation, shearing, and fracturing between N58.5H and N63H. This episode involved at least 1 to 1.5 m of vertical slip. If Colluvium I was originally a scarp-derived unit, it would provide evidence for at least one earlier event; however, available data do not preclude a slope colluvium origin for Colluvium I. Age constraints for this episode or episodes are only provided by the faulted dacite and the undeformed portion of Colluvium II. Containing chunks of Bandelier Tuff, Colluvium II must be younger than 1.22 Ma, but how much younger is uncertain; similarly, Colluvium II is overlain by deposits dated at about 4.2 cal ka and is clearly older, but how much older is uncertain. Thus, these older faulting episodes occurred sometime between the age of the

dacite, 5 Ma, and the age of Colluvium II, between < 1.22 Ma and > 4.2 cal ka. Following these earlier events, Colluvium II was shed across the older portion of the main fault zone. In the youngest event recognized in the trench (see below), Colluvium II was probably faulted at least 2 m down to the west. Independent of information from other faults in the trench, age relations for this episode of faulting are provided by the age of Colluvium II and the overlying undeformed Holocene fluvial deposits. Thus, the broad constraints for this faulting event are between < 1.22 Ma and 4.2 cal ka. Subsidiary faults in the younger portion of the main zone show orientations and age relations identical to the main fault at N57H to N58H; thus, we conclude these subsidiary faults formed during the same faulting event.

The mid-trench low-angle fault is depositionally overlain in the northeast wall of the trench by undeformed units S and P, both containing charcoal dated at about 3.8 cal ka. In the southwest wall of the trench, the fault cuts an unconsolidated overbank deposit and is depositionally overlain by younger overbank deposits. Charcoal from the faulted sediments (Unit yy) yielded a ^{14}C date of 6.5 cal ka, whereas the younger, unfaulted deposit (Unit SS) gave a date of about 4.8 cal ka. Stratigraphic relations of Unit SS with other dated units, and the fact that the dates are on detrital material, very strongly suggest that the 4.8 cal ka date is too old and that the most recent movements on this fault occurred between 4.2 and 6.5 cal ka. Given the geometric and spatial relations of the mid-trench low-angle fault with the main fault zone, as well as virtually identical youngest-age constraints on deformation for all faults in the trench, we conclude that this faulting represents deformation associated with the most recent surface-rupturing paleoseismic event recorded in the trench and on the Guaje Mountain fault.

The youngest units affected by deformation in the mid-trench strike-slip zone are G and F. Undeformed Unit P, containing charcoal dated at 3.8 cal ka, overlies the zone in both walls of the

trench. The youngest deformed units are unconsolidated and are, therefore, most probably Holocene in age; furthermore, they occupy the same stratigraphic position as dated units yy and SS. Thus, we conclude that the deformation in the mid-trench strike-slip zone occurred at the same time as that in the mid-trench low-angle fault.

B. Chupaderos Canyon Trench 1

For this section on the Chupaderos Canyon Trench 1 (CHU-1), refer to Plate 3.

1. Stratigraphy

Here, we discuss the general stratigraphic framework of trench CHU-1, specifically focused on those units that bear on paleoseismic interpretations. Detailed descriptions of all logged units are presented in Appendix B.

The oldest unit exposed in CHU-1 consists of poorly sorted gravels with cobbles and boulders of sub-rounded dacite in an orange, clay-rich matrix. We have called this unit the Puye Formation (Tpf; locally, 1.6 to 5 Ma), consistent with geologic maps of the area (Smith et al. 1970). This assignment is possibly problematic in that the Puye Formation is compositionally and texturally similar to deposits referred to as the "Cerro Toledo interval" whose age is 1.6 to 1.2 Ma (see, for example, Broxton and Reneau 1995). Commonly, position in the stratigraphic sequence can be used to tell the two units apart, with the Cerro Toledo interval occurring between the Tshirege and Otowi members of the Bandelier Tuff and the Puye Formation lying beneath the Bandelier Tuff. Also, subtle compositional variations can be found locally with the Cerro Toledo containing, in addition to the dacite-rich gravels, rare clasts of Bandelier Tuff and aphyric obsidian. CHU-1 did not offer sufficient exposure of the stratigraphic sequence nor did we note any of the rare diagnostic clasts; thus, we call the unit, which occurs only on the upthrown block of the fault zone, Puye Formation. Derived from the Puye Formation is a colluvial unit (Qc1-1) that, because of spatial relations to faults 1-B, we interpret to be a

tectonic colluvium. Separated from these units by an unconformity is the Tshirege Member of the Bandelier Tuff, which includes a basal lapillipumice fallout deposit (Qbtt; the Tsankawi Pumice) on the upthrown block of the fault zone and a fine-grained nonwelded ignimbrite (Qbt1) on the downthrown block. Overlying the Bandelier Tuff units, separated by a significant unconformity, is a sequence of late-Pleistocene fine-grained, alluvial deposits almost 4 m thick. Interfingering near the base of the late-Pleistocene alluvial sequence is a colluvial unit (Qc1-4), which consists exclusively of abundant clasts and fines of locally derived ignimbrite (Qbt1). Spatial relations with the main zone of faulting might imply that Qc1-4 is a scarp-derived colluvium. Although we entertain a scarp-derived scenario for Qc1-4, there are difficulties with it, discussed below. Alternatively, Qc1-4 may represent colluvium on a stream bank that was cut into Qbt1. Two units in the late-Pleistocene alluvial sequence (Qa11-1 and Qa11-3) can be traced most of the length of the trench and occur on both upthrown and down-dropped blocks of the fault zone, providing markers for estimation of magnitude of normal slip. The alluvial sequence extends to the modern ground surface, and it has been eroded. At least 1.4 m of the alluvial sequence (unit Qa11-4) has been stripped from the upthrown block. No Holocene units occur in proximity to the fault zone. Colluvium with an inferred Holocene age, based on characteristics similar to dated deposits in the surrounding area, occurs at the eastern and western ends of CHU-1 (units Qc1-5 and Qc1-6, respectively).

Three ^{14}C dates (Appendix A-1) were obtained on charcoal from units in CHU-1. The youngest date came from the lowest stratigraphic horizon sampled and represents either invasive material or contamination of the sample with young carbon. The other two dates suggest the late-Pleistocene fluvial sequence is around 40 to 32 ka. The date from the Holocene colluvium Qc1-6 reflects local reworking of charcoal from older deposits, likely Qa11-4 as implied by the OSL dates on that unit (see below). Six OSL dates (Appendix A-2) are consistent with the ^{14}C constraints and, given the uncer-

tainties, are stratigraphically consistent (Figure 9). The OSL dates also indicate the late-Pleistocene fluvial sequence is around 40 to 32 ka. Five soil profiles were measured in CHU-1 and exhibit internal consistency with strong correlations of soils among the profiles (see Appendix A-3). As expected, the two profiles on the upthrown block yield younger PDI age estimates for given horizons, reflecting the stripping of the stratigraphic section. The profiles on the downthrown block are generally consistent with each other but PDI age estimates deep in the fluvial sequence are too old given other age constraints. The reasons for these discrepancies are probably related to a depositional history and geomorphic setting at CHU-1 that differ significantly from the calibration sites for the soil chronofunction. The soil chronofunction is calibrated mainly on sites on a series of abandoned stream terraces (McDonald et al. 1996; Reneau and McDonald 1996). The alluvial sequence in CHU-1 represents an aggrading canyon floor that would have experienced repeated infiltration of flood waters over a period of at least eight thousand years. These conditions may have led to increased rates of soil-forming processes, relative to the chronofunction calibration sites in a different setting. For these reasons, together with evidence for erosion of the upper part of the alluvial sequence, we believe the PDI calculations do

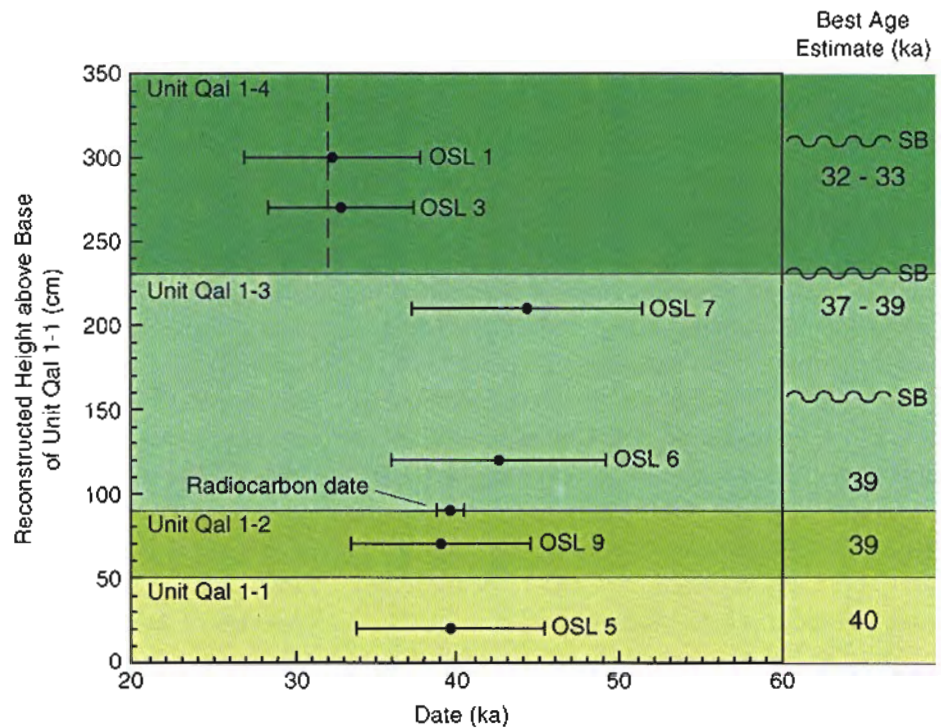


Figure 9. Age Constraints in Trench CHU-1. The plot shows age constraints with respect to stratigraphic position in the late-Pleistocene fluvial sequence in trench CHU-1. The dashed vertical line in unit Qal1-4 is the ^{14}C date on charcoal from unit Qc1-6, which is probably reworked from unit Qal1-4. The best age estimates are shown in the column at right along with stratigraphic positions of soil boundaries (wavy lines with SB). Although the soil boundaries are useful markers and indicate hiatuses in deposition, the associated PDI age estimates (Plate 3 and Appendix A) are not accurate in this setting (see discussion in text).

not provide reliable age estimates at CHU-1.

not provide reliable age estimates at CHU-1.

2. Structure

Most of the stratigraphic units exposed in CHU-1 are nearly flat-lying or have gentle dips of about 10 degrees to the northwest, approximately parallel to the modern hillslope. The contact of the Puye Formation (Tpf) with the Tsankawi Pumice (Qbt) also has shallow dips in the eastern part of the trench but steepens to about 25 degrees as it approaches the main fault (fault 1-D). Similarly, the ash layer within Qbt dips about 25 degrees into the fault zone. These changes in dip could be depositional, reflecting paleotopography that was blanketed by fallout deposits. The dip relations of these older units are also consistent with normal

drag during repeated normal displacements. Alternatively, these dip relations may have been caused by older monoclinical folding, as observed elsewhere in the fault system (Gardner et al. 1999, 2001), that has subsequently been ruptured by more recent faulting events.

CHU-1 exposed the main zone of faulting of the Guaje Mountain fault. Some subsidiary faults, if locally present in the hanging-wall block, may lie west of the west end of the trench, buried beneath the active channel of the Chupaderos Canyon drainage. The main zone of faulting in CHU-1 (between 28H and 40H) bears some remarkable geometric similarities to the main zone exposed in the Cabra Canyon trench. In CHU-1, the main fault zone is about 11 m wide and also consists of younger and older portions, based on relative ages of displacements. Similar to the Cabra Canyon trench exposure, the older portion of the main fault zone in CHU-1 (faults 1-A and 1-B) is about 5 m east of the younger portion. In both CHU-1 and the Cabra Canyon trench, strikes of structures related to the main fault zone are around N-S, with a range of strikes from N20W to N25E (Figures 8 and 10).

Remnants of the older portion of the main fault zone in CHU-1 are evident as faults 1-A and 1-B. These faults are expressed as vertical bands of foliated gouge 10 to 25 cm wide. The upward continuation of each fault is truncated at the top of the Tsankawi Pumice unit (Qbtt), and each is overlain by undeformed Qa1-1, the basal part of the late-Pleistocene alluvial sequence. Fault 1-A cuts the Puye Formation (Tpf) and vertically displaces an ash layer in Qbtt only a couple of centimeters down to the east; no vertical displacement of the Tpf-Qbtt contact is evident. Fault 1-B also cuts the Puye but separates it from a Tpf-derived colluvial deposit (Qc1-1), which is at least 50 cm thick, immediately west of the fault trace. Based on models of scarp evolution (Nash 1986; Forman et al. 1991; Nelson 1992; McCalpin et al. 1993), these relations suggest fault 1-B experienced movements that created a west-facing scarp at least one meter high post-Puye Formation but pre-Tshirege Member of the

Bandelier Tuff. Fault 1-B also displaces the ash layer within Qbtt about 25 cm down to the west but does not vertically displace the base of Qbtt. It is additionally incongruous that faults with such broad, well-developed zones of foliated gouge have only experienced less than 25 cm of displacement in the last 1.22 million years. These relations indicate that these faults must have experienced dominantly strike-slip displacements to develop such mature fabrics with only small to no apparent vertical displacements on unit contacts. In fault 1-B, a set of grooves, plunging shallowly (22 degrees) fault-parallel to the south, is consistent with this interpretation; these relations indicate a component of left slip. It is difficult to evaluate what other faults may have participated in these earlier episodes of deformation. Some faults (for example, those in between faults 1-D and 1-E, the eastern part of 1-F, and the western part of 1-G) have similar apparent age relations to faults 1-A and 1-B with deformation truncated at the top of the Bandelier Tuff (Qbt1), overlain by undeformed unit Qa1-1 (or the time equivalent Qc1-4). However, the Bandelier Tuff-late-Pleistocene alluvium contact represents such a significant unconformity that very probably much paleoseismic information is missing.

Faults 1-C, 1-D, and 1-E exhibit the youngest displacements with their ruptures propagated to the modern ground surface or lost in the near-surface zone of active bioturbation by roots. Fault 1-C, with a strike of about N25E, exhibits a 5-cm wide zone of foliated gouge, and it has near-vertical but erratic dips. Foliations within the gouge dip steeply to the southeast. The fault displaces numerous contacts about 10 cm down to the east; however, where fault 1-C cuts unit Qc1-1, it does not exhibit this sense of vertical displacement. In that all the displaced contacts or markers, from the ash layer in Qbtt to the youngest contact within the late-Pleistocene alluvial sequence, show the same magnitude and sense of displacement, these small vertical displacements occurred in one event, most probably the MRE. The upward terminations of the ruptures of fault 1-C are at the modern ground surface

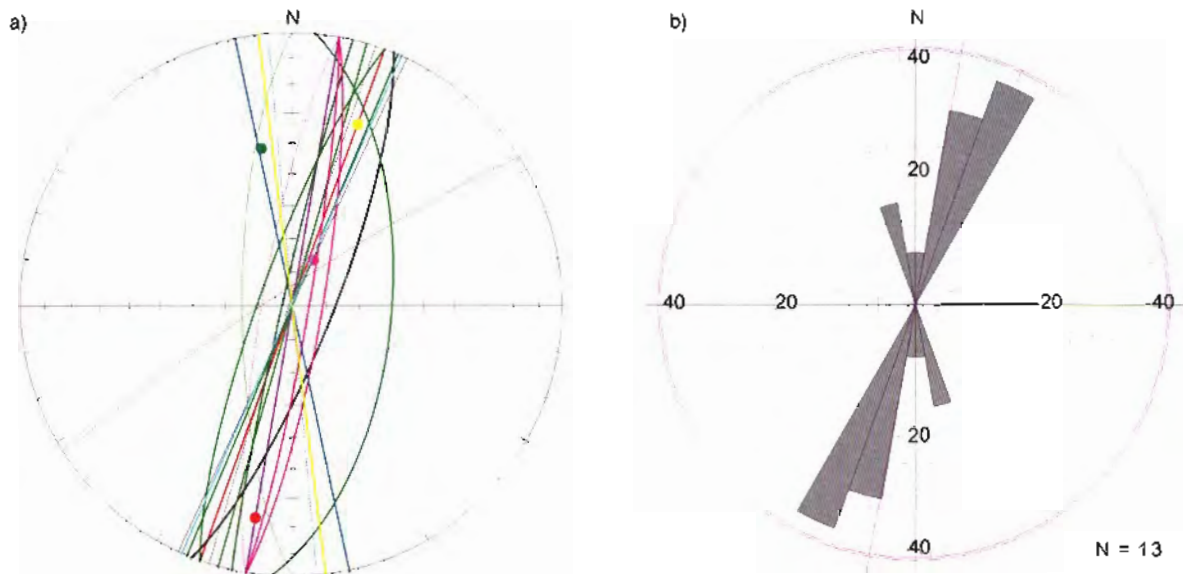


Figure 10. Structural Data from Trench CHU-1. a) Lower-hemisphere stereonet (Schmidt) plots of structures in trench CHU-1 showing the planes of faults (solid lines) and foliations (thin, dashed lines). Lineations (dots) are plotted as trend and plunge. Color coding as follows: 1-A = purple; 1-B = red; 1-C = black; 1-D = green; 1-E = pink; 1-F = blue; 1-G = yellow; and 1-H = light blue. b) Rose diagram of fault strikes in CHU-1 showing dominant trend between N10E and N30E.

where the fault fans into a 25-cm wide zone of intense shearing and fracturing that merges with the damage zone of the upper part of fault 1-D.

Fault 1-D appears to be the main fault trace based on the wide zone of gouge and the fact that it accommodates the greatest amounts of vertical displacement of all exposed faults. Very well-developed foliated gouge forms steeply dipping bands, typically about 30 cm wide, with the whole damage zone, including areas of intense shearing and cataclasite, typically about 50 cm wide. The attitude of fault 1-D is N20E, 60 to 80W, with the dip steepening with increasing depth near the base of the trench exposure. Fault 1-D displaces the base of a paleosol within unit Qa11-3 about 1.5 m and the Qa11-1–Qa11-3 contact about 2 m down to the west. Assuming the top of the Bandelier Tuff units once represented an erosional surface at the beginning of Qa11-1 deposition, this surface is displaced with about 2.5 m down-to-the-west normal slip. The upward terminations of the fault 1-D ruptures are at the modern ground surface where intense shearing

and cataclastic brecciation fan into a 50-cm wide zone that merges with the upper ruptures of fault 1-C. The mature fabric developed within the gouge is nearly fault-parallel and dips steeply to the northwest. In spite of the obvious vertical displacements of units across this fault, a well-developed lineation within the central parts of the gouge zone plunges 41 degrees to N11W, implying a component of right-oblique slip along with normal displacements.

Fault 1-E includes several individual faults grouped around a 10- to 40-cm wide zone of foliated gouge and cataclasite developed in the lower half of the exposed sequence. The zone of deformation strikes N10E and has dips from vertical to 85E. The upper part of fault 1-E is a thin, sharp rupture through all of the late-Pleistocene alluvial sequence, and it can be traced upwards toward the modern ground surface where it is obscured by bioturbation in the active root zone. Unit contacts in the late-Pleistocene sequence are apparently displaced about 30 cm down to the west, but a thick sand lens within unit Qa11-4 is abruptly truncated at the east

side of the fault, and no correlative sand lens is present west of the fault. These relations are best explained by an oblique component to the youngest movements. The lower portion of fault 1-E has the wide bands of gouge and cataclasite, truncates the eastern end of colluvium Qc1-4, and marks an east-facing step on the top of the Bandelier Tuff (Qbt1). Slickensides within the zone of gouge plunge steeply (75 degrees) to the north, implying a relatively minor component of horizontal slip in this portion of the fault.

Parts of faults 1-E, 1-F, and 1-G, as well as fault 1-H, form another age group based on how high in the stratigraphic sequence units are cut by the logged ruptures. The eastern splay of fault 1-E breaks only as high in the sequence as the Qal1-1–Qal1-3 contact horizon. Here the fault appears to displace the contact about 15 cm down to the west across a 40-cm wide fan of intense shearing and cataclastic brecciation. Fault 1-F strikes N12W and exhibits erratic dips. Most of the exposed fault is a sharp, thin break in Qbt1, but it fans upwards into a zone of cataclasite about 15 cm wide at the top of the tuff. Here the eastern splay and most of the cataclasite are overlain by undeformed colluvium (Qc1-4), whereas the western splay displaces the base of Qc1-4 about 10 cm down to the west. This western splay can be traced up through Qal1-1 and into the lower part of Qal1-3 where it is expressed as a prominent fracture with no displacement observable on the Qal1-1–Qal1-3 contact. Fault 1-G is a 40- to 60-cm wide zone of gouge and cataclasite, bounded by faults. The fault defining the eastern margin of 1-G has an attitude of N12W, vertical to 85W, and it displaces the Qc1-4 colluvium about 20 cm down to the west. The upward continuation of this fault was difficult to trace, but similar to the western fault of 1-F, it appears to break unit Qal1-1 and the base of Qal1-3 with no apparent displacement of the contact. The western fault of 1-F and the eastern fault of 1-G intersect and cross with no apparent mutual displacements. The zone of gouge and cataclasite and the fault at the western margin of 1-G are overlain by undeformed portions of unit Qc1-4. Foliation within 1-G has an attitude

of N18E, 71SE, contrary to the dips of the margins of the zone. A lineation within 1-G plunges 30 degrees to N20E. Fault 1-H is a vertical fault with a strike of N24E. No gouge or cataclastic breccia are associated with this fault. Fault 1-H displaces the Qbt1–Qal1-1 contact about 10 cm down to the west. The fault can be traced upward through unit Qal1-1 to where it is truncated at the Qal1-1–Qal1-2 contact.

3. Paleoseismic Implications

Trench CHU-1 provides a great deal of evidence, both direct and indirect, for multiple-faulting events since deposition of the Puye Formation. Best constrained are those two or three events that have occurred since the late Pleistocene, for which we use the conventional end-of-the-alphabet letter designations (i.e., Z is the most recent, Y is the penultimate event, and X is the next older event). Older events, because of erosional unconformities causing substantial missing stratigraphic section and damage from younger faulting events overprinting relations among faults, are difficult to address.

The oldest recognized faulting event in CHU-1 occurred sometime post-Puye Formation (Tpf) and pre-Tshirege Member of the Bandelier Tuff on fault 1-B. This event is inferred to have created a greater than 1 m, west-facing scarp in Tpf, from which colluvium Qc1-1 was derived and deposited at the base of the scarp. The record for many following paleoseismic events is no doubt lost because of the erosional bevelling of the top of Tpf and Qc1-1, creating the unconformity separating Tpf and Qc1-1 from the Bandelier Tuff (Qbt). Ensuing episodes of faulting are recorded by relations of faults 1-A and 1-B, which likely indicate multiple strike-slip events on those faults, as discussed above. As mentioned above, logged relations of many faults, including 1-C to 1-G, allow their participation in these older events; however, there is no way to constrain the nature of displacements on these other faults. Not much can be said about the actual number and timing of these older events except that they occurred post-1.22 Ma and prior to erosion of the top of Qbt-1 and Qbtt and deposition of Qal1-1.

Because of the large uncertainties in nature, number, and timing of these older events, we discuss them no further.

The youngest two, or possibly three, paleoseismic events are better constrained by relations within the late-Pleistocene sequence. Fault 1-D exhibits evidence for two of the youngest ruptures (events Z and Y) since the late Pleistocene with increasing displacements on progressively older units, as discussed above. If unit Qc1-4 is a tectonic, or scarp-derived, colluvium, it would indicate the possible third event (event X?).

Event X?, based on an assumption of tectonic origins for unit Qc1-4, is problematic in many respects. As discussed above, an alternative explanation of Qc1-4 as a stream-bank colluvium satisfies all observed relations. However, common practice in many paleoseismic studies is to assume tectonic origins for colluvial units in proximity to faults (for example, McCalpin 1996). Thus, we develop a scenario to embrace this possibility. Unit Qc1-4 is composed exclusively of angular blocks and fines derived from Bandelier Tuff ignimbrite (Qbt1), and the unit thickens to the west where it interfingers with Qal1-1. Thus, for a scarp-derived origin for Qc1-4, a west-facing scarp composed exclusively of Qbt1 is required, but where to place this scarp in reconstructions is the first problem. Qc1-4 pinches out against fault 1-E, but fault 1-E exhibits an east-facing step on the top of Qbt1. A west-facing scarp on fault 1-E would need to be completely removed in early Qal1-1 time and cannot be reconciled with the better-constrained displacements on fault 1-E in the ensuing younger events (events Y and Z, described below). Structural and geometric constraints, therefore, point to fault 1-D as a more-likely candidate for the hypothetical scarp.

A retrodeformation analysis (see McCalpin 1996) on the fault zone in CHU-1 yields Figure 11a, which shows a reconstruction of the setting in the main fault zone of CHU-1 immediately prior to event X?. Bandelier Tuff ignimbrite (Qbt1), restored on the

upthrown block, sits on both sides of the fault. Some of the tuff has already been downfaulted in earlier faulting episodes and erosion has planed off older scarps, leaving the eroded top of Qbt1 exposed at the ground surface. Fault event X? additionally displaces the tuff down to the west (Figure 11b). The reconstruction shows the displacement of event X? as about 1 to 1.5 m; however, this is largely unconstrained except to satisfy geometric and lithologic relations of the colluvial unit Qc1-4. From the free face of the scarp on fault 1-D, chunks of Qbt1 are shed across the fault zone, forming Qc1-4, which interfingers with earliest deposition of Qal1-1. These interfingering relations constrain the timing of event X? to about 40 ka, based on best-age estimates for Qal1-1 (Figure 9). Additionally, problematic with this scenario is that erosion must strip all of the ignimbrite (Qbt1) from the upthrown block and all of colluvium Qc1-4 between faults 1-D and 1-E in order to set the stage for the ensuing event Y (Figure 11c) at about the end of Qal1-1 deposition and in the early deposition of Qal1-3.

Parts of faults 1-E, 1-F, and 1-G, as well as fault 1-H, all have upper terminations of specific ruptures at essentially the same horizon, just above or at the upper Qal1-1 contact. We also note that, at this same horizon, the upward fanning patterns of intense shearing and cataclasite of fault 1-E and, perhaps, the lower portion of 1-D are remarkably similar to the fanning patterns of 1-D and 1-C where the youngest ruptures (event Z, see below) approach the modern ground surface. Additionally, the Qal1-1–Qal1-3 contact is displaced about 2 m down to the west on fault 1-D, whereas the base of the paleosol within the upper part of Qal1-3 is displaced only about 1.5 m down to the west on the same fault. All of these relations lead us to conclude that a discrete rupturing event, event Y, occurred at about the time of the beginning of deposition of unit Qal1-3 at about 39 ka (see Figure 9). Event Y caused small vertical displacements on fault 1-H and parts of 1-E, 1-F, and 1-G (all less than 25 cm, down to the west) and as much as 50 cm of down to the west on fault 1-D. These small vertical displacements may imply event Y was dominantly

continued on page 24

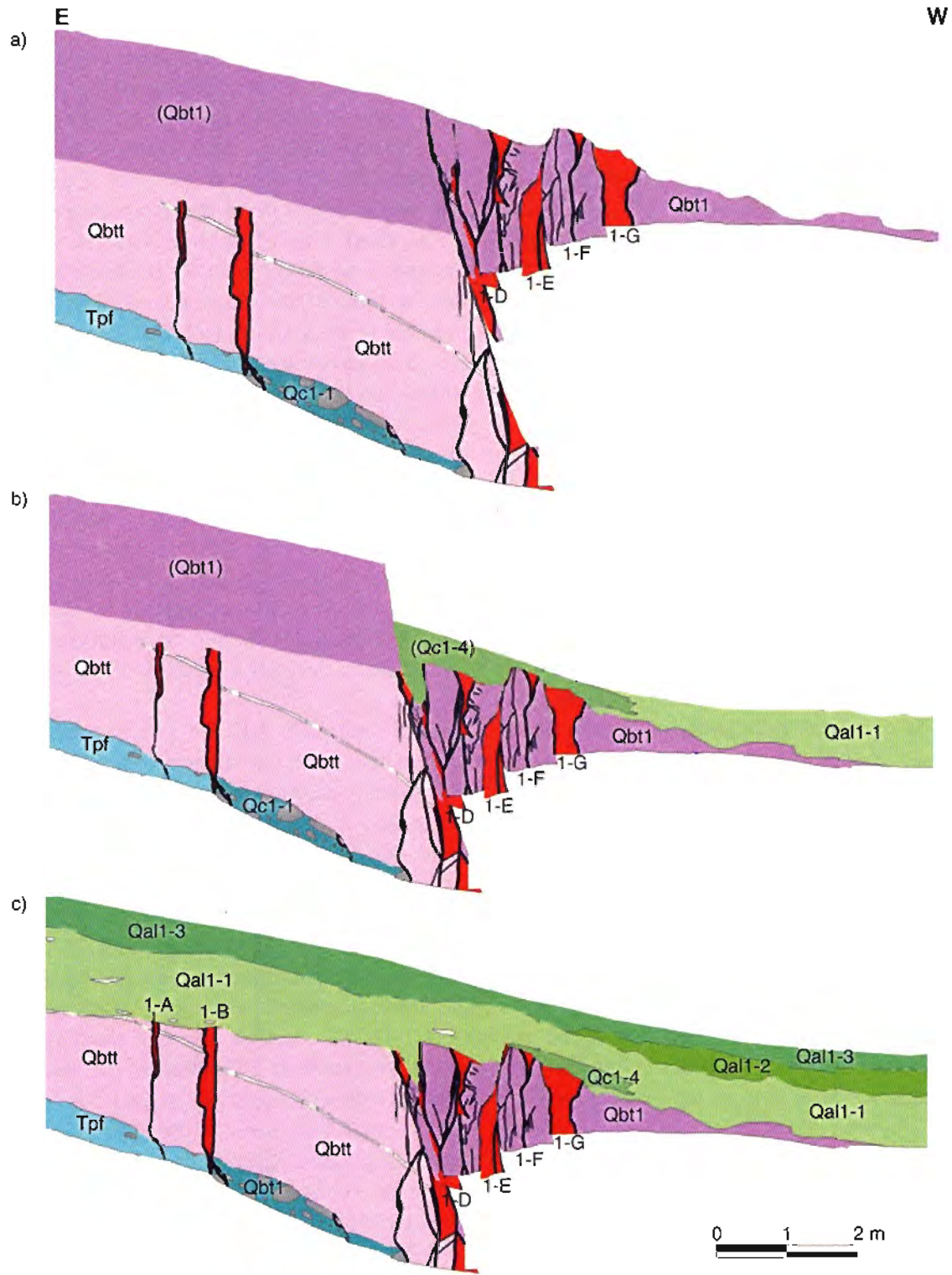
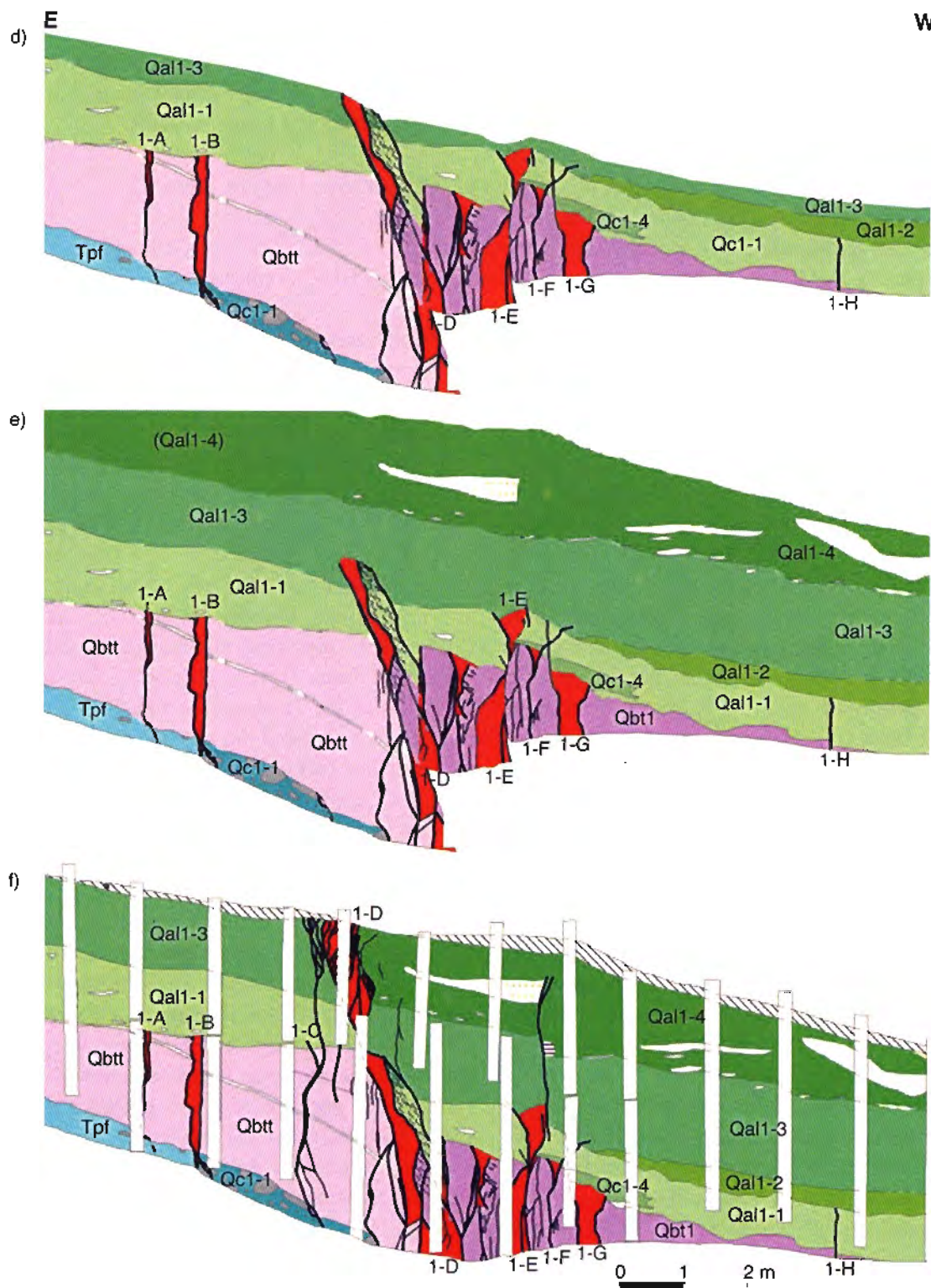


Figure 11. Reconstruction of Late-Pleistocene and Younger Events from Trench CHU-1. See text for discussion. Parentheses indicate a restored unit. Symbols and colors are the same as on Plate 3. The various sections show a) the setting in the fault zone just prior to paleoseismic event X?, about 40 ka; b) the setting immediately following paleoseismic event X?; c) the setting in the fault zone just prior to paleoseismic event Y, about 39 ka; d) the



setting immediately following paleoseismic event Y; e) the setting in the fault zone just prior to paleoseismic event Z, probably Holocene; and f) the trench as logged (white vertical bars are shores) following event Z and erosion of scarp and stripping of upthrown block on the east.

continued from page 21

strike slip. Figure 11c shows the setting in the fault zone immediately prior to event Y. As mentioned above, erosion has planed off the thin ignimbrite and scarp from the upthrown block and removed much of colluvial unit Qc1-4. Deposition of alluvial units Qa1-1 through the lower part of Qa1-3 proceeded across the fault zone. Event Y (Figure 11d) occurred, causing the vertical displacements on faults 1-D, 1-E, 1-F, 1-G, and 1-H just discussed. Available age constraints indicate event Y occurred at about 39 ka. Following event Y, deposition of the alluvial units up through Qa1-4 continued across the fault (Figure 11e).

Event Z (Figure 11f), the MRE, displaced markers in the upper portion of the alluvial sequence about 1.5 m down to the west on fault 1-D and caused ruptures on faults 1-C and 1-E to propagate to the modern ground surface. As discussed above, structural and stratigraphic relations surrounding faults 1-C and 1-E likely suggest more significant lateral displacements on these two faults during event Z. Timing constraints on event Z from CHU-1 alone are poor. Dates on stratigraphic units indicate event Z happened sometime since about 32 ka. Correlations of soils across the fault zone (see Appendix A-3) very strongly suggest that even the surface soil on the downthrown block has been faulted, but as discussed above, the numerical PDI age estimates for the soils are not reliable in this geomorphic setting. Since event Z, erosion has removed unit Qa1-4 and the scarp from the upthrown block, leaving the fault zone as logged (Figure 11f). It is worth noting that Holocene unit Qc1-6, containing charcoal dated at 32 ka, is probably a remnant of the colluvium that resulted largely from the stripping of Qa1-4 from the upthrown block. Given the inferences that can be drawn from CHU-1, including the faulted surface soil and likely age and origin of unit Qc1-6, together with results from other trenches on the Guaje Mountain fault zone, the simplest interpretation is that event Z occurred in the Holocene.

Relations in CHU-1 provide evidence for more than five faulting events. Significantly, two or three of

these events have occurred since deposition of Qa1-1 began about 40 ka. Cumulative vertical displacement since 40 ka is about 2 m, or as much as 3 m if event X? is a viable scenario.

C. Chupaderos Canyon Trench 2

For this section on the Chupaderos Canyon Trench 2 (CHU-2), refer to Plate 4.

1. Stratigraphy

The stratigraphy of CHU-2 was divided into four units, two of which are subdivisions of the Tshirege Member of the Bandelier Tuff. The oldest unit exposed in the trench was the Tshirege Member's basal fallout deposit, the Tsankawi Pumice (Qbt). About 1.5 m of the Tsankawi was exposed in CHU-2, which included two fining upwards sequences separated by a pair of ash layers (these ash layers were grouped as one on the logs). Conformably overlying the Tsankawi fallout is a white, fine-grained ignimbrite (Qbt1). Both the ash layers within the Tsankawi and the Qbt-Qbt1 contact have a strike and dip of N45E, 20NW. Thus, the Bandelier Tuff units are separated from the flat-lying units above by an angular unconformity. The angular unconformity is also a strath surface that has a strike and dip of N28W, 28NE. Above the angular unconformity is a fluvial sequence consisting of a discontinuous basal unit of coarse sands and gravels (Qa2-1) overlain by up to about 2 m of fine to very fine sands (Qa2-2). Based on available age constraints, the fluvial sequence is probably late Pleistocene to perhaps early Holocene in age, and the top of the sequence forms the modern ground surface. The upper 30 to 50 cm of Qa2-2 is extensively bioturbated in the active root zone, which made it difficult, if not impossible, to map the upwards terminations of most structures.

2. Structure

The Bandelier Tuff units exhibit a strike and dip of N45E, 20NW, whereas the late-Pleistocene to early Holocene fluvial sequence is essentially flat-lying. Although it is possible for pyroclastic fallout to accumulate on slopes of 20 degrees, it is unlikely

that the ash flows could be deposited on such slopes. Ponding of the ash flows against such slopes is a possibility that cannot be completely discounted, but the similarity of the strike of the attitude of the Bandelier Tuff units with the strikes of many local faults (Figure 12a) leads us to favor structural tilting as the cause for the dip of the Bandelier Tuff units.

The distribution of fault trends in CHU-2 is fairly uniform, but most fault strikes fall into two broad groups: N5-30W and N20-70E (Figure 12b). These two groups are mostly distinct from the dominant fault trends in CHU-1 of N5W to N25E and CHU-3 of N4W to N38E (Figures 10, 13, and 14). A couple of faults, or portions of zones, fall outside of these two groups with nearly east-west strikes. The larger variation of CHU-2 fault trends may imply there have been significant deviations in the stress field in the vicinity of CHU-2. These deviations may be related to a right stepover or bend in the trace of the Guaje Mountain fault as it passes

through Chupaderos Canyon (Figure 3).

Many of the faults exposed in CHU-2 have gouge and well-developed foliations that would appear to be inconsistent with the small discernable displacements. Most fault ruptures penetrate the late-Pleistocene–early Holocene fluvial sequence, but associated displacements are commonly equivocal. Zones 2-B, 2-C, 2-D, and 2-E form a tightly clustered group of anastomosing faults and fractures. Most of these structures are high angle and have strikes N65-80W or N50-71E, strongly oblique to the general trend of the Guaje Mountain fault zone (Figures 2, 3, and 14). Fault 2-B displaces an ash layer within the Tsankawi fallout deposit about 1 cm down to the south, but no comparable displacement could be found on the northeast wall of the trench. Above fault 2-B, associated fractures penetrate the fluvial sequence at least as high as the zone of active root bioturbation, but no vertical displacements of the Qbt1–Qal2-1 or the Qal2-1–Qal2-2 contacts could be found. Relations for

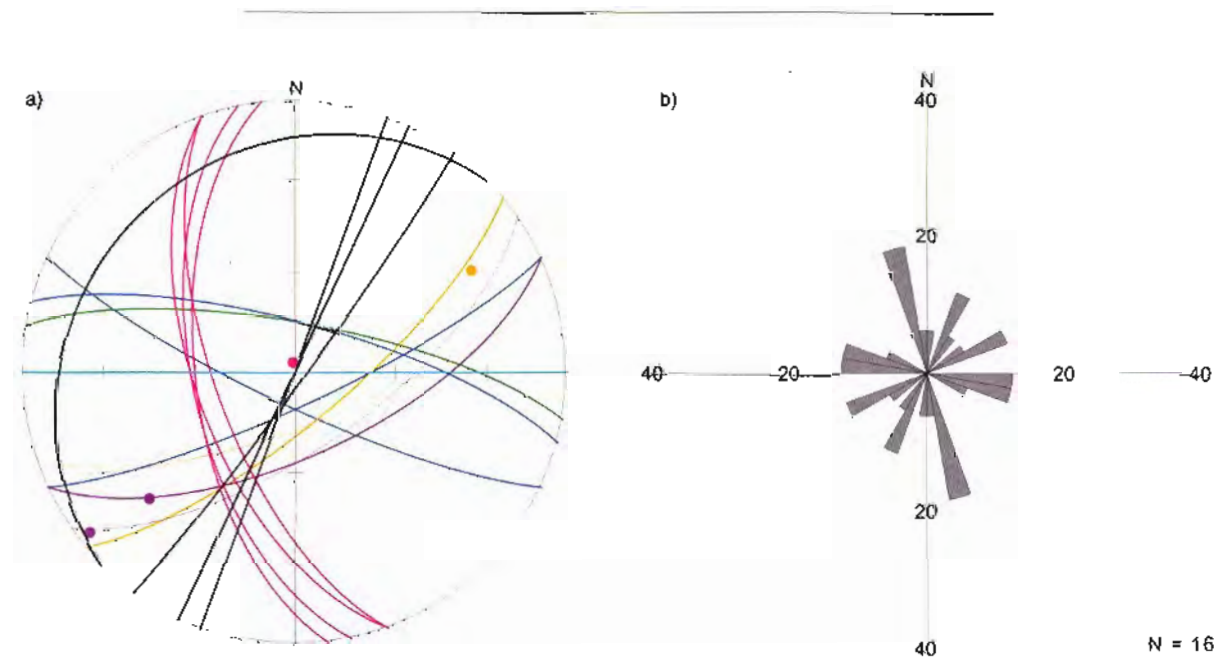


Figure 12. Structural Data from Trench CHU-2. a) Lower-hemisphere stereonet (Schmidt) plots of structures in trench CHU-2 showing planes of faults (solid lines) and foliations (thin, dashed lines). Lineations (dots) are plotted as trend and plunge. Color coding is as follows: 2-B = green; 2-C = blue; 2-D = orange; 2-E = purple; and 2-F = pink; 2-I, 2-K, and 2-L are black high-angle planes; strike and dip of Bandelier Tuff units is the black plane with shallow dip. b) Rose diagram of fault strikes in CHU-2 showing no dominant trend.

fault 2-C are quite similar to 2-B, except that before the upward continuations of associated ruptures are lost in the active root zone, there is a strong fault-parallel shear fabric. Fault 2-D shows no clear displacement of contacts, but it has a zone of foliated gouge about 5 to 7 cm wide. The foliation is fault-parallel and slickensides plunge at 26 degrees to the northeast. The upwards terminations of ruptures associated with fault 2-D are obscured by bioturbation but, similar to 2-C, exhibit strong fault-parallel shear fabric in the lower part of unit Qal2-2. Fault 2-E displaces the Qbt1-Qbt2 contact about 28 cm down to the southeast and exhibits a foliated zone of gouge up to about 8 cm wide. Relations of the upward terminations of ruptures of fault 2-E are similar to those of 2-C and 2-D; no clear displacements of contacts are evident, but the ruptures display a shear fabric in unit Qal2-2 before they are obscured in the active root zone.

In contrast to the faults previously discussed, fault 2-F strikes north-northwest. Fault 2-F appears to terminate against faults 2-E and possibly 2-H. Fault 2-F has zones of cataclasite and gouge. Slickensides within the gouge plunge steeply at 87 degrees to the north. These relations, in spite of a lack of stratigraphic markers, imply that this short fault has experienced repeated movements, the most recent of which has been dominantly dip slip. Between fault 2-F and fracture zone 2-G, there is a 20- to 45-cm down-to-the-north step on the strath surface (see Footnote 10 on the log of Plate 4). On both walls of the trench, this step on the strath surface occurred behind shores. Because the attitude of fault 2-F with respect to the trend of the trench created large slabs of tuff that would have spalled into the trench without the shores holding them back, we were unable to safely remove the shores to determine the exact nature of the step on the strath. If it is a fault, its strike is roughly east-west, and it must be vertical.

Fault 2-H is a high-angle structure that appears to truncate all other logged structures from the southeast. Its strike is north-south and the fault exhibits

cataclastic breccia on the northeast wall of the trench. The fault appears to displace the strath surface about 5 cm down to the east but not an overlying lens of coarse sand of unit Qal2-1. Similar to other CHU-2 faults previously discussed, rupture of fault 2-H persists upwards to within about 50 cm of the modern ground surface.

Faults 2-K and 2-L strike about N25E and are vertical. They displace the strath surface and the basal Qbt1-Qal2-1 contact about 5 to 10 cm, forming a small graben. On the southwest (logged) wall of the trench, the faults apparently do not displace the upper contact of Qal2-1 with Qal2-2, but on the northeast wall of the trench, the faults merge, bend to N65E, and displace the Qal2-1-Qal2-2 contact about 2 cm down to the south. About 12 cm above the contact, persistent shear fabric is evident along the rupture as elongate pebbles rotated to vertical in Qal2-2.

3. Paleoseismic Implications

The most significant paleoseismic information from trench CHU-2 is the penetration of ruptures, above small faults, into sediments that are late Pleistocene and possibly Holocene in age. Numerical age constraints from CHU-2 are few and broad but indicate that the most-recent deformation occurred since 12.5 cal ka. Fault displacements are so small, and the unconformity at the Bandelier Tuff-Qal2-1 contact is so significant, that we have not attempted a paleoseismic reconstruction as we have for trench CHU-1.

D. Chupaderos Canyon Trench 3

For this section on Chupaderos Canyon Trench 3 (CHU-3), refer to Plate 5.

1. Stratigraphy

The stratigraphy of CHU-3 is very similar to that of CHU-2. The oldest units exposed are ignimbrites of the Bandelier Tuff (Qbt1 and Qbt2). In the eastern portion of the trench, the tuff is the same fine-grained, nonwelded unit as seen in CHU-1 and CHU-2, but the underlying Tsankawi fallout

deposit is not exposed. In the western end of the trench, the ignimbrite (Qbt2) is a vapor-phase altered nonwelded tuff, which, based on exposures in surrounding outcrops, is the next unit above Qbt1 in the local Bandelier Tuff sequence. No reliable bedding indicators were found, so the attitude of the tuff is uncertain. It is possible, however, that the tuff in CHU-3 has a dip similar to that in CHU-2, which would explain two different Bandelier Tuff units at the same elevation at opposite ends of the trench.

A significant unconformity separates the tuff from the overlying fluvial sequence. Units within the fluvial sequence are flat-lying, and dates on detrital charcoal fragments from the upper part of the sequence range from 14 to 10.3 cal ka. At 32H, a stump hole with abundant charcoal dated at 3.4 cal ka provides a younger limiting age on the upper 1.5 m of the fluvial sequence. OSL dates are in agreement with the ^{14}C results with dates of 9.5 and 11.7 ka in the upper part of the fluvial sequence and 30.2 ka in the lower portion. PDI age estimates for the surface soil are consistent but may be too young; however, PDI age estimates for a buried soil appear to be in agreement with the OSL age estimate. Thus, the fluvial sequence in CHU-3 is late Pleistocene to Holocene in age. The base of the fluvial package overlying Qbt1 in the eastern half of the trench consists mainly of two coarse sand and gravel units (Qal3-1a and Qal3-2). Qal3-2 is unconsolidated, whereas Qal3-1a is consolidated and clay rich, implying a significant difference in ages as also is indicated by a soil boundary at their contact. The base of the fluvial sequence is not exposed between 30H and 40H where the sequence is greater than 4 m thick. The fluvial sequence is dominated by silty, fine-grained sands with lenticular pods of coarse sand (Qal3-3).

2. Structure

The eastern end of CHU-3 was about 10 m west of the estimated position of the main trace of the Guaje Mountain fault. The main trace was not excavated in this trench because of permit restric-

tions and the fact that extensive stripping of the alluvial section was evident. Instead, CHU-3 exposed a zone of hanging-wall deformation. Faults, in fact, were restricted to the eastern 25 m of the trench, making the entire zone of faulting about 35 m wide. This width is remarkably similar to the width of the fault zone in Cabra Canyon.

The strikes of faults in CHU-3 are dominantly north-northeast and range from N4W to N38E (Figure 13). The orientations of CHU-3 faults are very similar to those in CHU-1 and, with the notable exception of three faults (2-I, 2-K, and 2-L) at the northwest end of CHU-2, quite dissimilar from those in CHU-2 (Figures 6, 7, and 14). It is possible that these three CHU-2 faults are the same as some of the CHU-3 faults, but we have not attempted correlations.

Fault 3-A has an attitude of N5E, 62NW, and exhibits a shear fabric in unit Qbt1 that is slightly oblique to the fault. Shears and fractures of 3-A penetrate Qal3-1a, Qal3-2, and most of Qal3-3, but contacts are not appreciably displaced. On the north wall of the trench (not logged), the fault forms a 30-cm wide graben, which appears to be filled with Qal3-1a, in the tuff (Qbt1). Although elongate rocks in Qal3-1a are oriented parallel to the shear fabric, displaced contacts above Qbt1 are equivocal.

Faults 3-B and 3-C both exhibit a well-defined foliation, but do not appear to break units above the Qbt1 contact. Slickensides in fault 3-C plunge 15 degrees towards S19W. Fault 3-D does displace the Qbt1-Qal3-1a contact about 5 cm down to the east, but the faulting does not break the top of unit Qal3-1a. Fault 3-D displays a shear foliation nearly parallel to the fault and horizontal slickensides.

Fault 3-E has an attitude of N25-38E, 71SE, and is antithetic to the main trace of the Guaje Mountain fault. The fault displays gouge and cataclastic breccia 5 to 30 cm wide. Foliation in the gouge is fault-parallel to slightly oblique, and slickensides

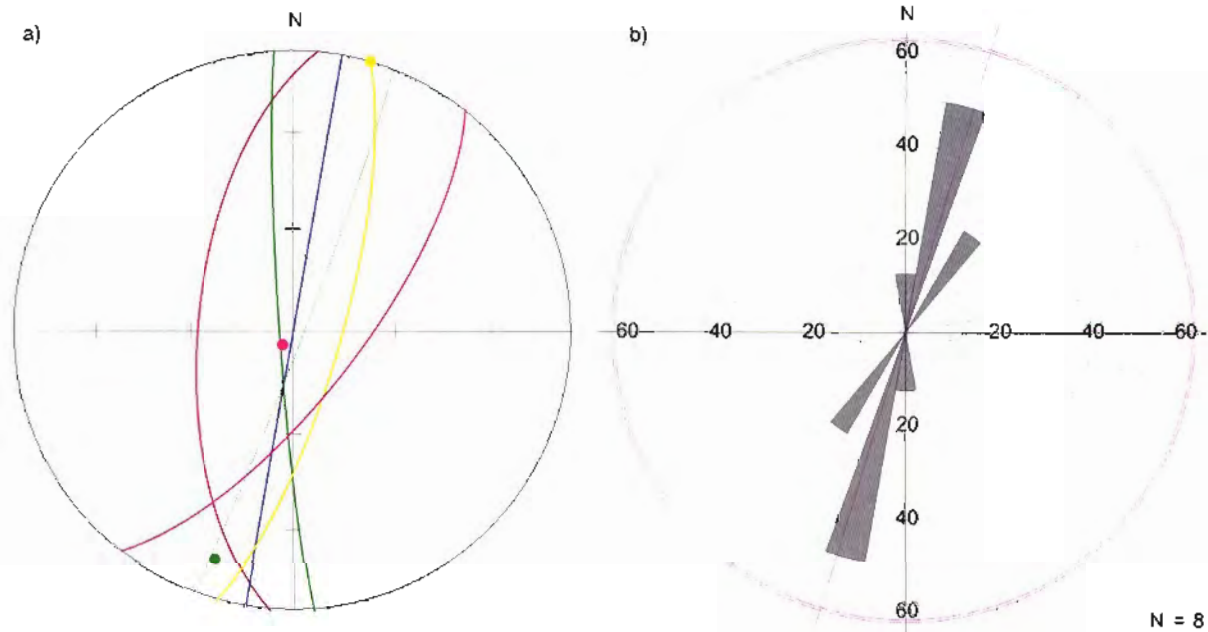


Figure 13. Structural Data from Trench CHU-3. a) Lower-hemisphere stereonet (Schmidt) plots of structures in trench CHU-3 showing planes of faults (solid lines) and foliations (thin, dashed lines). Lineations (dots) are plotted as trend and plunge. Color coding is as follows: 3-A = red; 3-B = blue; 3-C = green; 3-D = yellow; and 3-E = pink. b) Rose diagram of fault strikes in CHU-3 showing a dominant trend of N10E to N20E.

plunge at 85 degrees to S38W. The fault displaces the Qbt1–Qal3-1a contact and an oxidized zone in the tuff about 40 cm down to the east. The Qal3-1a–Qal3-2 contact appears to be displaced about 50 cm down to the east. Fault 3-E fans upwards through unit Qal3-2, shattering a boulder of Bandelier Tuff and forming a small graben about 75 cm wide. Ruptures continue upwards through Qal3-3 as several thin sharp breaks that displace a large sand lens 10 to 20 cm down to the east. Above the sand lens, the ruptures are obscured by bioturbation.

3. Paleoseismic Implications

Most faults in CHU-3 provide evidence of relatively small post-Tshirege Member displacements of unknown number and poorly constrained timing. Young ruptures with equivocal displacements project above these faults into units of early Holocene age. Fault 3-E, however, provides evidence for at least two ruptures since late-Pleistocene time with increasing displacements on

progressively older units. The older of these two events followed deposition of unit Qal3-2, displacing Qal3-2 and older units about 30 cm down to the east. Age constraints are broad, but this event occurred in the late Pleistocene, and it is probably the same as event X? or event Y discussed for CHU-1. Erosion of the soft material of unit Qal3-2 on the upthrown block followed this event with the large boulder of tuff armouring the downthrown block, creating a small obsequent scarp over which the basal parts of Qal3-3 were deposited. The younger event breaks, with small down-to-the-east displacements, the upper portion of unit Qal3-3, which age constraints indicate is younger than 10 ka but older than 3.4 cal ka. Thus, all constraints on timing relations are consistent with the youngest event in CHU-3, event Z in CHU-1, and the MRE of Cabra Canyon as being the same paleoearthquake.

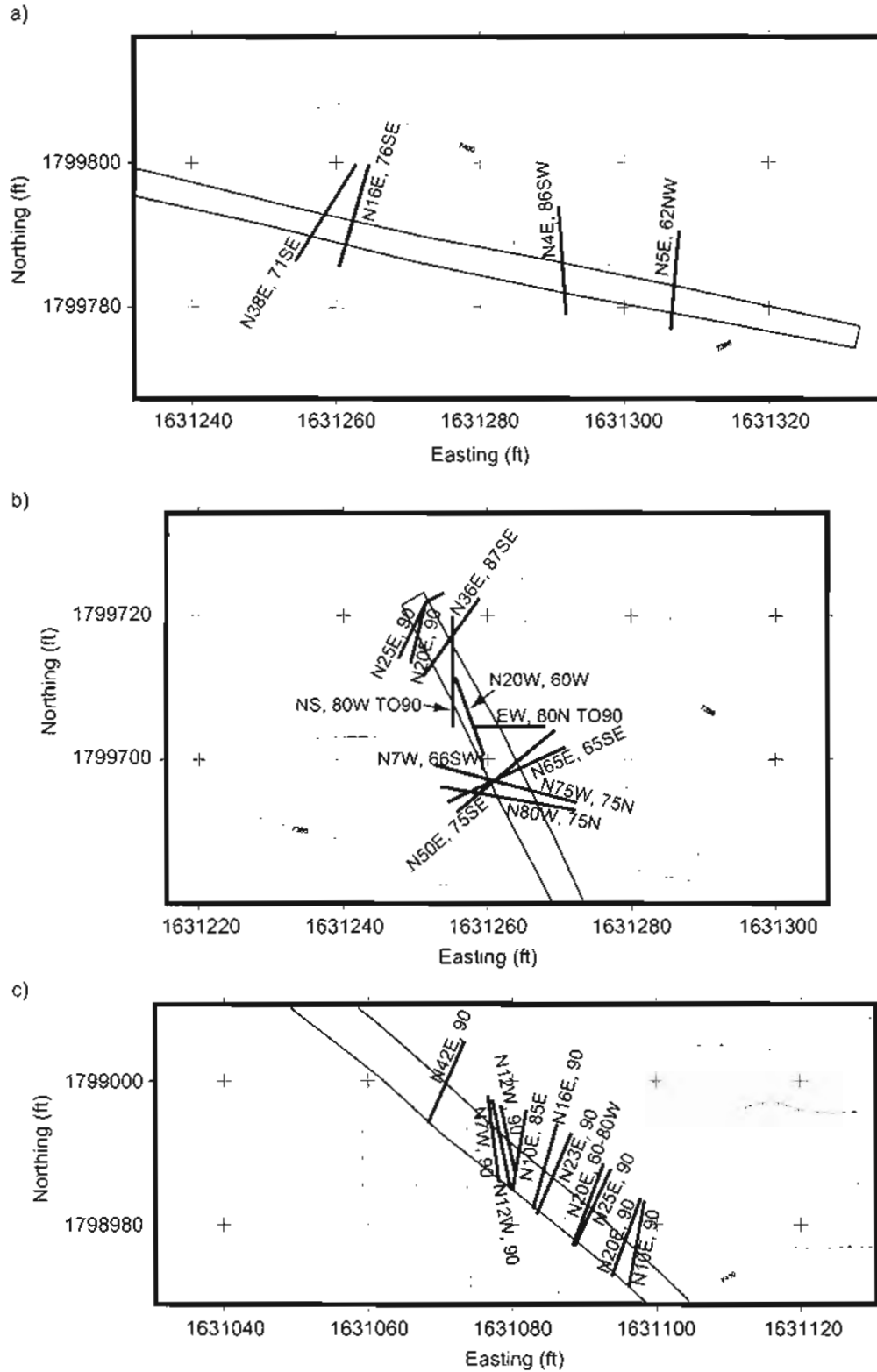


Figure 14. Detailed Maps of the Chupaderos Canyon Trenches Showing Strikes of Faults. The trenches are a) CHU-3, b) CHU-2, and c) CHU-1. Note that although maps are at the same scale, they are not spatially aligned. Numbers around borders are State Plane coordinates.

V. DISCUSSION AND CONCLUSIONS

All trenches that we have excavated along the Guaje Mountain fault provide direct or compelling evidence for a surface-rupturing paleoearthquake in the Holocene. The youngest paleoearthquake event in the Cabra Canyon trench was between 4 and 6.5 ka, in CHU-3 less than 10 ka, in CHU-2 less than 12.5 cal ka, and in CHU-1 probably Holocene. Furthermore, unless the Guaje Mountain fault has experienced more than one surface-rupturing event in the Holocene, the age constraints for the youngest event from each trench allow the events to be the same. Relations in CHU-1 strongly argue that there has only been one rupturing event since about 32 ka, with most of the late-Pleistocene fluvial sequence displaced the same amount in the youngest event, about 1.5 m down to the west. Additionally, relations in the Cabra Canyon trench indicate the youngest event probably displaced Colluvium II at least 2 m down to the west. The simplest interpretation is that the Guaje Mountain fault has had only one Holocene surface-rupturing event and that the youngest events observed in each trench are the same. Thus, we conclude the MRE for the Guaje Mountain fault occurred in the mid-Holocene, around 4 to 6.5 ka.

Both trenches CHU-1 and CHU-3 provide evidence for at least one surface-rupturing paleoearthquake in the late Pleistocene, which, based on relations from CHU-1, occurred around 39 ka. We believe that these relations provide constraints on the penultimate event for the Guaje Mountain fault. Results from trench CHU-1 also could indicate another surface-rupturing earthquake that happened at about 40 ka, but the event X? scenario is equivocal, and such an event has yet to be recognized from other trenches.

Trench data suggest or indicate that greater than 2 m and about 1.5 m of vertical displacement occurred during the MRE on the Guaje Mountain fault at Cabra Canyon and Chupaderos Canyon, respectively. Data from CHU-1 indicate a cumulative vertical displacement of 2 to 3 m in two or three

events since about 40 ka. Wong et al. (1995; summarized in Olig et al. 1996) infer three paleoseismic events with a maximum of 4 m of cumulative displacement since 150 to 300 ka, based on studies in Reudija Canyon, near the Sportsmen's Club, of a flight of stream terraces that flank both sides of the Guaje Mountain fault. With more recent age constraints on some of these terraces provided by Phillips et al. (1998), the oldest of these events occurred > 144 ka but less than 300 ka. Since that oldest event, the terrace data appear to only allow an additional 2.5 m of vertical displacement in the vicinity of the Sportsmen's Club. Assuming little along-strike variation in displacement, Wong et al. (1995) accounted for 2 m of terrace displacement with the MRE based on results of the Cabra Canyon trench, and they inferred a penultimate event with small vertical displacement sometime between the Holocene and less than 144 ka to account for the remaining 0.5 m of terrace displacement. These inferences are remarkably consistent with our trenching results. The Guaje Mountain fault MRE may well account for much of the terrace displacement, but the penultimate event at about 39 ka seen in the Chupaderos trenches caused only small vertical displacements in both Chupaderos Canyon and around the Sportsmen's Club locale. Combining available data, therefore, we recognize the following paleoseismic events on the Guaje Mountain fault: 1) 4 to 6.5 ka with 1.5 to > 2 m vertical displacement; 2) around 39 ka, probably dominantly a strike-slip event with only small vertical displacement of about 50 cm; 3) perhaps about 40 ka with 1 m of vertical displacement at Chupaderos Canyon (event X?); and 4) between 144 and 300 ka with 1.5 to 2 m of vertical displacement near the Sportsmen's Club.

VI. ACKNOWLEDGEMENTS

We are particularly grateful for the support and feedback we get from the Seismic Hazards Program manager Larry Goen. Also giving support from the Office of Infrastructure, Facilities, and Construction have been Jim Holt, Carolyn Zerkle, and

Scott Gibbs. We thank Laurel Goodwin and Jennifer Wilson for providing expert assistance with interpretations of structural textures and fabrics. Craig DePolo gave an insightful field review of the Chupaderos Canyon trenches. Danielle Katcher digitized the ancient logs from the Cabra Canyon trench. We are grateful to the U.S. Forest Service, the land manager in Chupaderos Canyon. In particular, Robert Remillard, Greg Kuyumjian, Annie Apodaca, and John Bruin of the U.S.F.S. were very helpful with permitting and oversight of the field project and with site restoration. Mike Hertrich and Buschman Construction provided excavation and shoring of the Chupaderos Canyon trenches. Mary Miller, Vangie Trujillo, and Jesse Castañon handled contracting. Brad Vicerra and Ellen McGee provided archeological support, surveys, and enlightenment. Ryan Channel was a helpful field assistant. We thank Jim Aldrich for a thorough review.

VII. REFERENCES

- Aitken, M. J. 1998. *An Introduction to Optical Dating*. New York, NY: Oxford University Press.
- Aldrich, M. J., and Dethier, D. P. 1990. Stratigraphic and tectonic evolution of the northern Espanola basin, Rio Grande rift, New Mexico. *Geological Society of America Bulletin* 102: 1695–1705.
- Banerjee, D., Murray, A. S., Botter-Jensen, L., and Lang, A. 2001. Equivalent dose estimation using a single aliquot of polymineral fine grains. *Radiation Measurements* 33: 73–94.
- Beers, R. S., Rogers, D. B., and Turney, W. R. 2000. Surface water, groundwater, and sediments. In *Environmental Surveillance at Los Alamos during 1999*, pp. 161–306. Los Alamos National Laboratory report LA-13775-ENV.
- Berger, G. W. 1999. Optical dating of sediments from Pajarito Fault trenches at Los Alamos, New Mexico. Unpublished report for Los Alamos National Laboratory. Reno, Nevada: Desert Research Institute.
- Broxton, D. E., and Reneau, S. L. 1995. Stratigraphic nomenclature of the Bandelier Tuff for the Environmental Restoration Project at Los Alamos National Laboratory. Los Alamos National Laboratory report LA-13010-MS, 21 pp.
- Broxton, D. E., Heiken, G. H., Chipera, S. J., and Byers, F. M. 1995a. Stratigraphy, petrography, and mineralogy of the Bandelier Tuff and Cerro Toledo deposits. In *Earth Science Investigations for Environmental Restoration—Los Alamos National Laboratory Technical Area 2I*, Broxton, D. E., and Eller, P. G., editors, pp. 33–63. Los Alamos National Laboratory report LA-12934-MS.
- Broxton, D. E., Vaniman, D., Byers, F. M., Chipera, S. J., Kluk, E. C., and Warren, R. G. 1995b. Stratigraphy, mineralogy, and chemistry of bedrock tuffs at Pajarito Mesa. In *Geological Site Characterization for the Proposed Mixed Waste Disposal Facility—Los Alamos National Laboratory*, Reneau, S. L., and Raymond, R., editors, pp. 5–30. Los Alamos National Laboratory report LA-13089-MS.
- Carter, K. E., and Gardner, J. N. 1995. Quaternary fault kinematics in the northwestern Espanola basin, Rio Grande rift, New Mexico. *New Mexico Geological Society Guidebook* 46: 97–103.
- Foreman, S. L., Nelson, A. R., and McCalpin, J. P. 1991. Thermoluminescence dating of fault-scarp-derived colluvium: Deciphering the timing of paleoearthquakes on the Weber segment of the Wasatch fault zone, north central Utah. *Journal of Geophysical Research* 96: 595–605.
- Gardner, J. N., and Goff, F. 1984. Potassium-argon dates from the Jemez volcanic field: Implications for tectonic activity in the north-central Rio Grande rift. *New Mexico Geological Society Guidebook* 35: 75–81.

- Gardner, J. N., and House, L. 1987. Seismic hazards investigations at Los Alamos National Laboratory, 1984 to 1985. Los Alamos National Laboratory report LA-11072-MS, 76 pp.
- Gardner, J. N., and House, L. S. 1994. Surprisingly high intensities from two small earthquakes, northern Rio Grande rift, New Mexico. *EOS, Transactions of the American Geophysical Union* 75 (16): 128.
- Gardner, J. N., Goff, F., Garcia, S., and Hagan, R. C. 1986. Stratigraphic relations and lithologic variations in the Jemez volcanic field, New Mexico. *Journal of Geophysical Research* 91: 1763–1778.
- Gardner, J. N., Baldrige, W. S., Gribble, R., Manley, K., Tanaka, K., Geissman, J. W., Gonzalez, M., and Baron, G. 1990. Results from seismic hazards trench #1 (SHT-1), Los Alamos Seismic Hazards Investigations. Los Alamos National Laboratory unpublished report EES1-SH90-19.
- Gardner, J. N., Lavine, A., WoldeGabriel, G., Krier, D., Vaniman, D., Caporuscio, F., Lewis, C., Reneau, P., Kluk, E., and Snow, M. 1999. Structural geology of the northwestern portion of Los Alamos National Laboratory, Rio Grande rift, New Mexico: Implications for seismic surface rupture potential from TA-3 to TA-55. Los Alamos National Laboratory report LA-13589-MS, 112 pp.
- Gardner, J. N., Reneau, S. L., Lewis, C. J., Lavine, A., Krier, D. J., WoldeGabriel, G., and Guthrie, G. D. 2001. Geology of the Pajarito fault zone in the vicinity of S-site (TA-16), Los Alamos National Laboratory, Rio Grande rift, New Mexico. Los Alamos National Laboratory report LA-13831-MS, 86 pp.
- Harden, J. W. 1982. A quantitative index of soil development from field descriptions: Examples from a soil chronosequence in central California. *Geoderma* 28: 1–28.
- Harden, J. W., and Taylor, E. M. 1983. A quantitative comparison of soil development in four climatic regimes. *Quaternary Research* 20: 342–359.
- Izett, G. A., and Obradovich, J. D. 1994. $^{40}\text{Ar}/^{39}\text{Ar}$ age constraints for the Jaramillo normal subchron and the Matuyama-Brunhes geomagnetic boundary. *Journal of Geophysical Research* 99: 2925–2934.
- Kelson, K. I., Hemphill-Haley, M. A., Olig, S. S., Simpson, G. D., Gardner, J. N., Reneau, S. L., Kolbe, T. R., Forman, S. L., and Wong, I. G. 1996. Late-Pleistocene and Possibly Holocene Displacement along the Rendija Canyon fault, Los Alamos County, New Mexico. *New Mexico Geological Society Guidebook* 47: 153–160.
- Kolbe, T., Sawyer, J., Gorton, A., Olig, S., Simpson, D., Fenton, C., Reneau, S., Carney, J., Bott, J., and Wong, I. 1994. Evaluation of the potential for surface faulting at the proposed Mixed Waste Disposal Facility, TA-67. Unpublished consulting report prepared for Los Alamos National Laboratory by Woodward-Clyde Federal Services, Oakland, CA, 3 volumes.
- Kolbe, T., Sawyer, J., Springer, J., Olig, S., Reneau, S., Hemphill-Haley, M., and Wong, I. 1995. Evaluation of the potential for surface faulting at TA-63. Unpublished consulting report prepared for Los Alamos National Laboratory by Woodward-Clyde Federal Services, Oakland, CA.
- Lamothe, M., Duller, G. A. T., Huot, S., and Wintle, A. G. 2001. Measuring a laboratory radiation dose in feldspar using SAR. *The First North American Luminescence Dating Workshop Abstracts*. Tulsa, OK.
- Lawson, C. L., and Hanson, R. J. 1974. *Solving Least Squares Problems*. Upper Saddle River, NJ: Prentice-Hall.
- Lepper, K. 2001. Development of an objective dose distribution analysis method for OSL dating and pilot studies for planetary applications. Ph.D.

- thesis, Oklahoma State University.
- Lepper, K., Agersnap-Larsen, N., McKeever, S. W. S. 2000. Equivalent dose distribution analysis of Holocene eolian and fluvial quartz sands from Central Oklahoma. *Radiation Measurements* 32: 603–608.
- Lepper, K., Wilson, C., Gardner, J., Reneau, S., and Lavine, A. 2003. Comparison of SAR techniques for luminescence dating of sediments derived from volcanic tuff. *Quaternary Science Reviews* 22: 1131–1138.
- Lewis, C. J., Lavine, A., Reneau, S. L., Gardner, J. N., Channell, R., and Criswell, C. W. 2002. Geology of the western part of Los Alamos National Laboratory (TA-3 to TA-16), Rio Grande rift, New Mexico. Los Alamos National Laboratory report LA-13960-MS, 98 pp.
- McCalpin, J. P., editor. 1996. *Paleoseismology*. San Diego, CA: Academic Press, 588 pp.
- McCalpin, J. P. 1998. Late Quaternary faulting on the Pajarito fault, west of Los Alamos National Laboratory, north-central New Mexico: Results from the seven-trench transect excavated in summer of 1997. Unpublished consulting report prepared for Los Alamos National Laboratory by GEO-HAZ Consulting Inc., Estes Park, CO.
- McCalpin, J. P. 1999. Late Quaternary faulting on the Pajarito Fault, west of Los Alamos National Laboratory, north-central New Mexico: Results from seven trenches excavated in summer of 1998. Unpublished consulting report prepared for Los Alamos National Laboratory by GEO-HAZ Consulting, Inc., Estes Park, CO.
- McCalpin, J. P. 2000. Late Quaternary faulting on the Pajarito fault, west of Los Alamos National Laboratory, north-central New Mexico: Summary chronology of Quaternary faulting events. Unpublished report. Estes Park, CO: GEO-HAZ Consulting, Inc.
- McCalpin, J. P., Zuchiewicz, W., and Jones, L. C. A. 1993. Sedimentology of fault-scarp-derived colluvium from the 1983 Borah Peak rupture, central Idaho. *Journal of Sedimentary Petrology* 63: 120–130.
- McDonald, E. V. 1999. LANL seismic hazard trench investigations: Soil stratigraphy and pedologic age estimates for Late Quaternary faulting on the Pajarito fault, west of Los Alamos National Laboratory: Results from 1997 and 1998 trench excavations. Unpublished report submitted to the Seismic Hazards Program, LANL, and GEO-HAZ Consulting, Inc., Estes Park, CO.
- McDonald, E. V., Reneau, S. L., and Gardner, J. N. 1996. Soil-forming processes on the Pajarito Plateau: Investigation of a soil chronosequence in Rendija Canyon. *New Mexico Geological Society Guidebook* 47: 367–374.
- Murray, A. S., and Wintle, A. G. 2000. Luminescence dating of quartz using an improved single-aliquot regenerative-dose protocol. *Radiation Measurements* 32: 57–73.
- Nash, D. B. 1986. Morphologic dating and modeling of degradation of fault scarps. In *Active Tectonics—Studies in Geophysics*, pp. 181–194. Washington, D. C.: National Academy Press.
- Nelson, A. R. 1992. Lithofacies analysis of colluvial sediments—an aid in interpreting the recent history of Quaternary normal faults in the Basin and Range province, western U.S. *Journal of Sedimentary Petrology* 62, 607–621.
- Olig, S., Kelson, K. I., Gardner, J. N., Reneau, S. L., and Hemphill-Haley, M. 1996. Earthquake potential of the Pajarito fault system, New Mexico. *New Mexico Geological Society Guidebook* 47: 143–151.
- Phillips, W. M., McDonald, E. V., Reneau, S. L., and Poths, J. 1998. Dating soils and alluvium with cosmogenic ^{21}Ne depth profiles: Case studies from the Pajarito Plateau, New Mexico, USA. *Earth and*

Planetary Science Letters 160: 209–223.

Prescott, J. R., and Hutton, J. T. 1988. Cosmic ray and gamma ray dosimetry for TL and ESR. *Nuclear Tracks and Radiation Measurement* 14: 223–227.

Reneau, S. L., and McDonald, E. V. 1996. Landscape history and processes on the Pajarito Plateau, northern New Mexico: Rocky Mountain Cell, Friends of the Pleistocene Guidebook. Los Alamos National Laboratory report LA-UR-96-3035, 195 pp.

Reneau, S. L., Gardner, J. N., and Forman, S. L. 1996. New evidence for the age of the youngest eruptions in the Valles Caldera, New Mexico. *Geology* 24: 7–10.

Reneau, S. L., Gardner, J. N., Lavine, A., McDonald, E. V., Lewis, C., Katzman, D., WoldeGabriel, G., Krier, D., Bergfeld, D., and Heikoop, J. 2002. Paleoseismic investigation of trench EOC-2, Pajarito fault zone, Los Alamos National Laboratory, New Mexico. Los Alamos National Laboratory report LA-13939-MS, 65 pp.

Smith, R. L., Bailey, R. A., and Ross, C. S. 1970. Geologic map of the Jemez Mountains, New Mexico. U.S. Geological Survey miscellaneous investigations map I-571.

Soil Survey Staff. 1981. Examination and description of soils in the field. In *Soil Survey Manual (USDA-ARS)*. Washington, D.C.: U.S. Government Printing Office.

Stuiver, M., Reimer, P. J., Bard, E., Beck, J. W., Burr, G. S., Hughen, K. A., Kromer, B., McCormac, F. G., Van der Plicht, J., and Spurk, M. 1998. INT-CAL98 radiocarbon age calibration 24,000–0 cal BP. *Radiocarbon* 40: 1041–1083.

Taylor, E. M. 1988. Instructions for the soil development index template—Lotus 1-2-3. U.S. Geological Survey open-file report 233A.

Tikhonov, A. N., and Arsenin, V. Y. 1977. *Solution of Ill-posed Problems*. New York, NY: Wiley.

Tikhonov, A. N., Goncharsky, A. V., Stepanov, V. V., and Yagola, A. G. 1995. *Numerical Methods for Ill-posed Problems*. Kluwer Academic Publishers.

Toyoda, S., Goff, F., Ikeda, S. and Ikeya, M. 1995. ESR dating of quartz phenocrysts in the El Cajete and Battleship Rock members of Valles Rhyolite, Valles Caldera, New Mexico. *Journal of Volcanology and Geothermal Research* 67: 29–40.

Wohletz, K. H. 1995. Measurement and analysis of rock fractures in the Tshirege Member of the Bandelier Tuff along Los Alamos Canyon adjacent to Technical Area 21. In *Earth Science Investigations for Environmental Restoration—Los Alamos National Laboratory Technical Area 21*, Broxton, D. E., and Eller, P.G., editors. Los Alamos National Laboratory report LA-12934-MS, pp. 19–32.

Wong, I., Kelson, K., Olig, S., Kolbe, T., Hemphill-Haley, M., Bott, J., Green, R., Kanakari, H., Sawyer, J., Silva, W., Stark, C., Haraden, C., Fenton, C., Unruh, J., Gardner, J., Reneau, S., and House, L. 1995. Seismic hazards evaluation of the Los Alamos National Laboratory. Unpublished consulting report prepared for Los Alamos National Laboratory by Woodward-Clyde Federal Services, Oakland, CA, 3 volumes.

Wong, I., Kelson, K., Olig, S., Bott, J., Green, R., Kolbe, T., Hemphill-Haley, M., Gardner, J., Reneau, S., and Silva, W. 1996. Earthquake potential and ground shaking hazard at the Los Alamos National Laboratory, New Mexico. *New Mexico Geological Society Guidebook* 47: 135–142.

APPENDIX A. GEOCHRONOLOGY

A-1. Radiocarbon Geochronology

Samples of one or more discrete charcoal fragments were hand picked from units in all of the trenches for possible radiocarbon (^{14}C) dating. Because roots, burned in situ, and bioturbation provide avenues for introduction of young charcoal into older deposits, areas with discolored or disrupted soil were avoided for sampling to minimize these possibilities. Recycling of old charcoal into younger deposits is a possibility that cannot be evaluated in the field, and contamination of samples with young (modern) carbon can occur. Thus, the ^{14}C dates need to be evaluated in the geologic context of the samples and in light of results of independent dating methods (see discussions in text).

Before submission to the analytical laboratory, each sample was air dried, examined under a binocular microscope, and cleaned to remove dirt and roots. All samples were analyzed by Beta Analytic, Inc. Sample pretreatment by Beta Analytic included a standard hot acid (HCl) bath to remove carbonates, followed by an NaOH treatment to remove secondary organic acids and a second HCl treatment. Samples from the Cabra Canyon trench were analyzed in 1989. Consequently, most analyses, with three exceptions (Table A-1), of Cabra Canyon samples were done by standard or extended beta counting with no analysis or correction for $\delta^{13}\text{C}$. Beta Analytic informs us (personal communication, 2003) that, for these samples, this correction makes a difference of only a couple of decades in the date, which is negligible for our purposes. The three exceptions from Cabra Canyon, as well as all samples from Chupaderos Canyon, were analyzed by accelerator mass spectrometry (AMS) with corrections for $\delta^{13}\text{C}$ and dates from analysis reported as conventional radiocarbon years (Table A-1). Carbon-14 dates from analysis were converted to calibrated (cal) ages to correct for temporal fluctuations in $^{14}\text{C}/^{12}\text{C}$ in the atmosphere and to allow direct comparison with age estimates obtained by other methods. All dates were calibrated by the

methods of Stuiver et al. (1998) using the latest version (version 4.3) of their CALIB program available on-line at <http://depts.washington.edu/qil/calib/calib.html>. Results for three samples from trench CHU-1 are not calibrated because they yielded dates beyond the range of available calibration data (Table A-1). Table A-1 provides the results of successful radiocarbon analyses for samples from the Cabra Canyon and Chupaderos Canyon trenches. The values in Table A-1 under "Best Age Estimate" are determined by consideration of the sample's calibrated age and calibrated two sigma uncertainty with respect to stratigraphic constraints and other dated samples. Thus, "4.2 cal ka" refers to a specific date, whereas, in this example, "4.2 ka" would refer to an approximate time based on stratigraphic context and other constraining dates.

A-2. Optically Stimulated Luminescence (OSL) Geochronology

The sediments of the Pajarito Plateau and its narrow, sharply incised canyon systems are challenging to date with luminescence techniques because they are derived predominantly from volcanic tuffs, they have been transported for relatively short distances, and they are likely to have been deposited from highly turbid water. X-ray diffraction analyses of numerous samples representing all units of the Bandelier Tuff indicate that the dominant mineralogies are alkali feldspars and quartz polymorphs (Broxton et al. 1995a, 1995b). However, the total crystalline quartz content in the tuff samples is low, ranging from 3 to 26% with 10 to 15% being most common. Many tuff samples also have a very high glass content ranging from 32 to 88%. Sediments derived from this source material are characterized by low crystalline quartz content and a fine sand fraction that contains a significant proportion of glass shards. Due to the friable nature of the parent material, sand-sized quartz crystals may also be transported within tuff clasts, shielding them from solar exposure. Typical suspended sed-

Table A-1. Radiocarbon Analyses*

Sample Number	Laboratory Number	¹⁴ C Age [†] (yr BP)	Calibrated Age [‡] (cal yr BP)	Calibrated 2σ [‡] (cal yr BP)	δ ¹³ C (‰)	Best Age Estimate [#] (cal ka)
Cabra Canyon Trench						
SHT1-10a	Beta 26084 (ETH 4139)	2840 ± 75	2950	2780–3210	NR	3.0
SHT1-10b	Beta 26085	2970 ± 100	3080–3160	2850–3380	NA	3.0
SHT1-15b	Beta 26086	3800 ± 100	4150–4220	3890–4500	NA	4.2
SHT1-18	Beta 26087	300 ± 70	310	0–510	NA	0.3
SHT1-19	Beta 26088 (ETH 4140)	4240 ± 80	4830	4530–5020	NR	4.8
SHT1-20	Beta 26089 (ETH 4160)	3495 ± 70	3730–3820	3590–3960	NR	3.8
SHT1-21	Beta 26090	3600 ± 170	3890	3470–4410	NA	3.8
SHT1-22	Beta 26091	1610 ± 160	1520	1190–1880	NA	1.5
SHT1-23	Beta 26092	5690 ± 250	6450–6470	5930–7160	NA	6.5
SHT1-26d	Beta 28720	3730 ± 90	4090	3830–4410	NA	4.2
Chupaderos Canyon Trenches						
CHU1-c2 [¥]	Beta 158056	32280 ± 330	—	—	-23.3	32.3
CHU1-c6 [¥]	Beta 158058	31450 ± 290	—	—	-26.9	31.5
CHU1-c11 [¥]	Beta 158061	39580 ± 760	—	—	-25.7	39.6
CHU2-c3	Beta 158392	10460 ± 50	12360–12610	11960–12860	-25.6	12.5
CHU3-c1	Beta 158393	11970 ± 60	13870–14050	13650–15300	-24.4	14.0
CHU3-c3	Beta 158394	9210 ± 50	10290–10400	10240–10480	-25.2	10.3
CHU3-c5	Beta 158396	3160 ± 60	3380	3210–3470	-23.0	3.4
CHU3-c6	Beta 158397	9430 ± 50	10600–10670	10510–11060	-23.0	10.7
CHU3-c8	Beta 158398	9440 ± 50	10600–10690	10510–11060	-23.3	10.7
CHU3-c10	Beta 158399	10210 ± 50	11770–11940	11640–12340	-23.1	11.9
CHU3-c11	Beta 158400	9580 ± 50	10790–11070	10690–11160	-24.4	10.9

*All analyses done by Beta Analytic, Inc. NA = not analyzed; NR = not reported.

†For Cabra Canyon Trench samples, radiocarbon age is measured by standard beta counting, except for samples SHT1-10a, SHT1-19, and SHT1-20, which were analyzed by accelerator mass spectrometry and reported as conventional radiocarbon ages, corrected for δ¹³C. For Chupaderos Canyon Trenches samples, conventional radiocarbon age after δ¹³C correction was determined.

‡Calibrated age and calibrated 2σ uncertainty range determined by the methods of Stuiver et al. (1998); the age is reported as a range for samples with multiple intercepts of the calibration curve.

#Best age estimate as used in text and on plates (see explanation in Section A-1, "Radiocarbon Geochronology").

¥Sample with age beyond the range of available calibration data.

iment loads in modern streams within the canyons of the Pajarito Plateau range from < 1000 mg/L to > 25,000 mg/L (Beers et al. 2000). Overbank flooding events that contribute to floodplain aggradation can have sediment concentrations up to 150,000 mg/L.

Because of these challenges, the present OSL dating investigation was carried out in two phases. The first phase was an evaluation of several proposed optically stimulated luminescence single-aliquot regeneration (OSL SAR) procedures for fine-grained polymineral and quartz sand samples, including single-grain laser luminescence (SGLL), carried out on a set of four samples to determine which techniques have the greatest potential to yield accurate dates for samples collected from alluvial deposits on the Pajarito Plateau. The second phase of the investigation was an application of the most promising technique from phase one to a larger, more complete set of samples.

1. General OSL Methods

In its simplest expression, an OSL age is the total radiation dose absorbed by the mineral grains since deposition (their last exposure to sunlight), referred to as the equivalent dose (D_e), divided by the environmental radiation dose rate. Equivalent doses can be measured by a variety of experimental procedures but are generally made on fine-grained (4–11 μm) polymineral or quartz sand (90–250 μm) extracts from sediment samples.

In this project, the fine-grained polymineral sediment fraction (4–11 μm) was obtained from field samples by Stoke's settling and centrifugation following standard luminescence-dating pretreatment procedures including HCl to remove carbonates and H_2O_2 digestion of organic matter. Measurement aliquots were prepared by evaporation plating. Quartz sand separates (90–250 μm fraction) were obtained by wet sieving and aggressive etching (45 minutes in 48% HF solution with constant stirring), followed by standard HCl and Na-pyrophosphate treatments to remove precipitates and particulates. Sand grains were attached to aliquots for SAR

measurements using a nonluminescent medical adhesive. Substrates for SGLL contain regularly spaced surface indentations and do not require adhesives. It was found during the course of the project that a majority of the usable quartz grains were obtained from the 90- to 150- μm fraction, but the larger initial fraction (90–250 μm) was retained to maintain experimental consistency.

All measurements and irradiations were conducted using a Risø DA-15 automated TL/OSL reader system with single-grain attachment. The system is equipped with a 40-mCi $^{90}\text{Sr}/^{90}\text{Y}$ β source, a blue diode array (OSL; 470 ± 30 nm), an infrared laser diode assembly (infrared stimulated luminescence [IRSL]; 830 ± 10 nm), a green laser (SGLL; Nd:YVO₄; 532 nm), an EMI model 9235QA PMT, and a 48-position sample carousel. Stimulated luminescence was measured in the ultraviolet emission range (5 mm Hoya U-340) for all data sets in this report.

Equivalent doses from the tuff-derived sediments were determined using several proposed OSL SAR procedures including: IRSL and post-IR blue OSL on polymineral fine-grains (Banerjee et al. 2001), IRSL with thermoluminescence (TL) annealing between regeneration cycles on polymineral fine-grains (Lamothe et al. 2001; Lamothe, personal communication, 2001), and blue OSL on quartz fine-sand (Murray and Wintle 2000). The experimental details for each of the SAR methods used are listed in Table A-2. IRSL multi-aliquot additive dose (MAAD) procedures (Aitken 1998) were also used to determine D_e for each sample from polymineral fine-grains. The IRSL MAAD ages are useful for comparison with those from SAR methods, and they help link the current study to past luminescence dating efforts in the area (Toyoda et al. 1995; Wong et al. 1995; Kelson et al. 1996; Reneau et al. 1996; McCalpin 1998, 1999, 2000).

An SGLL procedure for quartz sand was also evaluated (Table A-2). SGLL-derived D_e data were filtered based on the following three rejection criteria: 1) grains/pits with background-subtracted natural

Table A-2. Evaluation of Data Collection Operations Used for the SAR and SGLL Procedures

Operation	Method				
	IRSL SAR*	Post-IR Blue SAR*	IRSL w/TL annealing†	Quartz OSL SAR‡	Single-grain‡
Preheat	10 s @ 200°C	10 s @ 200°C	60 s @ 260°C	10 s @ 160°C	10 s @ 240°C
Measure natural signal	IRSL 200 s @ 60°C	OSL 100 s @ 125°C	IRSL 100 s @ 125°C	OSL 50 s @ 125°C	SGLL 1 s @ 125°C
Irradiate test dose	Sample specific	Sample specific	Sample specific	Sample specific	Sample specific
Preheat	Cut heat 160°C	Cut heat 160°C	Annealing cycle TL to 500°C	10 s @ 160°C	Cut heat 160°C
Measure test dose	IRSL 200 s @ 60°C	OSL 100 s @ 125°C	Sample specific	OSL 50 s @ 125°C	SGLL 1 s @ 125°C
Irradiate regen. dose	Sample specific	Sample specific	Sample specific	Sample specific	Sample specific
Preheat	10 s @ 200°C	10 s @ 200°C	60 s @ 260°C	10 s @ 160°C	10 s @ 240°C
Measure regen. dose	IRSL 200 s @ 60°C	OSL 100 s @ 125°C	IRSL 100 s @ 125°C	OSL 50 s @ 125°C	SGLL 1 s @ 125°C
Irradiate test dose	Sample specific	Sample specific	Sample specific	Sample specific	Sample specific
Preheat	Cut heat 160°C	Cut heat 160°C	Annealing cycle TL to 500°C	10 s @ 160°C	Cut heat 160°C
Measure test dose	IRSL 200 s @ 60°C	OSL 100 s @ 125°C	Sample specific	OSL 50 s @ 125°C	SGLL 1 s @ 125°C
Irradiate check dose	Sample specific	Sample specific	Sample specific	Sample specific	Sample specific
Preheat	10 s @ 200°C	10 s @ 200°C	60 s @ 260°C	10 s @ 160°C	10 s @ 240°C
Measure check dose	IRSL 200 s @ 60°C	OSL 100 s @ 125°C	IRSL 100 s @ 125°C	OSL 50 s @ 125°C	SGLL 1 s @ 125°C
Irradiate test dose	Sample specific	Sample specific	End of sequence	Sample specific	Sample specific
Preheat	Cut heat 160°C	Cut heat 160°C	End of sequence	10 s @ 160°C	Cut heat 160°C
Measure test dose	IRSL 200 s @ 60°C	OSL 100 s @ 125°C	OSL 50 s @ 125°C	OSL 50 s @ 125°C	SGLL 1 s @ 125°C

*Banerjee et al (2001)

†Lamothe et al. (2001); Lamothe, personal communication (2001)

‡Murray and Wintle (2000) with modified preheat treatment as per Lepper et al. (2000)

#Murray and Wintle (2000) modified for single grains

signals (in the initial 3 channels; 0.06 s) less than or equal to zero were excluded, 2) grains/pits having regeneration curves with a negative slope were excluded, and 3) grains/pits whose δD_c (defined in the following paragraph) was greater than 100% were excluded.

The last regeneration dose in a SAR/SGLL procedure set is used to gauge the success of the procedures in compensating for sensitivity changes in the material. Lepper et al. (2000) and Lepper (2001) have proposed using the midpoint dose in the regeneration range as a “check dose.” In this investigation, we introduce the parameter δD_c , which is the difference between the observed/calculated check dose and the administered check dose divided by the administered check dose. Scrutiny of the check dose and its distribution can provide a measure of the accuracy (mean δD_c) associated with recovering a known dose using a particular SAR/SGLL procedure.

Dose rates for samples in this investigation were determined by the method presented by Aitken (1998). Elemental concentrations of K, Rb, U, and Th were obtained via instrumental neutron-activation analysis (INAA) at the Ohio State University research reactor (Table A-3). The cosmic-ray dose at depth was calculated using the equation of Prescott and Hutton (1988) adjusted for the local surface “hard” component (muon) dose rate of 0.30 mGy/a. The average water content was estimated to be $10 \pm 3\%$ and $15 \pm 5\%$ for the samples collected from trench CHU-3 and CHU-1, respectively. Because a majority of the usable quartz grains were obtained from the 90- to 150- μm fraction, a beta-dose attenuation factor of 0.91 was used with the single-grain data. Because measured alpha efficiencies were not available, we have used a value of 0.055 for all fine-grain samples in this investigation based on the average of 15 measured values from past IRSL dating studies in the area (Table A-4; Berger 1999; S. Forman and J. Pierson, unpublished data). Anomalous fading has not been evaluated for the sediments in this study due to the large number of methods evaluated and the time

requirements associated with fading measurements.

It was noted during sample preparation that CHU1OSL4 (unit Qal1-1) contained numerous highly indurated lenses of sediment that were lighter in color than the surrounding sediment and would have been oriented vertically in the deposit. They did not contain carbonates (no HCl reaction) but were very well consolidated. Based on their orientation and distinct texture and results of preliminary tests, these lenses were interpreted to be post-depositionally emplaced material. They could have resulted from infilling of tectonic fractures or desiccation cracks. Regardless of their origin, the lenses are a potential source of “contamination” by younger sediment, and therefore, age determination from this sample was considered inadvisable.

2. Summary of Phase-One Results: Evaluation of Techniques

The results of phase one of this study have been presented and discussed in Lepper et al. (2003) and are only summarized here (Table A-5). Of the polyminerall fine-grain methods tested, the IRSL SAR and traditional IRSL MAAD procedures produced reasonable results for the Pleistocene-aged samples. The two less-well-established SAR methods, post-IR blue OSL and IRSL with TL annealing, yielded ages that were in agreement with the abundant ^{14}C age controls for the late-Pleistocene/early Holocene sample (unit Qal3-3). However, these two methods result in overestimates for the older sediments from Trench CHU-1.

An effort to apply the quartz-sand OSL SAR procedure to the sample from unit Qal3-3 was largely unsuccessful. A vast majority of the aliquots measured (37 of 40) exhibited “early saturation,” that is, their regeneration curves were sublinear and saturated at a signal level less than the natural signal making age calculations impossible for over 90% of the aliquots. Because the behavior of this sample violates fundamental assumptions required for successful application of the OSL SAR method and due to the poor data return, the quartz-sand OSL SAR procedure was not investigated further.

Table A-3. Dosimetry-Related Data in Support of OSL Age Determinations

Sample ID	Depth (m)	Average Water Content (%)	Elemental Concentrations from Instrumental Neutron-Activation Analysis				Dose Rate (Gy/ka)
			K (ppm)	Rb (ppm)	Th (ppm)	U (ppm)	
CHU1OSL1	0.65	15 ± 5	29745 ± 4829	107.3 ± 16.7	12.96 ± 1.90	3.27 ± 0.33	4.385
CHU1OSL3	0.80	15 ± 5	26894 ± 4512	171.7 ± 24.9	15.19 ± 2.25	5.02 ± 0.57	4.679
CHU1OSL4	3.40	15 ± 5	23928 ± 6022	183.9 ± 20.7	21.63 ± 2.41	5.26 ± 0.50	4.822
CHU1OSL5	1.95	15 ± 5	22997 ± 4476	159.9 ± 23.5	21.48 ± 3.19	5.41 ± 0.58	4.790
CHU1OSL6	0.70	15 ± 5	25211 ± 4970	139.3 ± 21.5	15.85 ± 1.75	4.44 ± 0.46	4.441
CHU1OSL7	1.50	15 ± 5	28068 ± 4944	120.1 ± 17.8	12.07 ± 1.77	4.18 ± 0.43	4.361
CHU1OSL9	2.75	15 ± 5	23424 ± 4173	130.1 ± 20.54	12.61 ± 1.87	3.60 ± 0.43	3.838
CHU3OSL2	3.70	10 ± 3	28839 ± 4465	101.2 ± 15.4	14.32 ± 2.11	4.67 ± 0.52	4.620
CHU3OSL3	1.30	10 ± 3	26604 ± 5185	124.0 ± 17.3	14.26 ± 1.65	5.11 ± 0.59	4.831
CHU3OSL4	0.90	15 ± 5	28778 ± 5629	135.9 ± 20.1	13.62 ± 2.00	4.31 ± 0.50	4.819

Table A-4. Alpha-Efficiency Values Measured in Past IRSL Dating Studies on the Pajarito Plateau

Sample Number	Source	Alpha Efficiency
LOSA98-1	Berger 1999	0.054
LOSA98-2	Berger 1999	0.077
LOSA98-3	Berger 1999	0.058
LOSA98-4	Berger 1999	0.069
LOSA98-5	Berger 1999	0.065
LOSA98-6	Berger 1999	0.076
OTL/UIC 519	Forman and Pierson, unpublished	0.027
OTL/UIC 518	Forman and Pierson, unpublished	0.046
OTL/UIC 633	Forman and Pierson, unpublished	0.028
OTL/UIC 634	Forman and Pierson, unpublished	0.039
OTL/UIC 635	Forman and Pierson, unpublished	0.040
OTL/UIC 636	Forman and Pierson, unpublished	0.090
OTL/UIC 637	Forman and Pierson, unpublished	0.063
OTL/UIC 638	Forman and Pierson, unpublished	0.059
OTL/UIC 639	Forman and Pierson, unpublished	0.031
Average:		0.055

Single-grain laser luminescence measurements were conducted on 400 grains/pits for each sample in this study. Depending on the sample, 207 to 258 grains/pits provided data suitable, after filtering, for D_e calculations (Table A-4) corresponding to a 52 to 65% data yield. The resulting SGLL D_e data sets formed continuous and positively skewed distributions for all samples evaluated. Because the mean D_e of this type of distribution is not an appropriate estimator of representative dose (affected by positive asymmetry), the mode D_e was examined. The mode of an asymmetric distribution can be influenced by data binning; therefore, the mode- D_e value can be shifted to higher or lower dose values by simply altering the arbitrary bin width. The limits of this shifting effect were investigated for each sample, and the ranges of possible mode- D_e values are presented in Table A-5.

Table A-5. Tabulated Results from the Various OSL SAR and SGLL Methods Evaluated in Phase One

Sample	SGLLIRSL		SAR*		Method		IRSL MAAD† ($D_e \pm$ uncert.)
	(Range of mode D_0)	(mean $D_e \pm$ std. dev.)	post-IR Blue SAR* (mean $D_e \pm$ std. dev.)	IRSL w/ TL SAR† (mean $D_e \pm$ std. dev.)			
CHU3OSL3	N = 252 of 400	N = 48 of 48	N = 48 of 48	N = 36 of 36			n/a
Representative Dose (Gy)	32.5–50.0	45.2 ± 7.4	72.7 ± 8.5	89.3 ± 20.3			44.3 ± 22.7
Dose Rate (Gy/ka)	4.83	5.83	5.83	5.83			5.83
Age Estimate (ka BP)	6.7–10.4	7.7 ± 1.6	12.5 ± 2.1	15.3 ± 3.9			7.6 ± 4.8
Mean dDc	0.74%	0.88%	4.89%	8.12%			n/a
CHU1OSL1	N = 258 of 400	N = 5 of 5	N = 5 of 5	N = 5 of 5			n/a
Representative Dose (Gy)	135.0–150.0	169.2 ± 16.2	238.5 ± 22.0	339.7 ± 40.4			150.7 ± 33.1
Dose Rate (Gy/ka)	4.39	5.10	5.10	5.10			5.10
Age Estimate (ka BP)	30.8–34.2	33.2 ± 5.2	46.8 ± 7.2	66.6 ± 11.4			29.6 ± 7.4
Mean dDc	4.94%	0.37%	1.59%	no data			n/a
CHU1OSL3	N = 244 of 400	N = 5 of 5	N = 5 of 5	N = 5 of 5			n/a
Representative Dose (Gy)	162.5–172.5	178.5 ± 12.8	242.9 ± 36.0	440.4 ± 90.6			168.2 ± 37.7
Dose Rate (Gy/ka)	4.68	5.64	5.64	5.64			5.64
Age Estimate (ka BP)	34.7–36.9	31.7 ± 4.4	43.1 ± 8.1	78.1 ± 18.5			29.8 ± 7.5
Mean dDc	4.12%	0.15%	0.63% (n/a)	5.16%			n/a
CHU1OSL9	N = 207 of 400	N = 4 of 4	N = 4 of 4	N = 3 of 3			n/a
Representative Dose (Gy)	140.0–157.5	191.7 ± 12.1	314.9 ± 43.2	440.9 ± 152.0			177.2 ± 85.2
Dose Rate (Gy/ka)	3.84	4.58	4.58	4.58			4.58
Age Estimate (ka BP)	36.5–41.0	41.9 ± 5.8	68.8 ± 12.7	96.4 ± 35.3			38.7 ± 19.2
Mean dDc	12.63%	0.46%	4.64%	no data			n/a

*Banerjee et al. (2001)

†Lamothe et al. (2001); Lamothe, personal communication, 2001

‡Allken (1998)

The mode- D_e analysis of the quartz-sand SGLL dose distribution resulted in luminescence age ranges that were stratigraphically consistent with radiocarbon and PDI age controls for the tuff-derived sediments in phase one of this study and appears to be the most promising method for OSL dating in this area. Therefore, it was this method, SGLL on quartz sand, that was used in phase two of this study.

3. Phase Two: Single-Grain Laser Luminescence Dating

Following data filtering, as described in Section 1, "General OSL Methods," the single-grain data sets for the samples in this investigation ranged in size from $N = 113$ to $N = 312$, corresponding to a data yield of 28 to 65% (Table A-6). These data sets are sufficient for meaningful dose-distribution analysis; however, no accepted analytical methods exist to determine a unique, nonarbitrary representative dose and corresponding uncertainty from single-grain data sets. Therefore, we have attempted to modify existing analytical methods for SAR data, including error deconvolution (Lepper et al. 2000; Lepper 2001) for use in this study.

An experimentally measured dose distribution is the convolution of the distribution arising from natural sedimentary processes and an experimental error distribution. This relationship can be expressed by the following Fredholm equation:

$$M(D) = \int g(D_e) f(D, D_e) dD_e \quad (\text{Eq. 1})$$

where D is the calculated equivalent dose, $M(D)$ is the measured distribution, $g(D_e)$ is the sedimentary process distribution, and $f(D, D_e)$ is the experimental error distribution. The convolution equation belongs to a class of equations called Fredholm integrals. The standard approach to solving such an equation is to reduce it to a set of discrete linear equations. However, the resulting set of equations forms an "ill-posed" problem. A regularization method developed by Tikhonov is required to recast the equations in a form that can be solved (Tikhonov and Arsenin 1977; Tikhonov et al. 1995). This research uses a nonparametric, non-negative least-squares algorithm adapted from Lawson and Hanson (1974) by V. Whitley and N. Agersnap-Larsen (unpublished) to solve the Tikhonov-regularized Fredholm equation and obtain the sedimentary process distribution, $g(D_e)$. It is this

Table A-6. SGLL Ages Presented in Stratigraphic Approximation for Each Trench

Sample ID	Unit	N^{\dagger}	Data Yield	Mean δD_e	Bin Width (Gy)	Deconvolution Parameter (Gy)	Deconvolved D_e (Gy)	Dose Probability Density	Rate (Gy/ka)	Age (ka)
CHU1OSL1	Qal 1-4	258/400	65%	4.94%	15.8	38.9	142.2 ± 15.8	0.47	4.385	32.4 ± 5.4
CHU1OSL3	Qal 1-4	244/400	61%	4.12%	11.0	35.5	154.0 ± 11.0	0.40	4.679	32.9 ± 4.5
CHU1OSL7	Qal 1-3	296/500	59%	5.36%	19.2	54.8	193.5 ± 19.2	0.47	4.361	44.4 ± 7.1
CHU1OSL6	Qal 1-3	312/500	62%	6.43%	17.2	53.3	189.2 ± 17.2	0.44	4.441	42.6 ± 6.6
CHU1QSL9	Qal 1-2	207/400	50%	12.63%	11.5	42.7	149.5 ± 11.5	0.48	3.838	39.0 ± 5.5
CHU1OSL4	Qal 1-1	—	—	—	—	—	Contaminated	—	—	—
CHU1OSL5	Qal 1-1	113/400	28%	1.32%	15.8	58.9	189.6 ± 15.8	0.79	4.790	39.6 ± 5.7
CHU3OSL3	Qal 3-3	252/400	63%	0.74%	5.4	10.0	45.9 ± 5.4	0.33	4.831	9.5 ± 1.6
CHU3OSL4	Qal 3-3	252/400	63%	1.07%	8.7	18.4	56.6 ± 8.7	0.37	4.819	11.7 ± 2.3
CHU3OSL2	Qal 3-3	182/400	46%	0.06%	9.3	43.3	144.2 ± 9.3	0.69	4.620	30.2 ± 4.0

[†]Number of usable grains/number of grains attempted

deconvolved distribution that is then analyzed to obtain a single age-representative dose (Table A-6).

In addition to the primary data—the set of measured equivalent doses, $M(D)$ —the deconvolution routine requires that two additional parameters be specified. The first, referred to as the deconvolution parameter, defines the error distribution, $f(D, D_e)$, which is represented in the program with a Gaussian model. The deconvolution parameter is the standard deviation of the check-dose (D_c) distribution that was obtained experimentally (Table A-6). The second input is a binning criterion for the resulting deconvolved histogram, $g(D_e)$. In this study, we have determined the bin width by dividing the 90/10 data range (the 90th percentile value minus the 10th percentile value) into 20 units (Table A-6). Additional information regarding the error deconvolution methodology used in this study can be found in Lepper (2001).

Figure A-1 is an example of the output from the deconvolution routine. It shows the nearly continuous, strongly positively skewed “as-measured” distribution expected from a fluvial sample on the left and the deconvolved, or “reconstructed,” distribution on the right. The deconvolved data were then transformed into probability density distributions (Figure A-2), and the age-representative D_e was defined as the midpoint value of the data cluster having the highest combined probability density (also represented on Figure A-2). This analysis

method was applied to all of the SGLL data sets. As none of the age-representative age clusters exceeded 2 bins in width, the uncertainty in D_e was taken to be ± 1 bin width. The foundations for these definitions of D_e and uncertainty were peer reviewed in Lepper (2001), but as stated earlier, the analytical methods used in this study are adaptations of existing techniques. This research should be viewed as an early stage in the development of objective analytical methods for single-grain OSL data.

SGLL ages and their corresponding uncertainties are given in the final column of Table A-6. In trench CHU-1, these values suggest a period of rapid deposition between ~ 37 and 43 ka BP in which units Qal1-1, Qal1-2, and Qal1-3 were deposited (CHU1OSL5, CHU1OSL9, CHU1OSL6, and CHU1OSL7). This age range includes and is consistent with reliable ^{14}C dates from this trench. Based on SGLL ages, unit Qal1-4 appears to have been deposited in a separate but also rapid event ~ 32 to 33 ka BP (CHU1OSL1 and CHU1OSL3). This interpretation implies a depositional hiatus or erosional event between units Qal1-3 and Qal1-4. Soil analyses support the depositional hiatus as pedogenic development was observed between these two units (Section A-3).

The SGLL ages for samples taken from the upper portions of unit Qal3-3 (CHU3OSL3 and CHU3OSL4) are consistent with numerous ^{14}C dates from trench CHU-3 within 50 vertical cm of

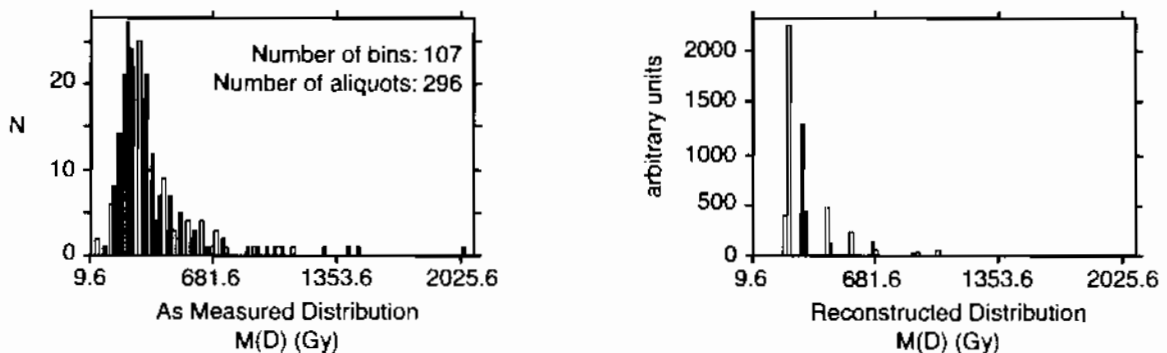


Figure A-1. Dose Distributions for Sample CHU1OSL7. The “as measured” distribution is on the left; the deconvolved distribution is on the right.

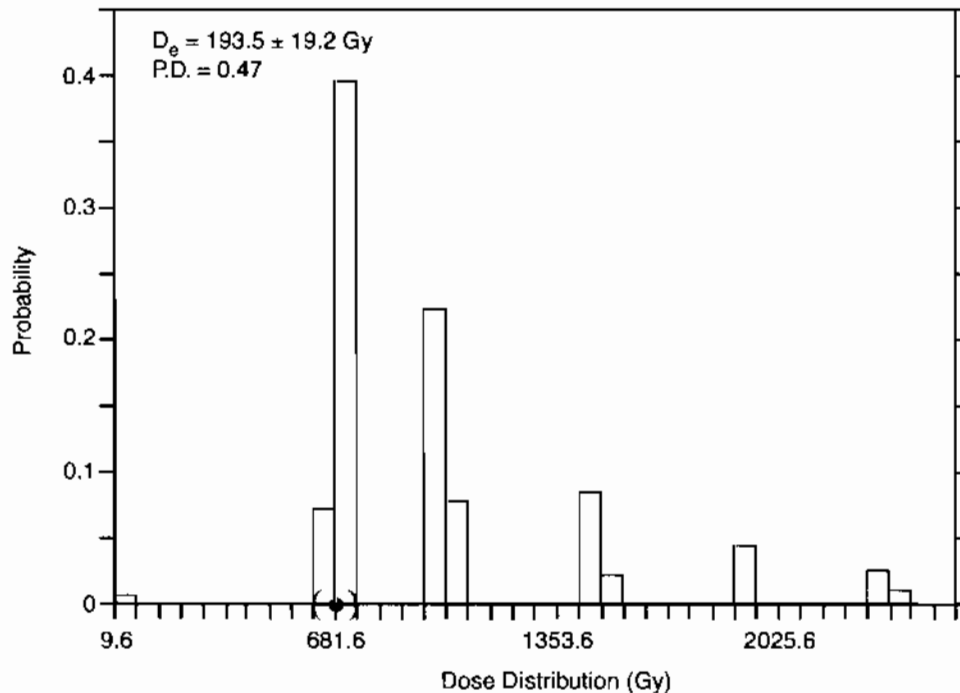


Figure A-2. Deconvolved Probability Density Distribution for Sample CHU1OSL7. The plot shows a graphical representation of the deconvolved probability density distribution for the single age-representative D_e and its uncertainty (---).

the OSL samples. The SGLL age from the lower portion of unit Qal3-3 (CHU3OSL2) suggests that these sediments were likely deposited during the same depositional period as unit Qal1-4. However, the stratigraphic and temporal separation between SGLL samples in trench CHU-3 is not consistent with deposition at the rate recorded in trench 1. This result suggests slower continuous deposition for unit Qal3-3, perhaps due to its geomorphic position, or that a hiatus in deposition did occur. The soil stratigraphy (Section A-3; profile CHU-3-1) at the site of OSL sample CHU3-OSL2 does indicate buried soils within unit Qal3-3, one of which may have formed between deposition of the sediments sampled for OSL.

A-3. Soil Stratigraphy and Pedologic Age Estimates for Chupaderos Canyon Trenches

This section summarizes the technical approach, soil stratigraphy, and age estimations for surface and buried soils described as part of the Seismic

Hazards Program investigations conducted in the Chupaderos Canyon trenches. Soil age estimates are calculated using a soil chronofunction derived from the quantification of soil morphology using a common soil-development-index technique. Morphologic information and radiometric ages for soils formed in the vicinity of LANL, based on detailed regional studies of soils, geomorphic processes, and late Quaternary geology conducted during previous years near LANL, were used to develop and refine a soil chronofunction (McDonald et al. 1996; McDonald 1999; Reneau et al. 2002). Application of this soil chronofunction to surface and buried soils in geomorphic settings significantly different from those of the chronofunction calibration sites may yield inaccurate numerical age estimates; nonetheless, soils provide relative age comparisons and indicate hiatuses in the sedimentary record.

1. Methods

Soil morphology was described according to the

standard methods and nomenclature of the Soil Survey Staff (1981). Two or five soil-stratigraphic sections were described in each trench. The location of each profile was chosen based upon vertical soil sections that provided 1) key soil-stratigraphic information regarding any critical structural features and/or 2) the most complete, vertical record of deposition and soil formation. Descriptions reflect soil morphology exposed within approximately 0.5 m on either side of the horizontal position.

2. Quantification of Soil Morphology

Soil morphology was quantified using the Soil Development Index (SDI) procedures according to Harden (1982), Harden and Taylor (1983), and Taylor (1988). Calculation of SDI values is based on a conversion of soil morphology (i.e., color, structure) into numerical data to enable a quantitative comparison of the degree of soil development. Points are assigned to each property based on the difference between the described soil property and the parent material. Points for each property are normalized to a percentage scale of maximum property development based on comparison of each property to a published or conceptual maximum value of development for each particular property. Maximum soil property values from Taylor (1988) were used to normalize soil property values in this study. Normalized property values are summed for each horizon and averaged, yielding a Horizon Development Index (HDI) value that provides an estimate of overall horizon development relative to a conceptual idea of maximum possible horizon development. Horizon Development Index values are multiplied by horizon thickness and summed for each profile, yielding a Profile Development Index (PDI) value for that profile.

PDI values for trench soils were calculated for all described soils using morphologic properties of rubification, texture, structure, dry and moist consistence, and argillans (clay skins). An important consideration in applying the SDI is determining the soil parent-material values. Parent-material values for each profile were adjusted to reflect ver-

tical changes in texture, consistence, and color of the inferred parent material that correspond to vertical stratification associated with deposition. For most of the buried soils in this study, the weakly to nonaltered sediment common to the surface of many of the trenches was used as a starting point for assessing parent material (discussed in more detail below).

3. Pedologic Age Estimates Using PDI Values

Soil age estimates are calculated using a soil chronofunction developed specifically for use in the Los Alamos area. The chronofunction is based on a systematic increase in soil-profile morphology using simple linear-regression analysis of logarithmic relationships between PDI values for soils in the vicinity of Los Alamos that have been well dated using a variety of radiometric dating techniques (McDonald et al. 1996; Phillips et al. 1998; McDonald 1999; Reneau et al. 1996, 2002). Age estimates for soils described at each trench profile are determined using the soil chronofunction shown in Equation 2.

$$\text{Soil age} = 10 \frac{\log \text{PDI} + 1.347}{0.660} \quad (\text{Eq. 2})$$

4. Confidence Interval for Pedologic Age Estimates

Because of variations in parent material and in environmental factors governing soil-forming processes as well as the general uncertainties in the application of a soil chronofunction for providing age estimates, it is desirable to have some means of determining the accuracy and precision of age estimates generated by a soil chronofunction. Confidence intervals for PDI age estimates were calculated based on linear relationships between PDI values and best age estimates for chronosequence soils. At a 95% confidence level, variation in age estimates is ± 0.07 of the log of the estimated soil age. Soil ages based on the soil chronofunction average within $\pm 18\%$ of the "true" soil age for soils dated radiometrically (^{14}C and ^{21}Ne) and formed in both colluvium and alluvium (Reneau et al. 2002). PDI age estimates are calculated using Equation 2 and increasing or decreasing this estimate by 20%,

yielding three age estimates: best, lower range, and upper range.

5. Stratigraphic-Age Relations for Soils

PDI values were calculated to the base of each recognized soil, with the summed PDI of the entire overlying soil column (if more than one soil) used to calculate soil age. The PDI-based soil age therefore reflects the total time required to develop the overlying soil stratigraphy (i.e., the overlying stack of buried soils) down to a specific depth (the base of each buried soil). The PDI ages, therefore, reflect that time that the overlying strata have been exposed to soil-forming processes. This relation assumes that there is no missing soil between the surface and the base of each soil. This assumption is not realistic for all trench profiles because it is probable that some soils are either partially truncated or completely missing from within any trench section. Further, in cases where sediments or deposits have been exposed by erosion of overlying material (after initial post-deposition burial), the time of soil formation will reflect the time of exposure to soil-forming processes, not the age of the deposit. In other words, the degree of soil formation reflects the time interval that any surface or deposit has been exposed to soil-forming processes, which will generally occur whenever the deposit is within approximately 1 to 2 m of the land surface. In most cases, this time interval should be equivalent to the age of the deposit. In some cases, however, in which erosion has exposed previously buried deposits, the degree of soil formation is a result of pre-burial exposure (if any) to soil-forming processes and the length of time after post-burial exposure. In cases for which erosion has resulted in missing strata (based on stratigraphic, sedimentologic, or soil information), PDI-based ages should be considered minimum ages.

6. Description of Soil Stratigraphy Exposed in Trenches

Vertically stacked sequences of multiple buried soils are exposed in each trench (designated by the suffix "b" at the end of each horizon designation). Buried soils are former surface soils that have been

buried by subsequent periods of colluvial or alluvial deposition. In most cases, the top of each buried soil is recognized as an increase in B horizon properties, especially an increase (relative to the overlying horizon) in argillans (vertically translocated clay, also called clay skins), rubification (increase in soil redness), and the strength of soil structure. The top of each buried soil, therefore, is often recognized as the top of the strongest B horizon of each buried soil. When soils form at the land surface, B horizons normally lie below the surface and are usually overlain by some combination of A, E, and transitional horizons (e.g., AB, BA, EB). In many cases, these former surface horizons are preserved within the base of the overlying soil; however, subsequent soil-forming processes have altered the original morphology of these soils. The base of the overlying soil is pedogenetically "welded" to the underlying soil. Horizons of the buried soil can be pedologically transformed because the zone of soil-forming processes, such as oxidation and the translocation and accumulation of clay, extends through the new layer of soil and into the top of the underlying soil. The resulting morphology of these welded or overlapping soil horizons (i.e., horizons that are now part of both soils) can appear more like B horizons rather than the original A and B. A lack of recognizable A, E, or related transitional horizons may also be due to truncation of soils prior to burial. Truncation of soils is often recognized by sharp contacts with the overlying deposit and/or abrupt changes in sediment texture. Furthermore, many of the soils described in these trenches are in geomorphic settings that are more conducive to deposition than erosion, promoting preservation of buried soils.

Most of the soils exposed in these trenches contain a similar range of genetic horizons. The horizons at the top of the soil profile, A horizons, usually contain slightly higher concentrations of disseminated organic matter that impart a slightly darker coloration (i.e., lower soil chroma and value). Transitional horizons, BA and AB horizons, have dominant properties that are similar to both A and underlying B horizons. Weakly developed B hori-

zons, Bw horizons, have either redder soil color (i.e., higher value and chroma) due to the accumulation of iron (oxy)hydroxides relative to the parent material and/or development of soil structure. Horizons that are 1) usually better developed than Bw horizons and 2) have noticeable accumulation of translocated clay (argillans) are designated as Bt horizons. In these soils, argillans are commonly developed as coatings on ped faces and clasts and lining pores. Former E horizons that have had B-horizon properties overprinted on them from subsequent soil formation related to burial are BE horizons. The E horizon is usually very light colored (chroma < 2) due to the lack of appreciable accumulation of either organic matter or iron (oxy)hydroxides on mineral particles. Skeletans (bleached quartz or feldspar grains) are common along ped faces in E horizons. Transitional horizons that have dominant properties similar to both B and C horizons are designated as BC or CB horizons. Horizons that are poorly altered to unaltered are C horizons and may represent the properties of the original soil parent material.

7. Results

The following text provides a general overview of the soil stratigraphy described in the Chupaderos Canyon trenches. Nine soil-stratigraphic profiles were described among the three trenches (CHU-1, CHU-2, and CHU-3). Profiles were located to characterize key stratigraphic intervals and to provide information about the tectonic history. A summary of soil morphology is presented in Table A-7, and a summary of PDI results and correlations of soils to designated trench units are shown in Table A-8. Soil-horizon designations used in this report reflect interpretation of soil features and processes based on Los Alamos County-wide studies of soils and soil-forming processes (McDonald et al. 1996; Reneau and McDonald 1996).

a. Trench CHU-1 Profiles

Profile CHU-1-1. Soil characteristics were described to a depth of 410 cm (Table A-7). The top of the profile description begins at the original surface that underlies the spoil of material excavated

from the trench. Three buried soils were identified below the surface soil.

Surface Soil: The surface soil is 43 cm thick, is weakly to moderately developed, and coincides with the upper part of unit Qa11-4. The top of the soil contains a moderately developed A horizon with a distinct accumulation of organic matter. The soil B horizon is a weakly developed Bt horizon with few argillans bridging sand grains. Dry soil color ranges from 10YR 5/3 to 8.75YR 5/4. Soil structure is predominantly platy and subangular blocky. A PDI age of 1.8 to 2.9 ka was estimated for this soil (Table A-8). The age may underestimate the true age of this soil because the soil is thin (< 50 cm) and it is likely that the degree of rubification and development of argillans require more than 2 or 3 thousand years.

Buried Soil b1: The first buried soil is 88 cm thick (43 to 131 cm depth) and is moderately developed. This soil coincides with the lower portion of unit Qa11-4. This soil is denoted by the presence of a weakly developed Bt horizon that has considerably better development of argillans, prismatic structure, and dry color hue than the overlying surface soil. Dry soil color is 7.5 YR 5/6. Soil structure consists of prismatic structure parting to subangular blocky structure. Argillan development ranges from common to few coatings lining prismatic pedfaces and pores. A PDI age of 9 to 15 ka was estimated for this soil (Table A-8).

Buried Soil b2: The second buried soil is moderately developed and is 56 cm thick (131 to 187 cm depth). This soil coincides with the upper part of unit Qa11-3. The upper soil boundary is based on the contact between unit Qa11-4 and Qa11-3 and is further denoted by an increase in the development of structure and argillans relative to the overlying soil Cb1 horizon. Moreover, the top of the soil is denoted by the presence of faunal burrows and krotovina indicating that Bt1b2 horizon was at or near the land surface and subjected to active biologic processes characteristic of surface horizons. Dry soil color is 10YR 6/3. Soil structure consists of

continued on page 56

Table A-7. Summary of Soil Morphology for Chupaderos Trench Excavations, 2001 (notes on page 56)

Horizon	Lower Depth (cm)*	Gravel (%)	Dry Color (matrix)	Moist Color (matrix)	Field Texture†	Structure‡	Consistence‡		Wet	Argillans‡	Lower Horizon Boundary‡	Carbo-nates‡	Notes
							Dry	Moist					
Trench CHU-1-1 Profile													
A	12	5-10	10YR 5/3	10YR 3/3	sil-	1-2 m + c pl: 1 m + f sbk	so	vfr	ss, ps		as		Surface soil
Bt1	24	4-8	8.75YR 6/4	7.5YR 4/4	sil-sicl	m + 1 m sbk in places	sh	fr-vfr	ss, ps-p	2 f br	as		
Bt2	35	5-15	6.75YR 5/4	7.5YR 4/4	sil+	2-3 m pl + 1 m + f sbk in places	sh	vfr-fr	ss, ps	2 f-d br	as		
Bt3	43	5-15	8.75YR 5/4	7.5YR 4/4	sil	2-1 m + f sbk	h-sh	fr-vfr	ss, ps	2 d-f co + br	cs		
Btb1	82	5-10	7.5YR 6/4	7.5YR 4/4	sicl-sil	1-2 m pr: 1 m sbk	h-sh	fr-vfr	ss, p-ps	4 d-f po	cs		Faunal burrows
Cb1	131	5-10	10YR 6/3	8.75 YR 4/4	l	m	h-so	fr-vfr	ss-vs, p-ps	3 d-f bk:pf	cs-aw		Bedded sands/silts
Bt1b2	151	4-8	10YR 6/3	8.75YR 4/4	sil	1-2 m pr: 1 m sbk	h	fr-vfr	ss, ps	2-1 pr:pf	cs		Faunal burrows, krotovina
Bt2b2	187	5-10	10YR 6/3	10YR 3/3	sil	1 m + c pr: 1 m sbk in places	h-sh	fr-vfr	ss, ps	3 f po, 1 pr:pf	cs		
Bt1b3	214	5-10	8.75YR 6/3	7.5YR 4/3	sil-	2-1 m pr: 1-2 m sbk	h	fr	ss, ps	3 d-f po, 2 f pr:pf	cs		Faunal burrows
Bt2b3	240	5-10	7.5YR 6/3	7.5YR 4/3	st-sicl	2 m + f pr: 2 m + f sbk	vh	fi-fr	ss, p-ps	4 d-f po, 3 f-d co pr:pf	cs		
Bt3b3	266	5-10	7.5YR 5/4	7.5YR 4/3	sil	2-1 m + f pr: 2-1 m + f sbk	h	fr-vfr	ss, ps	4 d-f po, 3 f-d pr:pf	cs		
Bt4b3	305	5-15	7.5YR 5/4	7.5YR 3/3	sil	1 m pr	h	fr-vfr	ss, ps	2 vfr-f pr, 2 f po	aw-cw		Bedded sands/silts
Cbb3	365	20-35	10YR 6/4	7.5YR 4/4	l	m	sh	vfr	ss, ps-yps		a-cw		Weathered tuff
Cr	410		10YR 6/4	7.5YR 4/4									

Table A-7 Continued. Summary of Soil Morphology for Chupaderos Trench Excavations, 2001 (notes on page 56)

Horizon	Lower Depth (cm)*	Gravel (%)	Dry Color (matrix)	Moist Color (matrix)	Field Texture†	Structure‡	Consistence‡		Wet	Argillans‡	Lower Horizon Boundary‡	Carbo-nates‡	Notes
							Dry	Moist					
Trench CHU-1-2 Profile													
Bt1	23	10-20	8.75YR 6/4	7.5YR 4/4	sil	2 c + m pl; 2-1 c + m sbk	h	fi-fr	ss, ps	3 f br + co	cs		Stripped A horizon
Bt2	48	5-10	8.75YR 6/4	7.5YR 4/4	silt+	1-2 c + m pr; 1 c pl	h-sh	fr-vfr	ss, ps	3 d-f co pr:pf	as		
Bt3	64	4-8	8.75YR 6/3	7.5YR 4/3	sl	m	sh-h	fr	so, vps	2 d pr:pf	aw		
Bt1b1	93	4-8	7.5YR 6/4	7.5YR 4/4	sicl	1-2 c + pr; 1 m + csbk	sh	fr	ss, ps-p	4 d-p pr:pf; 4 f po	cs		Faunal burrows
Bt2b1	116	4-8	7.5YR 6/4	7.5YR 4/4	sicl	1 c + m pr; 1 c + m sbk in places	h	fr	ss-s, p-ps	2 f-d co pr:pf; 2 f po	cs		
BCb1	139	2-5	8.75YR 6/3	7.5YR 4/4	sil	1 c-m pr	sh	fr	ss, ps	1-2 f-p pr:pf	cs		
Bt1b2	175	2-8	7.5YR 6/3	7.5YR 4/4	sil	1-2 c-m pr; 1 c + m sbk	h	fi	ss, ps	2 f po; 1-2 f co pr:pf	cs		Faunal burrows
Bt1b3	203	4-8	7.5YR 6/3	7.5YR 4/4	sil-sicl	2-1 m, pr; 1 c + m, sbk	sh-h	fr	ss, ps-p	2 f pr:pf	cs		
Bt2b3	231	4-8	7.5YR 6/3	7.5YR 3/4	silt+	1-2 m + f pr; 1 m sbk	h	fi	ss, ps-p	2 f-d pr:pf; 2 f po	cs		
Bt3b3	254	5-10	7.5YR 5/4	7.5YR 4/4	sicl	2-1 m + f pr; 3-2 m + f sbk	h-sh	fr-vfr	ss-s, ps-p	3 f-d co pr:pf; 3 d-f po	cs		
Bt3b3	288	5-15	7.5YR 6/4	7.5YR 4/4	silt+	1 m + c pr in places	h-sh	fr-vfr	ss, ps-p	5 d-f po; 2 f co pr:pf; 2 f-d br	cs		
Bt4b3	321	5-15	7.5YR 6/4	7.5YR 4/4	l	m	h-sh	vfr	ss, ps	5 d po, 2 f br	aw		Pumice Weakly weathered tuff
Cr1b3	351		7.5YR 7/4	7.5YR 4/4	l		h-sh	fr	vss, vps				Fractured, unweath- ered tuff
Cr2b3	461		10YR 8/2	10YR 5/4	ls		sh	fr-vfr	so, vps-po				

Table A-7 Continued. Summary of Soil Morphology for Chupaderos Trench Excavations, 2001 (notes on page 56)

Horizon	Lower Depth (cm)*	Gravel (%)	Dry Color (matrix)	Moist Color (matrix)	Field Texture†	Structure‡	Consistence‡		Wet	Argillans‡	Lower Horizon Boundary‡	Carbo-nates‡	Notes
							Dry	Moist					
Trench CHU-1-3 Profile													
Bt1	12	5-10	7.5YR 6/3	8.75YR 4/4	sil	2 m + f pl	h-sh	fr	ss, ps	2 d-f br	cs		
Bt2	36	5-10	7.5YR 6/3	7.5YR 4/4	sil	3-2 c + m pl; 1-2 m abk	h	fr	ss, ps	3 f-d po, 2 d-f co pr:pf	as		2 d pf
Bt3	56	5-10	7.5YR 6/3	7.5YR 4/4	sil	1-2 c pr to nearly m in places, 1-2 c pl	h-vh	fr-fi	ss, ps	2 f po, 2 d-f pr:pf	cs		3 d pr:pf
Bt1b1	78	10-15	7.5YR 6/3	7.5YR 4/4	sil	1 m pr; 1-2 m sbk	h	fr	ss, ps	4 d-f po	cs		Faunal burrows 2 f-d pf
Bt2b1	111	5-15	7.5YR 6/3	7.5YR 4/4	sicl	1-2 m pr; 1-2 m + f sbk	h-sh	fr	ss, ps-p	5 d po, 2 f-d pr:pf	cs		1 f pr:pf
Bt1b2	145	25-35	7.5YR 6/4	7.5YR 4/4	sicl-sil	1 m pr to m	h-sh	fr	ss, ps-p	4 d-f, br, po	cs		Faunal burrows
Bt2b2	218	30-40	7.5YR 6/4	7.5YR 4/4	sicl-sil	m	sh-h	fr	ss, ps-p	1-2 f br, po	gs		
Bt3b2	247	30-40	7.5YR 7/4	7.5YR 4/6	ls-l	m	sh	fr-vfr	vs-so, vps	2 f br	cs		
Bt4b2	281	30-40	8.75YR 7/3	8.75YR 4/6	s-ls	m	sh-so	vfr	so, vps-po	2 f br	as-aw		Pumice
Trench CHU-1-4 Profile													
Bt1	17	4-8	7.5YR 6/3	7.5YR 4/3	sil	2-1 c + m pl; 1-2 m, sbk	h	fr	ss, ps	2 d-f co bk:pf	as		
Bt2	42	4-8	7.5YR 5.5/4	7.5YR 3/4	sil-sicl	3-2 vc-m pl; 1-2 m sbk	h	fr-fi	ss, ps-p	4 d-f po, 3 co bk:pf	as		1-2 f pf
Bt3	59	5-10	7.5YR 6/4	7.5YR 4/4	sil-sicl	1 vc-c pr	h	fr-vfr	ss, ps-p	2 f-d po, 2 f-d co pr:pf	cs		3 f c pr:pf
Bt1b1	94	5-10	7.5YR 6/3	7.5YR 4/4	sil	1-2 vc-c pr; 2-1 c + m sbk + 2-1 m pl	h-sh	vfr	ss, ps	4 d-f po, 3 f-d pf	as-aw		Faunal burrows 2 f-d vert pf
Bt2b1	110	15-20	7.5YR 6/4	7.5YR 4/4	sil+	1 m pr; 2-3 m + f sbk+abk	h-sh	fr	ss, p-ps	2 d pf	cs		2 f co + sf, 1 f co pr:pf

Table A-7 Continued. Summary of Soil Morphology for Chupaderos Trench Excavations, 2001 (notes on page 56)

Horizon	Lower Depth (cm)*	Gravel (%)	Dry Color (matrix)	Moist Color (matrix)	Field Texture†	Structure‡	Dry Moist Consistence‡	Wet	Argillans‡	Lower Horizon Boundary‡	Carbo-nates‡	Notes
Trench CHU-1-4 Profile Continued												
Bl3b1	128	15-25	7.5YR 6/4	7.5YR 4/4	sil+	1-2 m + f sbk + abk	h-sh	fr	2 d-f co pl, 2 f br	cs	1 f sf pt	
Bl4b1	173	15-25	7.5YR 6/4	7.5YR 4/4	l	m	sh-h	fr-vfr	2 f-d br	cs-as		Pumice
Bt1b2	194	20-30	7.5YR 6.5/4	7.5YR 6/4	l	1 m + f sbk	h-sh	vfr	5 f-d po, 3 d pr	cs	1 f po	Pumice
Bt2b2	234	40-55	7.5YR 7/4	7.5YR 4/6	l	1 m sbk nearly m in places	sh	vfr	2 d co + br	cs		Pumice
Bt3b2	267	70-85	8.75YR 7/4	8.75YR 4/6	ls	m	sh	vfr	1 f br	cs		Pumice
Bt4b2	303	70-85	10YR 7/3	8.75YR 4/6	ls	m	sh	vfr	so, vps-po	ai		Pumice
Trench CHU-1-5 Profile												
A	9	4-8	10YR 6/3	8.75YR 4/4	sil	2-3 c + m + f pl; 2-1 m + f sbk	sh	vfr	ss, ps	as		
Bt1	26	5-15	7.5YR 6/4	7.5YR 4/4	sil-scl	2 vf + f + m pl; 1-2 m sbk-abk	sh	fi	3 p-d po, 2 d-f co pl	as		poorly bedded sands
Bt2	44	5-15	7.5YR 6/4	7.5YR 4/4	sil	1-2 m pr; 1 m sbk	sh-h	fr	2 f-d po, 2 f-d co pr; pt	cs		
Bt1b1	65	5-15	7.5YR 6/4	7.5YR 4/4	sil	1-2 m pr; massive	sh-h	fr	3 f-d pr pt; po	cs		crudely bedded sands grading to silts
Bt2b1	86	5-15	7.5YR 5/4	7.5YR 3/4	sil	1 c+m pr	h-sh	fr-vfr	ss, ps-p	aw		scattered weather pumice
Bwb2 (Ab)	124	4-8	10YR 6/3	8.75YR 4/3	sil	1 m pr; 1 m sbk	h	fr	1 f po	cs		Buried A, faunal burrows
Bt1b2	162	4-8	8.75YR 6/3	7.5 YR 4/4	sil	1 m + c pr; nearly m	h	fr	4 f-d po	cs		
Bt1b3	198	4-8	7.5YR 6/3	7.5YR 3.5/3	sil	1 c-m pr; 1 m + f sbk	h	fr-vfr	4 d-f po	cs		

Table A-7 Continued. Summary of Soil Morphology for Chupaderos Trench Excavations, 2001 (notes on page 56)

Horizon	Lower Depth (cm)*	Gravel (%)	Dry Color (matrix)	Moist Color (matrix)	Field Texture†	Structure‡	Consistence‡		Wet	Argillians‡	Lower Horizon Boundary‡	Carbo-nates‡	Notes
							Dry	Moist					
Trench CHU-1-5 Profile Continued													
Bl2b3	223	4-8	8.75YR 6/3	7.5YR 4/3	sil	1 m pr: 1 m sbk, nearly m	h	fr	ss, ps	4 f-d po, 2 f co pr:pf	cs		Crude bedding in places
Bl3b3	244	5-10	7.5YR 6/3	7.5YR 3/4	sil	1 m-c, pr, nearly m	h-sh	fr	ss, ps	3 f-d po	aw-cs		
Bl1b4	267	10-15	7.5YR 6/4	7.5YR 4/4	sil	2 m pr: 2-3 m sbk + 1-2 m-c p	h	fr	ss, ps	5 d po, 2 f-d pr:pf	cs		
Bl2b4	300	20-30	7.5YR 5.5/4	7.5YR 3/4	sicl	1 m pr, nearly m	h-vh	fr	ss, ps	3 d-f br, 2 d-f co pr:pf	cs		
BCb4	322	10-20	7.5YR 6/4	7.5YR 4/4	l	m	sh	vfr-fr	ss, ps-vps	1-2 f br			
Trench CHU-2-1 Profile													
A	19	4-8	7.5YR 5/4	7.5YR 3/3	sil	2 m + f pl: 2-1 m + f abk	sh-so	vfr	ss, ps		cs		
Bl1	45	4-8	7.5YR 6/4	7.5YR 4/4	sil	2-3 c + m pl: 1-2 m abk	h	fr	ss, ps	2 f-d bk:pf, 4 f po	cs-as	2 f sf vert pf	
Bl2	75	4-8	7.5YR 6/4	7.5YR 4/4	sil	1-2 c+m pr: 1 m sbk	h	fr	ss, ps	3 f po, 2 f co-pr:pf	cs	3 f-d co pr:pf	
Bl3	106	4-8	7.5YR 6/4	7.5YR 4/4	sil	2-1 c + m pr: 1 m abk	h	fr	ss, ps	4 f po	as	3 d pr:pf	Bedded sands in places
Bl1b1	130	4-8	7.5YR 6/4	7.5YR 4/4	sicl	1-2 c + m pr: 2-1 m sbk	h	fr-fi	ss, p-ps	4 f-d po, 1-2 f co pr:pf	cs	2 d-f co pr:pf	Faunal burrows
Bl2b1	172	5-10	7.5YR 6/4	7.5YR 4/4	sil	2-1 c + m, pr: 1-2 m, sbk	h	fr	ss, ps	4 f po	as-aw	2 d-f co pr:pf	
Bl3b1	184	20-35	7.5YR5.5/4	7.5YR 4/4	sil	m-sg	sh-lo	vfr	ss, ps	2 f-d br	aw		Bedded sand
Crb1	210		7.5YR 7/4	7.5YR 4/6	sl	m	sh	fr	so, vsp	1 f br	as		Weathered tuff

Table A-7 Continued. Summary of Soil Morphology for Chupaderos Trench Excavations, 2001 (notes on page 56)

Horizon	Lower Depth (cm)*	Gravel (%)	Dry Color (matrix)	Moist Color (matrix)	Field Texture†	Structure‡	Consistence‡		Wet	Argillens‡	Lower Horizon Boundary‡	Carbo-nates‡	Notes
							Dry	Moist					
Trench CHU-2-1 Profile Continued													
Cr1b1	233		8.75YR 7/4	7.5YR 4/4	ls		sh	vfr	so, vps-po		cs		Weakly weathered tuff
Cr2b1	267		8.75YR 7/3	8.75YR 4/4	ls		sh	vfr	so, vps-po				Fractured, unweathered tuff
Trench CHU-2-2 Profile													
A	13	4-8	8.75YR 5/4	7.5YR 4/4	sil	3-2 m + f + v pl	so	vfr	ss, ps		as		
B1	42	4-8	7.5YR 6/4	7.5YR 4/4	sil+	3-2 c + m + f pl; 1-2 c + m abk	h	fi-fr	ss, ps	4 d-f po, 3 f-d vert pf	as	3 co vert pf	
B2	67	4-8	7.5YR 6/3	7.5YR 3/3	sil	2-3 vf + c pl; 2-1 c + m abk	h	fi	ss, ps	4 po	cs-as	3 co vert pf	
B3	86	15-25	7.5YR 6/3	7.5YR 4/3	l	1-2 m sbk	h-sh	vfr	vss-vps	1 f po	as-cs		Bedded sand
B4	98	10-15	7.5YR 6/4	7.5YR 4/3	sil	m + 1 m sbk	h	fr	ss, ps	1 f po	as-aw		Bedded sand
A1b1	102	4-8	7.5YR 5/4	7.5YR 4/3	sil	2 m + f sbk-abk, 2-1 m pl	h	fr	ss, ps	2 f-d pf	aw		Buried A, faunal burrows
A2b1	113	<5	7.5YR 6/3	7.5YR 4/3	sil	1-2 c + m pr	h	fr	ss, ps		cs		Faunal burrows
B11b1	144	4-8	7.5YR 6/4	7.5YR 4/4	sil	1-2 m pr; 1 m sbk	h-sh	fr	ss, p-sp	5 d f po	as-cs		
B11b2	174	10-20	7.5YR 5/6	7.5YR 4/6	sid	1 m, pr; 1-2 m + f, sbk	sh	vfr-fr	ss, ps-p	5 f-d br, 1 f po	cs		Crudely bedded pumice

Table A-7 Continued. Summary of Soil Morphology for Chupaderos Trench Excavations, 2001 (notes on page 56)

Horizon	Lower Depth (cm)*	Gravel (%)	Dry Color (matrix)	Moist Color (matrix)	Field Texture†	Structure‡	Consistence‡		Wet	Argillans‡	Lower Horizon Boundary‡	Carbo-nates‡	Notes
							Dry	Moist					
Trench CHU-2-2 Profile Continued													
Bt2b2	205	10-20	7.5YR 5/6	7.5YR 4/6	sil-sacl	1 m pr: 1 m + f sbk	sh-so	fr-vfr	ss, ps	4 f-d br, 2 f po	cs		Weakly weathered pumice
Bt3b2	232	10-20	7.5YR 5/6	7.5YR 4/6	sil-sacl	1 m sbk	so-sh	fr-vfr	ss, ps	3 f-d br	as-aw		Weakly weathered pumice
CBb2	267	10-20	7.5YR 7/4	7.5YR 4/6	ls	m	so	vfr	vss, po	1-2 f br			Weakly weathered pumice
Trench CHU-3-1 Profile													
A	15		10YR 6/3	8.75YR 3/2	sil	2 vc-m pl: 1-2 c + m sbk	sh	fr	vss, vps		cs		
Bw1	31		10YR 6/3	8.75YR 4/3	sil	3 m + f pl: 2 m + f sbk	sh	vfr-fi	ps, ss	2 f br	as		
Bw2	51		10YR 6/3	8.75YR 3/3	sil-	3 m + f pl: 2 m + f sbk	sh-h	fr	ss, ps		cs		
Bw3	68		10YR 6/2	10YR 3/3	sil-	2 vc-m pl	sh-h	fr-vfr	vss, ps		cs		
C	118		10YR 6.5/2	10YR 3/3	l	m	h-sh	fr	vss, vps		as-aw		Crude bedding
Bt1b1	133		8.75YR 6/3	7.5YR 4/4	sil+	2-1 m + f pr: 1 m sbk	sh	fr	ss, ps-p	3 d pr, pl, 3 d-f po	cs		Bioturbation
Bt2b1	147		8.75YR 6/3	7.5YR 4/4	sil-sicl	2-1 c-m pr: 1 c + m sbk	vh-h	fr	vss, ps-s	1 f po	as		
Btb2	166		8.75YR 6/3	7.5YR 4/4	sil+	2-3 c + m pr: 1 m + f sbk	h-vh	fr-vfr	ss, p-ps	1-2 f pl, 2 f-d po	cs		
BCb2	189		8.75YR 6/3	7.5YR 4/4	sil-	1-2 c-m pr	h-sh	fr-vfr	ss, ps		cs		
CBb2	228		8.75YR 6/3	87.5YR 4/4	l	m	sh-h	fr-vfr	vss-ss, vps-ps		aw		Bedded sand/silt

Table A-7 Continued. Summary of Soil Morphology for Chupaderos Trench Excavations, 2001 (notes on page 56)

Horizon	Lower Depth (cm)*	Gravel (%)	Dry Color (matrix)	Moist Color (matrix)	Field Texture†	Structure‡	Consistence‡		Wet	Argillans‡	Lower Horizon Boundary‡	Carbo-nates‡	Notes
							Dry	Moist					
Trench CHU-3-1 Profile Continued													
C1b2	308		8.75YR 6.5/3	10YR 4/4	l	m	sh-h	fr-vfr	ss, ps		gs		
C2b2	397		7.5YR 6/4	7.5YR 4/4	l-sil	m	sh-h	fr-vfr	vss-ss, ps				
Trench CHU-3-2 Profile													
A	16		7.5YR 5/3	7.5YR 3/3	sil	1-2 c + m pl: 1 m sbk	sh	vfr-fr	ss, ps		cs		
Bw1	32		7.5YR 5/4	7.5YR 5/4	sil-l	1-2 c + m pl: 1 m sbk	sh	fr-vfr	ss, ps		cs		
Bw2	53		7.5YR 5.5/4	7.5YR 3/3	sil	1 m + 1 1-2 pl, nearly m	sh-so	vfr	ss, ps		cs-aw		
Bw3	70		7.5YR 6/3	7.5YR 3/3	sil	2-1 c + m pl: 2 m + f sbk	sh	fr-vfr	ss, ps		aw		
CB	137		10YR 6/3	8.75YR 4/4	l-sil	m	h, vh	fi, fr-vfr	vss, ps		cs-aw		Crude bedded silt
B11b1	160		7.5YR 7/3	7.5YR 4/4	sil	1-2 c + m pr: 1-2 m + f sbk	sh	fr-vfr	ss, ps	2 f pr:pf, 2 f po	cs		Bioturbation
B12b1	207	10-20	7.5YR 6/3	6.25YR 4/4	sil-sicl	3-2 m pr: 2 m + f sbk	h-sh	fr-	ss, ps-p	3 f-d pr:pf, 2 f po	aw		
BCb1	237	40-60	6.25YR 5/4	6.25YR 4/4	l+	m-9g	lo-h	fr-vfr	ss-vps	1 f pr	cs		
B11b2	251	20-35	7.5YR 6/3	7.5YR 4/4	l-cl	m + 1-2 m sbk	h-sh	fr-vfr	ss, ps-p	4 f-d pr	ai-w		
Cr/Btb2	277		7.5YR 6/4	7.5YR 4/4		m				3 f-d po	cs-gs		Weathered tuff
Cr/b2	346		7.5YR 6/4	7.5YR 4/6		m					cs		Weathered tuff

Notes for Table A-7

***Lower Depth:** the depth from the top of the profile where described.

†**Field Texture:** s = sand, ls = loamy sand, sl = sandy loam, l = loam, sil = silt loam, scl = sandy clay loam, silcl = silty clay loam, cl = clay loam

‡**Structure:**

Grade: 1 = weak, 2 = moderate, 3 = strong

Size: vc = very coarse, c = coarse, m = medium, f = fine, vf = very fine

Type: sbk = subangular blocky, abk = angular blocky, pr = prismatic, pl = platy, sg = single grain, m = massive

Other: a colon = parting to (e.g., 1–2 m pr:)

§**Consistence:**

Dry: lo = loose, so = soft, sh = slightly hard, h = hard, vh = very hard

Moist: vfr = very friable, fr = friable, fi = firm, vfi = very firm

Wet—Stickiness: so = nonsticky, vss = very slightly sticky, ss = slightly sticky, s = sticky, vs = very sticky

Wet—Plasticity: po = nonplastic, vps = very slightly plastic, ps = slightly plastic, p = plastic

¶**Cutans (Argillans and Carbonates):**

Abundance: 1 = very few (< 5%), 2 = few (2–25%), 3 = common (25–50%), 4 = many (50–75%), 5 = nearly continuous (75+%)

Thickness/(Distinctness): f = thin (faint), d = moderately thick (distinct), p = thick (prominent), vf = very thin

Location/Type: po = along pores; co = coating gravel, ped faces; br = bridging grains; pf = along ped faces (as co + br);

pr:pf = along prismatic ped faces; bk:pf = along blocky ped faces; Lam = lamellae; Non-lam = interspace between lamellae;

Pl: ped interior; prfc: pressure faces; irg = irregular shape

Type: man = mangans, skel = skeletans, si = silans

♠**Horizon Boundary:**

Thickness (first letter): a = abrupt (< 2 cm), c = clear (2–5 cm), d = diffuse (> 5 cm), g = gradual

Topography (second letter): s = smooth, w = wavy, i = irregular

prismatic structure parting to subangular blocky structure. Argillans range from common to few coatings lining prismatic pedfaces and pores. A PDI age of 18 to 29 ka was estimated for this soil (Table A-8).

Buried Soil b3: The third buried soil is strongly developed, is 178 cm thick (187 to 365 cm depth), and overlies weakly weathered and fractured tuff of unit Qbt1 of the Tshirege Member. This soil has formed in units Qa1-3, Qa1-2, and Qa1-1. The top of the soil is denoted by a noticeable increase in the development of structure and argillans relative to the overlying soil. Dry soil color ranges from 7.5 YR 5/4 to 8.75YR 6/3. Soil structure consists of prismatic structure parting to subangular blocky structure. Argillan development ranges from many to few coatings lining prismatic pedfaces and pores. A PDI age of 53 to 84 ka was estimated for this soil (Table A-8).

Profile CHU-1-2. Soil characteristics were described to a depth of 461 cm (Table A-7). The top of the profile description begins at the original surface that underlies the spoil of material excavated from the trench. Three buried soils were

identified below the surface soil.

Surface Soil: The surface soil is 64 cm thick, is weakly to moderately developed, and coincides with the upper part of unit Qa1-4. The A horizon appears to have been stripped, and the Bt1 now lies at the surface. The soil B horizon is a weakly developed Bt horizon with few argillans bridging sand grains. Dry soil color ranges from 8.75YR 6/4 to 8.75YR 6/3. Soil structure ranges from platy to subangular blocky. A PDI age of 4.7 to 7.4 ka was estimated for this soil (Table A-8). The age may underestimate the true age of this soil because the top of the soil appears to have been removed.

Buried Soil b1: The first buried soil is 75 cm thick (64 to 139 cm depth) and is moderately developed. This soil coincides with the lower portion of unit Qa1-4. This soil is denoted by the presence of a moderately developed Bt horizon that has considerably better development of argillans and prismatic structure than the overlying Bt3 horizon. Dry soil color ranges from 7.5YR 6/3 to 7.5YR 6/4. Soil structure consists of prismatic structure parting to subangular blocky structure. Argillans range from

Table A-8. PDI Age Estimates for Trenches CHU-1, CHU-2, and CHU-3

Lowest Horizon	Lower Horizontal Body Depth (cm)	Trench Unit	PDI Value	PDI Estimated Age (ka)			Composite PDI Estimated Age (ka)		
				Best	Upper Range	Lower Range	Best	Upper Range	Lower Range
Trench CHU-1-1									
Bt3	43	Qal 1-4	7.6	2.3	2.9	1.8			
CBb1	131	Qal 1-4	21.9	12	15	9			
Bt2b2	187	Qal 1-3	34.2	23	29	18			
CB3	365	Qal 1-3, 1-2, 1-1	68.3	66	84	53			
Trench CHU-1-2									
Bt3	64	Qal 1-4	14.2	5.9	7.4	4.7			
BCb1	139	Qal 1-4	33.0	22	27	17			
Bt1b2	175	Qal 1-3	42.1	32	40	25			
Bt5b3	321	Qal 1-3, 1-2, 1-1	85.5	94	118	75			
Trench CHU-1-3									
Bt3	56	Qal 1-3	15.1	6.5	8.2	5.2	26	33	21
Bt2b1	111	Qal 1-3	33.4	22	28	18	42	53	33
Bt4b2	281	Qal 1-1, Qbt	75.6	78	98	62	97	123	77
Trench CHU-1-4									
Bt3	59	Qal 1-3	16.7	7.6	9.6	6.0	27	34	22
Bt4b1	173	Qal 1-3	46.5	37	46	29	56	71	45
Bt4b2	303	Qal 1-1, Qbt	76.7	79	100	63	99	125	79
Trench CHU-1-5									
Bt2	44	Qal 1-6, Qal1-4	12.4	4.8	6.1	3.8			
Bt2b1	86	Qal1-4	23.7	13	16	10			
Btb2	162	Qal 1-3	42.5	32	40	25			
Bt3b3	244	Qal 1-3	65.7	63	79	50			
BCb4	322	Qal 1-2, Qal1-1	86.6	96	120	76			
Trench CHU-2-1									
Bt3	106	Qal2-2	30.7	19	24	15			
Bt3b1	184	Qal2-2	55.1	48	60	38			
Cr2b1	267	Qal2-2, Qbtt	63.0	59	74	47			
Trench CHU-2-2									
Bt4	98	Qal2-2	25.6	15	18	12			
Bt1b1	144	Qal2-2	40.4	30	37	23			
CBb2	267	Qal2-2, Qbtt	73.5	74	94	59			
Trench CHU-3-1									
C	118	Qal3-3	14.2	5.9	7.4	4.7			
Bt2b1	147	Qal3-3	21.5	11	14	9			
C2b2	397	Qal3-3	46.1	36	46	29			
Trench CHU-3-2									
CB	137	Qal3-3	14.0	5.8	7.3	4.6			
BCb1	237	Qal3-3, Qal3-2	36.6	25	32	20			
Cr2	346	Qal3-1a, Qbt1	49.8	41	51	32			

many to few coatings lining prismatic pedfaces and pores. A PDI age of 17 to 27 ka was estimated for this soil (Table A-8).

Buried Soil b2: The second buried soil is moderately developed and is 36 cm thick (139 to 175 cm depth). This soil coincides with the upper part of unit Qa1-3. The upper soil boundary is the contact between unit Qa1-4 and Qa1-3 and is denoted by an increase in the development of structure and argillans relative to the overlying soil BCb1 horizon. Moreover, the top of the soil is denoted by the presence of faunal burrows and krotovina indicating that the Bt1b2 horizon was at or near the land surface and subjected to active biologic processes characteristic of surface horizons. Dry soil color is 7.5YR 6/3. Soil structure consists of prismatic structure parting to subangular blocky structure. Argillan development ranges from common to few coatings lining prismatic pedfaces and pores. A PDI age of 25 to 40 ka was estimated for this soil (Table A-8).

Buried Soil b3: The third buried soil is strongly developed, is 146 cm thick (175 to 321 cm depth), and overlies 140 cm of weakly weathered and fractured tuff of unit 1 Qbt1 of the Tshirege Member. This soil predominantly has formed in units Qa1-3, Qa1-2, and Qa1-1. The top of the soil is denoted by a noticeable increase in the development of structure and argillans relative to the overlying soil. Soil structure consists of prismatic structure parting to subangular blocky structure. Argillans range from nearly continuous to few coatings lining prismatic pedfaces and pores and bridging sand grains and pumice. A PDI age of 75 to 118 ka was estimated for this soil (Table A-8).

Profile CHU-1-3. Soil characteristics were described to a depth of 281 cm (Table A-7). The top of the profile description begins at the original surface that underlies the spoil of material excavated from the trench. Two buried soils were identified below the surface soil.

Surface Soil: The surface soil is 56 cm thick and is

moderately developed. This soil coincides with the upper portion unit Qa1-3 and soil b2 in profiles CHU-1-1, CHU-1-2, CHU-1-5. The A horizon appears to have been recently stripped and the Bt1 now lies at the surface. Dry soil color for all horizons is 7.5YR 6/3. Soil structure consists of platy structure, prismatic structure parting to subangular blocky structure, and is nearly massive near the bottom of the soil. Argillan development ranges from common to few coatings lining prismatic pedfaces and pores. A PDI age of 5.2 to 8.2 ka was estimated for this soil (Table A-8). This value is a minimum age for this soil, however, because the soil is correlative with buried soil b2 in the CHU-1-1, CHU-1-2, and CHU-1-5 profiles that lie west of fault 1-D. Adding the average PDI ages of both the surface and buried soil b1 at profiles CHU-1-1, CHU-1-2, and CHU-1-5 yields a cumulative PDI age for this soil of 21 to 33 ka.

Buried Soil b1: The first buried soil is 55 cm thick (56 to 111 cm depth) and is moderately developed. This soil coincides with the lower portion of unit Qa1-3. This soil is denoted by the presence of a moderately developed Bt horizon that has considerably better development of argillans and prismatic structure than the overlying horizon (Bt3). Dry soil color is 7.5YR 6/3. Soil structure consists of prismatic structure parting to subangular blocky structure. Argillans range from nearly continuous to few coatings lining prismatic pedfaces and pores. A PDI age of 18 to 28 ka was estimated for this soil (Table A-8). This value is a minimum age for this soil, however, because this soil is correlative with buried soil b3 in the CHU-1-1, CHU-1-2, and CHU-1-5 profiles that lie west of fault 1-D. Adding the average PDI ages of the surface and overlying buried soils at CHU-1-1 and CHU-1-2 results in a cumulative PDI age for this soil of 34 to 54 ka.

Buried Soil b2: The second buried soil is moderately developed and is 170 cm thick (111 to 281 cm depth). This soil coincides with unit Qa1-1 and extends into the upper part of the Tsankawi Pumice of the Tshirege Member. The soil boundary is the contact between unit Qa1-3 and unit Qa1-1. Dry

soil color ranges from 8.75YR 7/3 to 7.5YR 6/4. Soil structure consists of prismatic structure to nearly massive in horizon Bt1b2 and is massive in underlying horizons. Argillan development ranges from many to few coatings lining pores and bridging sand grains and pumice. A PDI age of 62 to 98 ka was estimated for this soil (Table A-8). Adding the average PDI ages of the surface and overlying buried soils at CHU-1-1, CHU-1-2, and CHU-1-5 yields a cumulative PDI age for this soil of 78 to 124 ka.

Profile CHU-1-4. Soil characteristics were described to a depth of 303 cm (Table A-7). The top of the profile description begins at the original surface that underlies the spoil of material excavated from the trench. Two buried soils were identified below the surface soil.

Surface Soil: The surface soil is 59 cm thick and is moderately developed. This soil coincides with the upper portion unit Qal1-3. The A horizon appears to have been recently stripped and the Bt1 now lies at the surface. Dry soil color ranges from 7.5YR 5.5/4 to 7.5YR 6/3. Soil structure predominantly consists of platy structure parting to subangular blocky structure. Argillan development ranges from many to few coatings lining prismatic pedfaces and pores. A PDI age of 6.0 to 9.6 ka was estimated for this soil (Table A-8). This value is a minimum age for this soil, however, because this soil is correlative with buried soil b2 in the CHU-1-1, CHU-1-2, and CHU-1-5 profiles that lie west of fault 1-D. Adding the average PDI ages of the surface and overlying buried soil at CHU-1-1, CHU-1-2, and CHU-1-5 yields a cumulative PDI age for this soil of 22 to 36 ka.

Buried Soil b1: The first buried soil is at 114 cm thick (59 to 173 cm depth) and is moderately developed. This soil coincides with the lower portion of unit Qal1-3. This soil is denoted by the presence of a moderately developed Bt horizon that has considerably better development of argillans and prismatic structure than the overlying horizon (Bt3). Moreover, the top of the soil is

denoted by the presence of faunal burrows and krotovina indicating that the Bt1b2 horizon was at or near the land surface and subjected to active biologic processes. Dry soil color ranges from 7.5YR 6/4 to 7.5YR 6/3. Soil structure consists of prismatic structure parting to subangular blocky structure. Argillans range from many to few coatings lining prismatic pedfaces and pores. A PDI age of 29 to 46 ka was estimated for this soil (Table A-8). This value is a minimum age for this soil, however, because this soil is correlative with buried soil b3 in the CHU-1-1, CHU-1-2, and CHU-1-5 profiles that lie west of fault 1-D. Adding the average PDI ages of the surface and overlying buried soil at CHU-1-1, CHU-1-2, and CHU-1-5 results in a cumulative PDI age for this soil of 46 to 72 ka.

Buried Soil b2: The second buried soil is moderately developed and is 130 cm thick (173 to 303 cm depth). This soil coincides with unit Qal1-1 and the upper part the Tsankawi Pumice of the Tshirege Member. The soil boundary is based on the contact between unit Qal1-3 and unit Qal1-1. Dry soil color ranges from 8.75YR 7/3 to YR 6/4. Soil structure consists of subangular blocky structure grading downward to massive. Argillans range from nearly continuous to very few coatings lining pores and bridging sand grains and pumice. A PDI age of 63 to 100 ka was estimated for this soil (Table A-8). Adding the average PDI age of the surface and buried soils at CHU-1-1, CHU-1-2, and CHU-1-5 yields a cumulative PDI age for this soil of 79 to 126 ka.

Profile CHU-1-5. Soil characteristics were described to a depth of 322 cm (Table A-7). The top of the profile description begins at the original surface that underlies the spoil of material excavated from the trench. Four buried soils were identified below the surface soil.

Surface Soil: The surface soil is 44 cm thick, is weakly to moderately developed, and coincides with unit Qal1-4 and Qc1-6. The top of the soil contains a moderately developed A horizon with a

distinct accumulation of organic matter. The soil B horizon is a weakly developed Bt horizon with common to few argillans bridging sand grains. Dry soil color ranges from 10YR 6/3 to 7.5YR 6/4. Soil structure is predominantly platy and subangular blocky. A PDI age of 3.8 to 6.1 ka was estimated for this soil (Table A-8).

Buried Soil b1: The first buried soil is 42 cm thick (44 to 86 cm depth) and is moderately developed. This soil coincides with the lower portion of unit Qal1-4. This soil is denoted by the presence of a subtle change in structure, argillan development, and poor preservation of bedding in places. It is possible that this soil is not a separate soil but is instead related to the surface soil. Dry soil color is 7.5 YR 6/4. Soil structure consists of prismatic structure. Argillans range from common to few coatings lining prismatic pedfaces and pores. A PDI age of 10 to 16 ka was estimated for this soil (Table A-8).

Buried Soil b2: The second buried soil is moderately developed and is 76 cm thick (86 to 162 cm depth). This soil coincides with the upper part of unit Qal1-3. The upper soil boundary is the contact between unit Qal1-4 and Qal1-3 and is further denoted by the presence of a grayish pale-brown color and common faunal burrows indicating that the Bwb2 horizon was at the land surface and subjected to active biologic processes characteristic of surface horizons. Dry soil color ranges from 8.75 YR 6/3 to 10YR 6/3. Soil structure consists of prismatic structure parting to subangular blocky structure. Argillan development ranges from common to few coatings pore linings. A PDI age of 25 to 40 ka was estimated for this soil (Table A-8).

Buried Soil b3: The third buried soil is strongly developed and is 82 cm thick (162 to 244 cm depth). This soil has formed in the lower portion of units Qal1-3. The top of the soil is denoted by a noticeable change in structure and an increase in faunal burrowing. Dry soil color ranges from 8.75 YR 6/3 to 7.5YR 6/3. Soil structure consists of prismatic structure parting to subangular blocky structure. Argillans range from many to few coatings lining

prismatic pedfaces and pores. A PDI age of 50 to 79 ka was estimated for this soil (Table A-8).

Buried Soil b4: The fourth buried soil is strongly developed and is 78 cm thick (244 to 322 cm depth). This soil has formed in units Qal1-2 and Qal1-1 and overlies weathered and fractured Unit 1 (Qbt1) of the Tshirege Member. The top of the soil is denoted by a stratigraphic break between Qal1-3 and Qal1-2 and noticeable increase in the development of structure and argillans relative to the overlying soil. Dry soil color ranges from 7.5 YR 5.5/4 to 7.5YR 6/4. Soil structure consists of prismatic structure parting to subangular blocky structure and grades to massive with increasing soil depth. Argillans range from nearly continuous to few coatings lining prismatic pedfaces and pores and bridging sand grains and pumice. A PDI age of 76 to 120 ka was estimated for this soil (Table A-8).

b. Summary of Trench CHU-1 Soil Stratigraphy

Unit Qal1-4 consists of two soil units. The PDI age for the surface soils at profiles CHU-1-1, CHU-1-2, and CHU-1-5 range from 1.8 to 7.4 ka. This age may underestimate the true age of the soil because a few thousand years may be insufficient to account for the development of soil structure and argillans. The overall stronger degree of soil formation may be because the surface soil has formed in material likely derived from the erosion of pre-existing soils upslope and east of fault 1-D. The trench stratigraphy indicates that these three surface soils are the youngest soil units. A buried soil that lies about 50 cm below the surface was identified at all three profiles on the downthrown structural block. The boundary between the surface and the buried soil is subtle and is largely based on changes in soil structure, argillans, and the presence of faunal burrows. The PDI age for this buried soil ranges from 9 to 27 ka.

Unit Qal1-3 contains two soils. The two buried soils at profiles CHU-1-1, CHU-1-2, and CHU-1-5 (soils b2 and b3) that are formed in unit Qal1-3 are buried by unit Qal1-4. The boundary of the upper buried soil (soil b2) in unit Qal1-3 is largely based on the stratigraphic contact between units Qal1-4 and

Qal1-3, by an increase in soil rubification, structure, argillans relative to the overlying soil horizon, and by the presence of faunal burrows. The age of the upper soil (soil b2) ranges from 18 to 40 ka. The surface soil at profiles CHU-1-3 and CHU-1-4 are correlative to buried soil b2 in unit Qal1-3 at profiles CHU-1-1, CHU-1-2, and CHU-1-5. The PDI age for the surface soils at profiles CHU-1-3 and CHU-1-4 range from 5.2 to 9.6 ka; however, this value is a minimum age range because these soils would have started forming before deposition of unit Qal1-4. Cumulative PDI ages for the surface soils at CHU-1-3 and CHU-1-4, based on the average PDI ages for soils formed in unit Qal1-4, range from 22 to 36 ka. The upper boundary of the lower buried soil in unit Qal1-3 is subtle and is largely based on changes in soil structure, argillans, and the presence of faunal burrows. The PDI age for this buried soil at CHU-1-3 and CHU-1-4 (soil b1) ranges from 18 to 46 ka and the cumulative PDI age ranges from 34 to 72 ka. By comparison, the PDI range for correlative soil at profiles CHU-1-1, CHU-1-2, and CHU-1-5 (soil b3) is 50 to 118 ka.

c. Trench CHU-2 Profiles

Profile CHU-2-1. Soil characteristics were described to a depth of 267 cm (Table A-7). The top of the profile description begins at the original land surface. One buried soil was identified below the surface soil.

Surface Soil: The surface soil is 106 cm thick, is moderately developed, and coincides with the upper portion unit Qal2-2. The top of the soil contains a moderately developed A horizon with a distinct accumulation of organic matter and evidence of faunal burrowing. The soil B horizon is a weakly to moderately developed Bt horizon with many to few argillan coatings lining prismatic pedfaces and pores. Dry soil color ranges from 7.5YR 5/4 to 7.5YR 6/4. Soil structure is predominantly prismatic structure parting to angular and subangular blocky. A PDI age of 15 to 24 ka was estimated for this soil (Table A-8).

Buried Soil b1: A buried soil is 161 cm thick (106 to 267 cm depth) and is moderately developed.

This soil coincides with the lower portion of unit Qal2-2 and the upper 70 cm of the weathered and fractured unit Qbt1 of the Tshirege Member. This soil is denoted by the presence of a moderately developed Bt horizon that has considerably better development of argillans and blocky structure and an increase in faunal burrows than the overlying horizon. Dry soil color ranges from 8.75YR 7/3 to 7.5 YR 5/4. Soil structure consists of prismatic structure parting to subangular blocky structure, grading to massive near the bottom of the profile. Argillan development ranges from many to few coatings lining prismatic pedfaces and pores and bridging sand grains and pumice. A PDI age of 38 to 60 ka was estimated for this soil to the base of unit Qal2-2 and a PDI age of 47 to 74 ka including pedogenic alteration of the pumice bed off the Tshirege Member (Table A-8).

Profile CHU-2-2. Soil characteristics were described to a depth of 267 cm (Table A-7). The top of the profile description begins at the original land surface. Two buried soils were identified below the surface soil.

Surface Soil: The surface soil is 98 cm thick, is moderately developed, and coincides with the upper portion unit Qal2-2. The top of the soil contains a moderately developed A horizon with a distinct accumulation of organic matter and evidence of faunal burrowing. The soil B horizon is a moderately developed Bt horizon with many to few argillan coatings lining pores and prismatic pedfaces. Dry soil color ranges from 8.75YR 5/4 to 7.5YR 6/3. Soil structure is predominantly prismatic and platy structure parting to angular and subangular blocky. A PDI age of 12 to 18 ka was estimated for this soil (Table A-8).

Buried Soil b1: The first buried soil is 46 cm thick (98 to 144 cm depth) and is moderately developed. This soil coincides with the lower portion of unit Qal2-2. This upper boundary of this soil is denoted by the presence of a moderately developed A horizon and an increase in faunal burrows relative to the overlying horizon. Dry soil color ranges from

7.5YR 5/4 to 7.5 YR 6/3. Soil structure consists of prismatic, platy, and subangular blocky. Argillan development ranges from nearly continuous to few coatings lining pedfaces and pores. A PDI age of 23 to 37 ka was estimated for this soil.

Buried Soil b2: The second buried soil is moderately developed and is 123 cm thick (144 to 267 cm depth). This soil coincides with the upper part of the Tsankawi Pumice (Qbtt) of the Tshirege Member of the Bandelier Tuff. The soil boundary is based on the contact between unit Qal2-2 and the eroded top of Qbtt. It is not clear if pedogenic alteration of Qbtt is largely the result of soil formation that preceded burial or if pedogenic alteration largely occurred after burial and coincides with formation of buried soil b2. A lack of preserved bedding in the pumice in horizon Bt1b2 suggests that the top of the pumice was exposed to pedogenic processes for at least some time before burial by unit Qal2-2. Regardless, it is likely that pedogenic processes associated with formation of overlying soil have further altered soil b2. Dry soil color ranges from 7.5YR 7/4 to 7.5YR 5/6. Soil structure consists of prismatic structure parting to angular and subangular blocky structure, grading to massive towards the bottom of the profile. Argillan development ranges from nearly continuous to very few coatings lining pores and bridging grains. A PDI age of 59 to 94 ka was estimated for this soil (Table A-8). Soil b2 at profile CHU-2-2 appears to be correlative with soil b1 at profile CHU-2-1.

d. Summary of Trench CHU-2 Soil Stratigraphy

Unit Qal2-2 consists of two soil units. The PDI age for the surface soils at profiles CHU-2-1 and CHU-2-2 range from 12 to 19 ka. A buried soil (soil b1) that lies about 100 cm below the surface was identified at both profiles. The boundary between the surface and the buried soil is defined by a buried A horizon at CHU-2-2 and changes in soil structure, argillans, and the presence of faunal burrows at profile CHU-2-1. Soil b1 at profile CHU-2-2 overlies a second buried soil (soil b2). Soil b1 at profile CHU-2-1 appears to be correlative with soil b2 at profile CHU-2-2. This result indi-

cates that the top of soil b1 at CHU2-1 has been partially truncated. The PDI age for soil b1 at CHU-2-1 ranges from 38 to 60 ka and the PDI age for soil b2 ranges from 47 to 94 ka.

e. Trench CHU-3 Profiles

Profile CHU-3-1. Soil characteristics were described to a depth of 397 cm (Table A-7). The top of the profile description begins at the top of unit Qal3-4.

Surface Soil: The surface soil is 118 cm thick, is weakly to moderately developed, and coincides with the upper portion of unit Qal3-3. The top of the soil contains a moderately developed A horizon with a distinct accumulation of organic matter. The soil B horizon is a weakly to moderately developed Bw horizon. Dry soil color ranges from 10YR 6/3 to 10YR 6.5/2. Soil structure is predominantly platy and subangular blocky. A PDI age of 4.7 to 7.4 ka was estimated for this soil (Table A-8).

Buried Soil b1: The first buried soil is 29 cm thick (118 to 147 cm depth) and is moderately developed. This soil coincides with the upper to middle portion of unit Qal3-3. This soil is denoted by the presence of a moderately developed Bt horizon that has considerably better development of argillans, prismatic structure, and dry color hue than the overlying horizon and an increase in the abundance of faunal burrowing. Dry soil color is 8.75 YR 6/3. Soil structure consists of prismatic structure parting to subangular blocky structure. Argillans range from common to few coatings lining prismatic pedfaces and pores. A PDI age of 9 to 14 ka was estimated for this soil (Table A-8).

Buried Soil b2: The second buried soil is moderately developed and is 250 cm thick (147 to 397 cm depth). This soil coincides with the lower part of unit Qal3-3. The upper soil boundary is denoted by an increase in the development of structure and argillans and by an increase in the abundance of faunal burrowing relative to the overlying soil Bt2b1 horizon. Dry soil color ranges from 8.75 YR 6/3 to 7.5YR 6/4. Soil structure consists of prismatic structure parting to subangular blocky struc-

ture and grades to massive toward the bottom of the profile. Argillans range from few coatings lining pedfaces and pores in the Btb2 to no argillans in underlying horizons. A PDI age of 29 to 46 ka was estimated for this soil (Table A-8).

Profile CHU-3-2. Soil characteristics were described to a depth of 346 cm (Table A-7). The top of the profile description begins at the top of unit Qal3-4.

Surface Soil: The surface soil is 137 cm thick, is moderately developed, and coincides with unit Qal3-4 and the upper portion of unit Qal3-3. The top of the soil contains a moderately developed A horizon with a distinct accumulation of organic matter. The soil B horizon is a moderately developed Bw horizon. Dry soil color ranges from 8.75YR 6/3 to 7.5YR 5/4. Soil structure is predominantly platy and subangular blocky. A PDI age of 4.6 to 7.3 ka was estimated for this soil (Table A-8).

Buried Soil b1: The first buried soil is 100 cm thick (137 to 237 cm depth) and is moderately developed. This soil coincides with the lower portion of unit Qal3-3 and all of unit Qal3-2. This soil is denoted by the presence of a moderately developed Bt horizon that has considerably better development of argillans, prismatic structure, and dry color hue than the overlying CB horizon and an increase in the abundance of faunal burrowing. Dry soil color ranges from 6.25 YR 5/4 to 7.5YR 7/3. Soil structure consists of prismatic structure parting to subangular blocky structure. Argillans range from common to few coatings lining prismatic pedfaces and pores. A PDI age of 20 to 32 ka was estimated for this soil (Table A-8).

Buried Soil b2: The second buried soil is weakly to moderately developed and is 109 cm thick (237 to 346 cm depth). This soil coincides with units Qal1-1a and Qbt1 of the Tshirege Member. The upper soil boundary is denoted by an increase in the development of structure and argillans and by an increase in the abundance of faunal burrowing relative to the overlying soil BCb1 horizon. Dry soil color ranges from 7.5 YR 6/3 to 7.5YR 6/4. Soil

structure is massive with pockets of subangular blocky structure in horizon Bt1b2. Argillans range from many to few coatings lining pedfaces and pores in the Bt horizons. A PDI age of 32 to 51 ka was estimated for this soil (Table A-8).

f. Summary of Trench CHU-3 Soil Stratigraphy

Unit Qal3-3 consists of three soil units along the western half of the trench exposure and two soil units along the eastern half of the trench exposure. The PDI age for the surface soils range from 4.6 to 7.4 ka. A buried soil (soil b1) at profile CHU-3-1 that lies at 98 cm below the surface was identified along the western half of the trench. The boundary between the surface and the buried soil is defined by an increase in soil structure, argillans, and the presence of faunal burrows. The PDI age for soil b1 at profile CHU-3-1 ranges from 9 to 14 ka. The upper boundary of soil b1 at profile CHU-3-2 is also defined by an increase in soil structure, argillans, and the presence of faunal burrows relative to the overlying soil horizon. Soil b1 at profile CHU-3-2 and soil b2 at profile CHU-3-1 appear to be correlative. The PDI age for soil b2 at CHU-3-1 and soil b1 at CHU-3-2 ranges from 20 to 43 ka. Soil b2 at profile CHU-3-2 has formed in alluvium and tuff and predates deposition of unit Qal3-3 and Qal3-2. The top of this soil is denoted by an increase in the abundance of faunal burrowing relative to the overlying soil horizon. The PDI for this soil ranges from 32 to 51 ka.

APPENDIX B. CHUPADEROS CANYON TRENCHES—UNIT DESCRIPTIONS

For the most part, the units logged are considered to be unique to a given trench. With the exception of the Bandelier Tuff and related units, the unit symbols and colors used on the trench logs are not intended to imply correlations of units between or among the trenches. To emphasize this, most unit symbols are of the form Qc1-1, which is shorthand for Quaternary colluvium, trench CHU-1, first (i.e., oldest) colluvial unit in the sequence. Similarly, Qal2-1 would be shorthand for Quaternary alluvium, trench CHU-2, first alluvial unit in the sequence. Some of the Qal units may, in fact, represent terrace deposits, especially in light of their relations to what appears, in all the trenches in Chupaderos Canyon, to be a strath surface beveled on top of the Bandelier Tuff units. Furthermore, the Qal units represent fluvial deposits of the Chupaderos drainage that are now perched at elevations higher than the modern channel and floodplain. However, in the absence of clear topographic expressions of terraces at the trench sites we choose to refer to these deposits simply as alluvium.

B-1. Trench CHU-1

Tpf. Puye Formation. Poorly sorted, coarse sands and gravels; matrix is orange, dominantly medium to very coarse sand with pedogenic clays, supporting generally subrounded to rounded cobble to boulder-size clasts of Tschicoma Formation dacite up to 30 cm in diameter. Deposits likely are part of a Pliocene alluvial fan complex. Locally contains a < 10-cm-thick, very fine to fine sand on top, which may be an eolian deposit. Thickest exposure in trench is about 60 cm, but base is not exposed and upper contact with other units is an unconformity.

Qc1-1. Tpf-(Puye-)derived colluvium at base of trench from roughly 29H to 32H. Poorly sorted, orange, silt to very coarse sand matrix supporting subrounded dacite clasts up to 50 cm in diameter. Texturally and lithologically similar to the Tpf deposits, but clasts have carbonate rinds oriented

randomly, suggesting rotation of clasts during colluvial transport. Spatial relations to faults imply this unit may be a tectonic colluvium. Maximum exposed thickness is about 50 cm, but base is not exposed, and upper contact with the Tsankawi Pumice (Qbtt) is unconformable.

Qbtt. Tsankawi Pumice. Dominantly rhyolitic, white, pumice lapilli fallout deposit, with minor interbedded ash layers and variable amounts of pedogenic clays; forms the base of the Tshirege Member of the Bandelier Tuff. In the trenches and exposures on surrounding mesas, unit is extremely variable in volcanological detail. In trench CHU-1, a typical section is, from base up, approximately 1-m-thick, white pumice fall with pumice < 1 cm diameter, < 15% ash, < 15% crystals (mostly quartz); most pumice is 2 to 5 mm in diameter. This is capped by a 2- to 4-cm white ashy layer with minor pumice. Above ash, deposit is approximately 1 m thick and is same as pumice-rich fallout below, except for localized zones of abundant ashy fines. Unit thickens dramatically from east to west in trench CHU-1, with the thickest exposure of about 3 m at about 32H. Eastern end of unit in trench exhibits rounded pumices, implying local reworking, whereas the thickest part of the unit at 32H is a primary fallout sequence. Top and bottom contacts in CHU-1 are unconformities.

Qbt1. Fine-grained white rhyolitic ignimbrite of the Tshirege Member of the Bandelier Tuff that occurs, from about 33H to 40H, as fractured and sheared blocks in the fault zone and on the down-thrown block. The tuff is nonwelded and contains sparse (< 5%) 1- to 2-mm-diameter pumice, < 3% accidental lithic fragments, and < 10% phenocrysts (quartz and sanidine). West of 35.5H and the fault zone, unit appears coarser with more-abundant and larger pumice (up to 2 cm), 15% phenocrysts, and rare lithic fragments. Maximum thickness exposed in CHU-1 is about 1.8 m, but base is not exposed and upper contact with overlying units is an unconformity. Unit probably correlates with unit Qbt1g

of Broxton and Reneau (1995) farther south on the Pajarito Plateau.

Qc1-2. Pumiceous Colluvium. Poorly sorted, fine to medium sand with abundant Qbtt-derived pumice up to 2 cm in diameter and sparse subangular to subrounded dacite clasts up to 15 cm diameter. Pumice lapilli are glassy with quartz and sanidine phenocrysts. The upper approximately 20 cm of this unit is platy, with subhorizontal fractures. Basal contact with underlying Tpf is an unconformity but locally appears gradational due to bioturbation. Upper contact with Qc1-3 is gradational and apparently conformable. Maximum exposed thickness about 80 cm.

Qc1-3. Reworked Tsankawi Pumice. Subrounded reworked pumice is 2 to 12 mm in diameter in abundant clay. Unit exhibits moderate intertuff stratification at the east end of CHU-1. Contains rare clasts of subrounded Tschicoma Formation dacite up to 20 cm. Lower contact with Tpf is an unconformity, but with Qc1-2, it is gradational. Upper contact with overlying units appears to be locally gradational, but outcrop pattern on logs may imply that it is, at least in part, erosional. Maximum thickness about 40 cm.

Qal1-1. Pumiceous Alluvium. Poorly sorted, very fine to coarse sand consisting mostly of crystals and small lithic fragments with abundant pumice up to 1 cm diameter; contains subrounded to subangular clasts of Bandelier Tuff up to 25 cm diameter. Unit contains moderately well-sorted medium to coarse sand lenses up to about 20 cm thick. Locally, a Bt horizon was logged at the top of the unit and, generally, the unit exhibits weak to moderate reddish orange color. Maximum exposed thickness is about 1.6 m. Basal contact, mostly with Bandelier Tuff units, is an unconformity, but unit interfingers with Qc1-4. Upper contact with Qal1-2 and Qal1-3 is commonly gradational and apparently largely conformable, although the Bt horizon at the top of the unit between 16H and 26H indicates at least a local, upslope hiatus in the depositional sequence. The upper contact with Qal1-3 is marked by a decrease

in pumice pebbles and sand content and a relative increase in silt content. Upper contact with Qal1-2 is a gradational increase in silt content. This unit is one of two units that runs most of the length of the trench, occurring on both upthrown and downthrown blocks of the fault zone.

Qc1-4. Colluvium between roughly 34H and 36.5H, derived from white tuff blocks of Qbt1. Unit is poorly sorted, slightly silty, very fine to coarse sand with angular clasts of white tuff (Qbt1) to 6 cm in diameter, increasing in abundance to east and toward the base of the unit. Unit unconformably overlies zones of cataclasite and Qbt1, and it interfingers with the lower part of pumiceous alluvium unit Qal1-1. Maximum thickness about 40 cm. Spatial relations with faults may suggest this unit is a tectonic colluvium; however, as discussed in the text, we prefer the interpretation of the unit representing a stream bank colluvial deposit.

Qal1-2. Pumiceous Silty Alluvium. Weak to moderate reddish orange silty, very fine sand with abundant pumices 2 mm to 1 cm in diameter; pumices are larger and more abundant near the base of the unit. Unit is very similar to underlying Qal1-1 except for generally finer-grained matrix and generally decreasing pumice content towards the top. Unit contains moderately well-sorted coarse sand lenses up to about 10 cm thick, which increase in abundance to the west. Lower contact with Qal1-1 and upper contact with Qal1-3 are gradational and conformable. Upper contact with Qc1-6 is probably an unconformity. Unit pinches out to the east and thickens to a maximum of about 75 cm to the west.

Qal1-3. Silty Alluvium. Weak to moderate reddish orange unit exhibits weak stratification. Unit is very similar to underlying Qal1-2, except it is largely devoid of pumice clasts. Unit is silty, very fine sand with sparse thin lenses of fine to medium sand. Contains rare pumice < 1.5 cm diameter. Maximum thickness is about 1.75 m. This unit is one of two units that runs most of the length of the trench, occurring on both upthrown and downthrown

blocks of the fault zone. Lower contacts on the downthrown block in the western part of the trench are gradational with Qal1-2 and Qal1-1. Upper contact on the downthrown block with Qal1-4 is gradational and appears conformable.

On the upthrown block, lower contact is likely a minor unconformity with Qal1-1 and a major unconformity with Tpf, Qc1-2, and Qc1-3. The upper contact on the upthrown block is the stripped ground surface and an unconformity with Qc1-5. Where the unit forms the ground surface, the top 10 to 30 cm are extremely bioturbated.

Qal1-4. Sandy Alluvium. Very weak reddish orange unit of silty, very fine sand with prominent and abundant lenticular lenses of moderately well-sorted, coarser sand. Some sandy lenses contain interstratified layers of very coarse sand, pebbles, silt, and very fine sand. Coarser sandy lenses are up to 50 cm thick and laterally continuous for up to 1.75 m. Unit also contains sparse pumice lenses, with pumice up to 1 cm diameter, in the upper parts. Unit is up to 2 m thick, but its top is the modern ground surface, and upper portions may have been stripped on the downthrown block of the fault zone. Where the unit forms the ground surface, the top 10 to 30 cm are extremely bioturbated. The entire unit has been stripped off of the upthrown structural block. Lower contact with Qal1-3 is gradational and appears conformable.

Qc1-5. Colluvium in east end of trench beneath the modern ground surface. Very poorly sorted unit of silty, unconsolidated, light-grey, very fine to fine sand with pumice clasts up to 1 cm diameter and Qbt clasts to 15 cm diameter. Consists of lithologies found exposed farther up the modern slope. Maximum thickness about 50 cm.

Qc1-6. Colluvium in west end of trench beneath the modern ground surface. Weak to moderately reddish orange, poorly sorted, silty, very fine to coarse-grained sand. Unit is mostly derived from unit Qal1-4 and probably is a deposit that resulted mostly from the stripping of Qal1-4 from the

upthrown structural block. Lower contact is likely an unconformity. Maximum thickness about 1.1 m.

B-2. Trench CHU-2

Qbtt. Tsankawi Pumice. Dominantly rhyolitic, white, pumice lapilli fallout deposit, with minor interbedded ash layers and variable amounts of pedogenic clays; forms the base of the Tshirege Member of the Bandelier Tuff. In the trenches and exposures on surrounding mesas, unit is extremely variable in volcanological detail. In trench CHU-2, the unit is about 1.5 m thick, but the base is not exposed. The lower 1 m is a pumice fallout deposit, which fines upward, with pumice from 2 to 15 mm. On top of this deposit, there is a fine ash layer, about 2 to 3 cm thick, overlain by about 2 cm of very coarse sand-size pumice, crystal, and lithic fallout, which is, in turn, overlain by another ash layer about 2 to 8 cm thick. The pair of thin ash layers and intervening coarser layer are grouped as one layer on the logs. The ash layers are overlain by 20 cm of pumice lapilli fall, which also fines upward. Pumices in the upper-fining upward-fallout deposit range from 2 to 10 mm in diameter. Most of the primary textures in the fallout sequence are overprinted by abundant translocated clays. Upper contact with Qbt1 is conformable but, with Qal2-1, is an angular unconformity. Strike and dip on the ash layers and contact with Qbt1 is N45E, 20NW.

Qbt1. Fine-grained white rhyolitic ignimbrite of the Tshirege Member of the Bandelier Tuff. Pumice is sparse, < 5%, and small, up to 7 mm. The non-welded tuff is phenocryst poor, < 10% quartz plus sanidine, and has < 5% accidental lithic fragments. Maximum thickness is about 2.6 m, but upper contact with Qal2-1 is an angular unconformity. Basal contact with underlying Qbtt is conformable and dips N45E, 20NW. Unit probably correlates with unit Qbt1g of Broxton and Reneau (1995) farther south on the Pajarito Plateau.

Qal2-1. Coarse sand and gravels. Laterally discontinuous unit of moderately sorted coarse to very coarse sands and gravels. Clasts are generally sub-

angular dacite and Bandelier Tuff pebbles, but angular clasts of tuff up to 30 cm occur. Unit exhibits some cross-bedding. Maximum thickness is about 30 cm, but upper contact with Qal2-2 appears, in the northwestern portion of the trench, to be unconformable. Upper contact with Qal2-2 in southeastern part of trench appears largely conformable with interfingering relations. Lower contact with Bandelier Tuff units is an angular unconformity.

Qal2-2. Fine-grained alluvium. Mottled weak to moderate reddish orange, silty, very fine to fine sand. Unit contains moderately well-sorted lenses of coarse sands and gravels, 2 to 10 cm thick and laterally continuous for up to 40 cm. Top of unit is modern ground surface, and the upper 30 to 50 cm of the unit is extensively bioturbated. Lower contact with Qal2-1 is apparently unconformable in the northwestern portion of the trench and conformable, with interfingering relations, in the southeastern part of the trench. Maximum thickness about 2 m.

B-3. Trench CHU-3

Qbt1. Fine-grained, white, nonwelded, rhyolitic ignimbrite of the Tshirege Member of the Bandelier Tuff. Pumice content and size are variable with zones of sparse (< 5%) and small (up to 5 mm) pumice and zones of more abundant (10–15%) and larger (up to 3 cm) pumice. Accidental lithic fragments range 5 to 10%, and phenocrysts of quartz and sanidine constitute < 10%. The upper approximately 1 m is oxidized and has abundant fractures filled with clay or silica. Top of unit is variably weathered. Maximum thickness is about 2 m, but base is not exposed, top contact is an unconformity, and the attitude of the unit cannot be determined. Unit probably correlates with unit Qbt1g of Broxton and Reneau (1995) farther south on the Pajarito Plateau.

Qbt2. Tan to grey, nonwelded, ignimbrite with 5 to 10% phenocrysts of quartz and sanidine up to 2 mm in diameter, devitrified, vapor-phase-altered pumice up to 5 to 10 cm long, and < 5% accidental lithic

fragments up to 10 cm diameter. Unit probably correlates with unit Qbt2 of Broxton and Reneau (1995) farther south on the Pajarito Plateau.

Qal3-1a. Clay-rich, coarse sand and gravel with moderate to strong reddening. Cobbles of dacite up to 15 cm; coarse sand fraction is mostly crystals. Long axis of vertical clasts may reflect shearing in fault 3-A. Unit lies unconformably on the Bandelier Tuff unit Qbt1 and unconformably beneath Qal3-2 and Qal3-3. Unit has been extensively scoured, likely with deposition of unit Qal3-2, leaving laterally discontinuous patches in eastern part of trench. Maximum thickness about 40 cm.

Qal3-1b. Pocket of silt at approximately 29-30H. Unit has moderately strong red color and is clay rich silt, with very fine to fine sand. Sparse coarse to very coarse sand grains are crystals. Stratigraphic position, clay content, and stronger red color suggest an age comparable to unit Qal3-1a and that this unit may be a finer-grained facies of Qal3-1a.

Qal3-2. Gravel and sand. Coarse to medium sand matrix with abundant clasts of glassy pumice up to 10 cm in diameters and abundant, large cobbles and boulders of rounded to subrounded Tschicoma dacite and subrounded to angular Bandelier Tuff unit Qbt2. Clasts of unit Qbt2 are up to 1 m. Top and bottom contacts are unconformities and unit has maximum thickness of about 1 m.

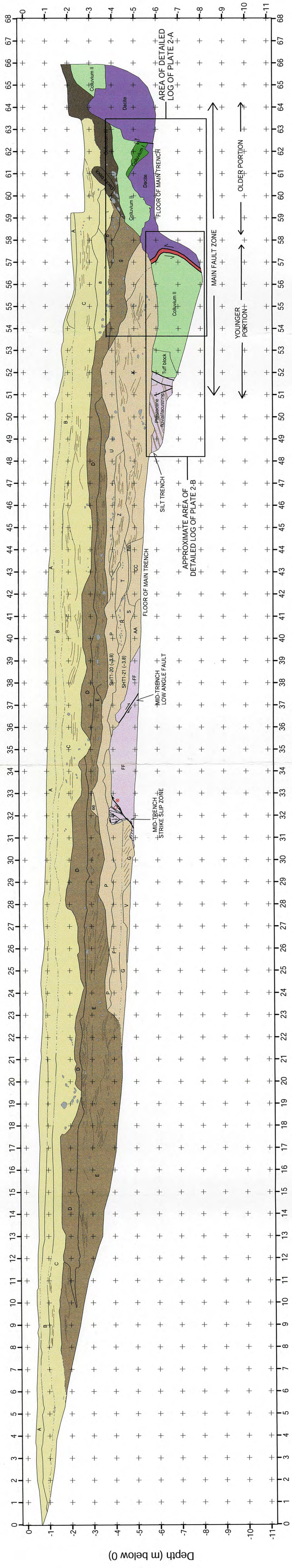
Qal3-3. Thick sequence of dominantly silty alluvium. Lower portion contains abundant sand lenses. Sand lenses are mostly 10 to 20 cm thick and 20 to 40 cm long, but one is up to 6 m long. Lenses are coarse sand and minor gravel with rounded to subrounded dacite clasts. The sand fraction is mostly crystals. Between sand lenses, unit is silt to very fine sand. Upper portion of unit generally lacks the sand lenses and is silty, very fine sand with sparse pebbles < 1 cm diameter. Boundary between upper and lower portions of unit is logged as a gradational internal contact. Unconformably overlies most

Paleoseismic Trenching in the Guaje Mountain Fault Zone

older units but may be partly conformable with Qal3-2. Top of unit commonly forms modern ground surface. Maximum exposed thickness is about 2.75 m.

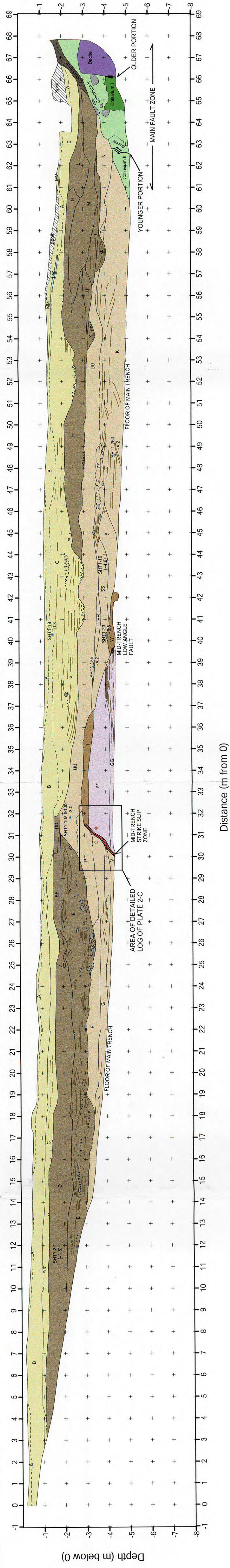
Qal3-4. Soft loose silt with very fine to fine sand with sparse scattered pebbles and crystals. Unit is probably the more intensely bioturbated top of unit Qal3-3. Maximum thickness about 1 m.

NORTHEAST WALL OF CABRA CANYON TRENCH (View to the northeast)



Distance (m from 0)

SOUTHWEST WALL OF CABRA CANYON TRENCH (View to the northeast)



Distance (m from 0)

LEGEND

- < 1 cal ka
- ~1.5 cal ka
- ~3-4 cal ka
- > 5 cal ka
- Pleistocene
- Dacite block or cobble
- Gouge or shear zone
- Colluvium III
- Colluvium II
- Colluvium I
- Dacite (~5 Ma)
- fault (dashed where inferred or queried)
- arrows indicate direction of displacement
- ⊗ displacement into the plane of figure
- ⊙ displacement out of the plane of figure
- fracture
- bedding
- internal contact
- shear fabric
- SHT1-21 ¹⁴C sample with approximate age in cal ka:
- ~4.0
- parentheses indicate composite sample

Plate 1: Generalized logs of the Cabra Canyon trench.

Plate 2: Detailed logs of selected zones in the Cabra Canyon trench.

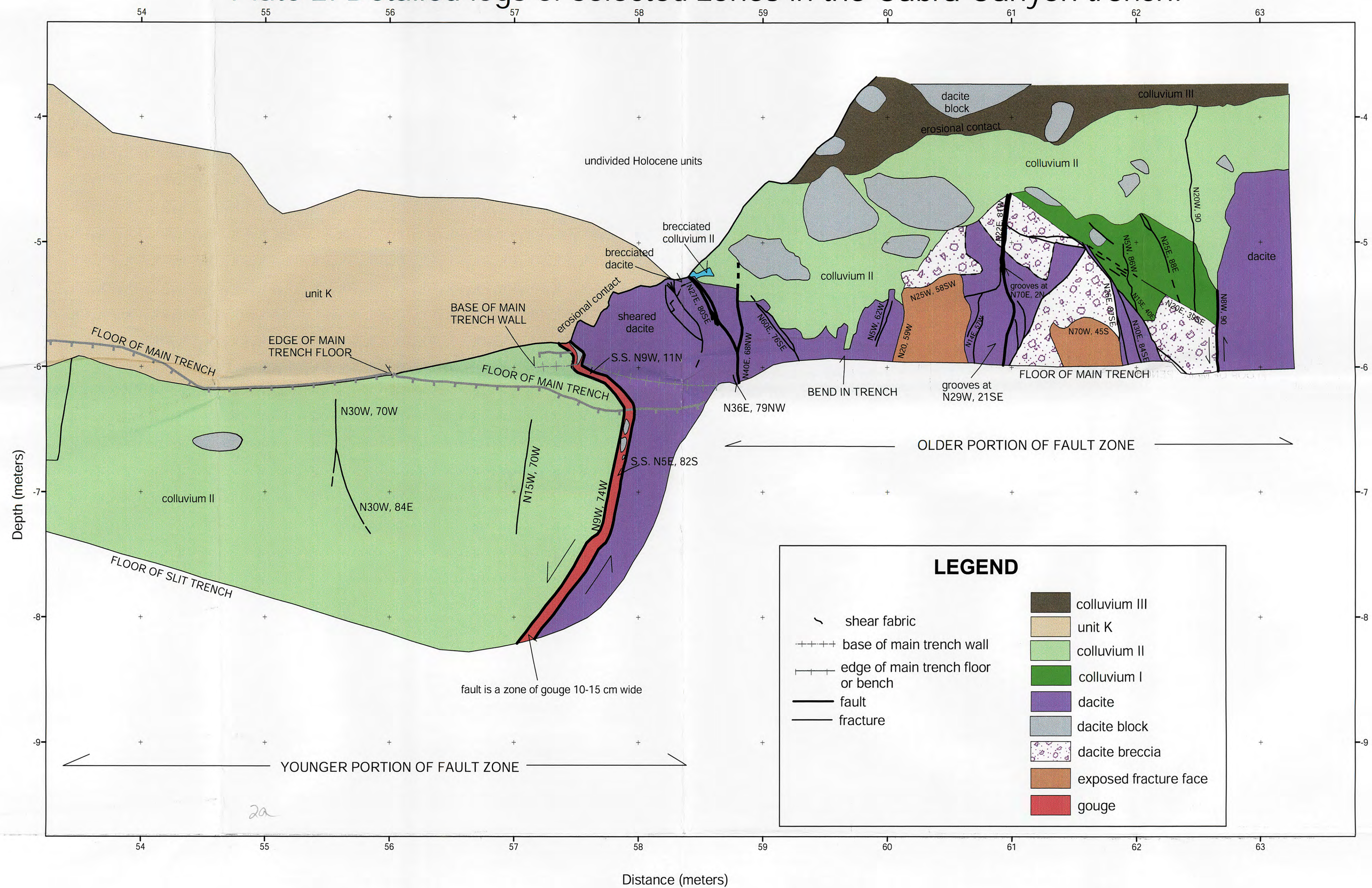


Plate 2-A: Detailed log of the main fault zone in the northeast walls of the main and slit trenches; note 3-D joining of the main and slit trench logs; S.S. = slickensides. View to the northeast.

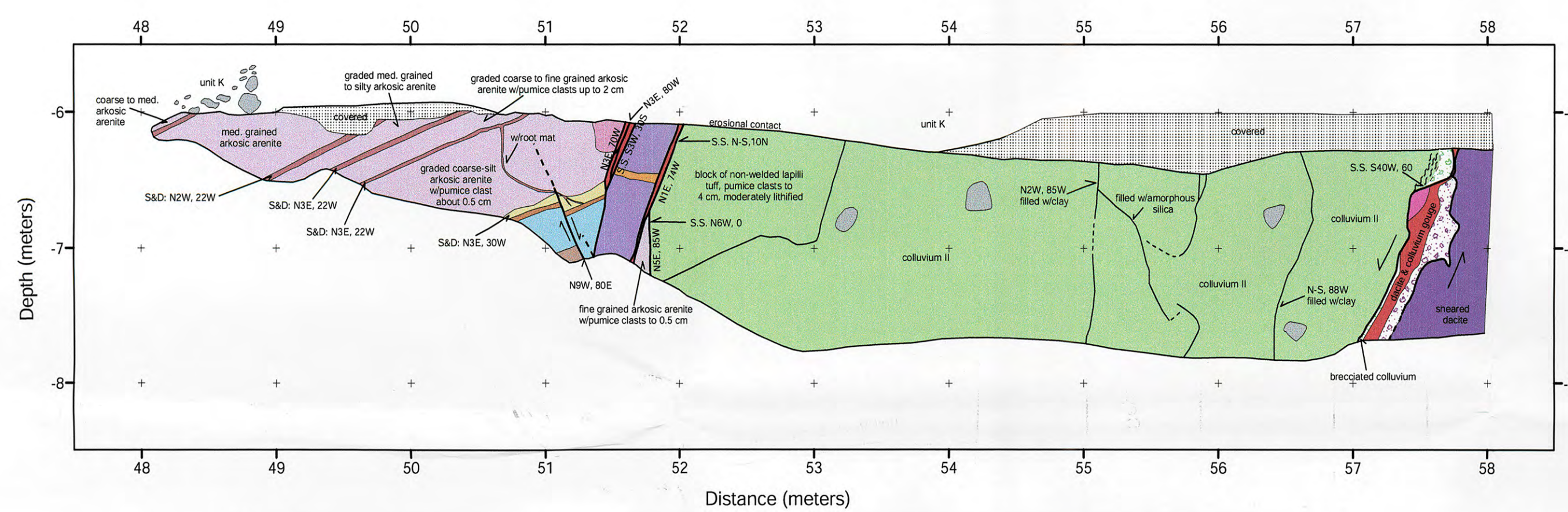


Plate 2-B: Detailed log of northeast wall of the slit trench (younger portion of main fault zone) displayed about 30 cm farther northeast from log of Plate 1 and Plate 2-A because of re-excavation. S&D = strike and dip of bedding; S.S. = slickensides. View to the northeast.

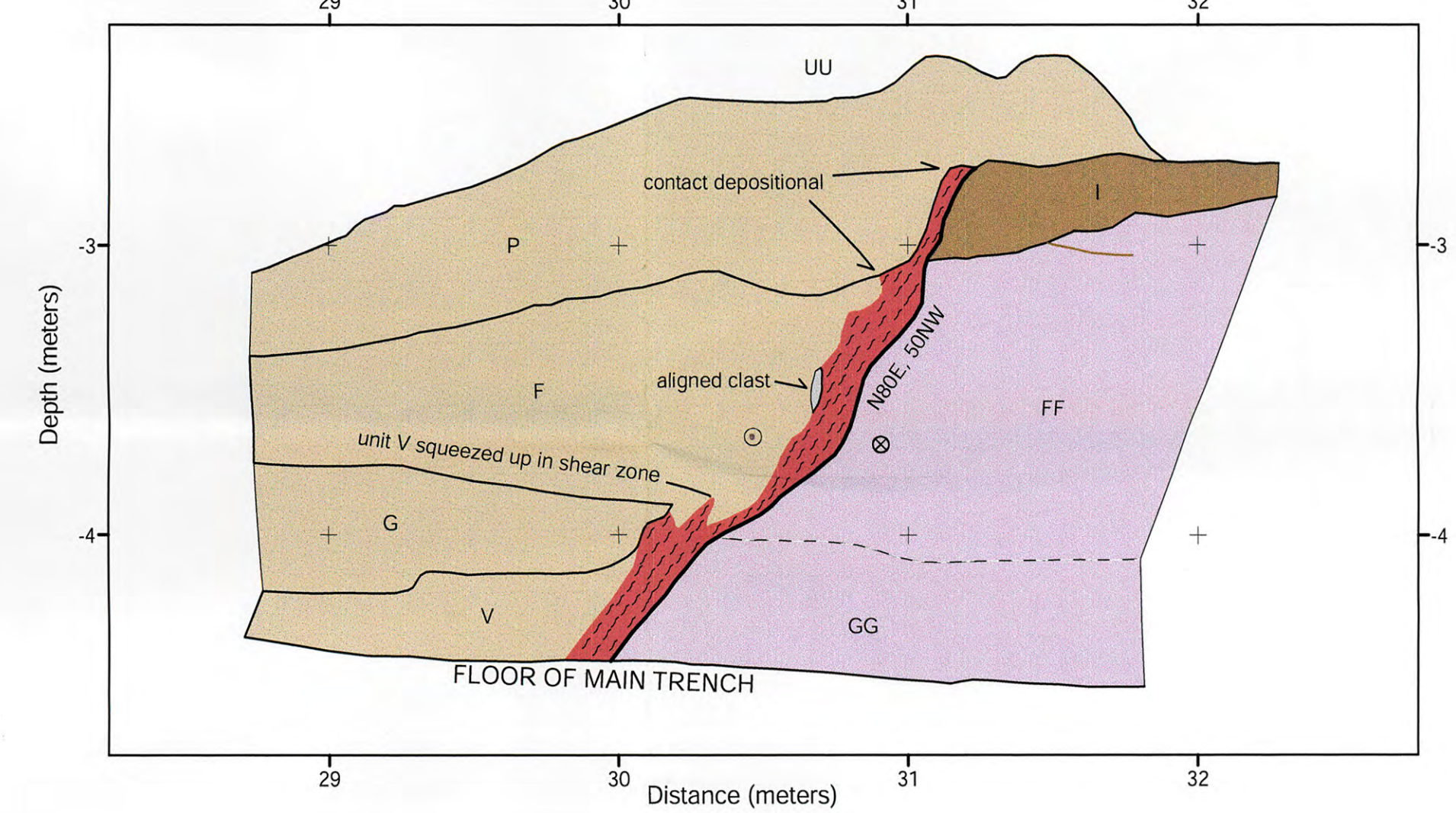
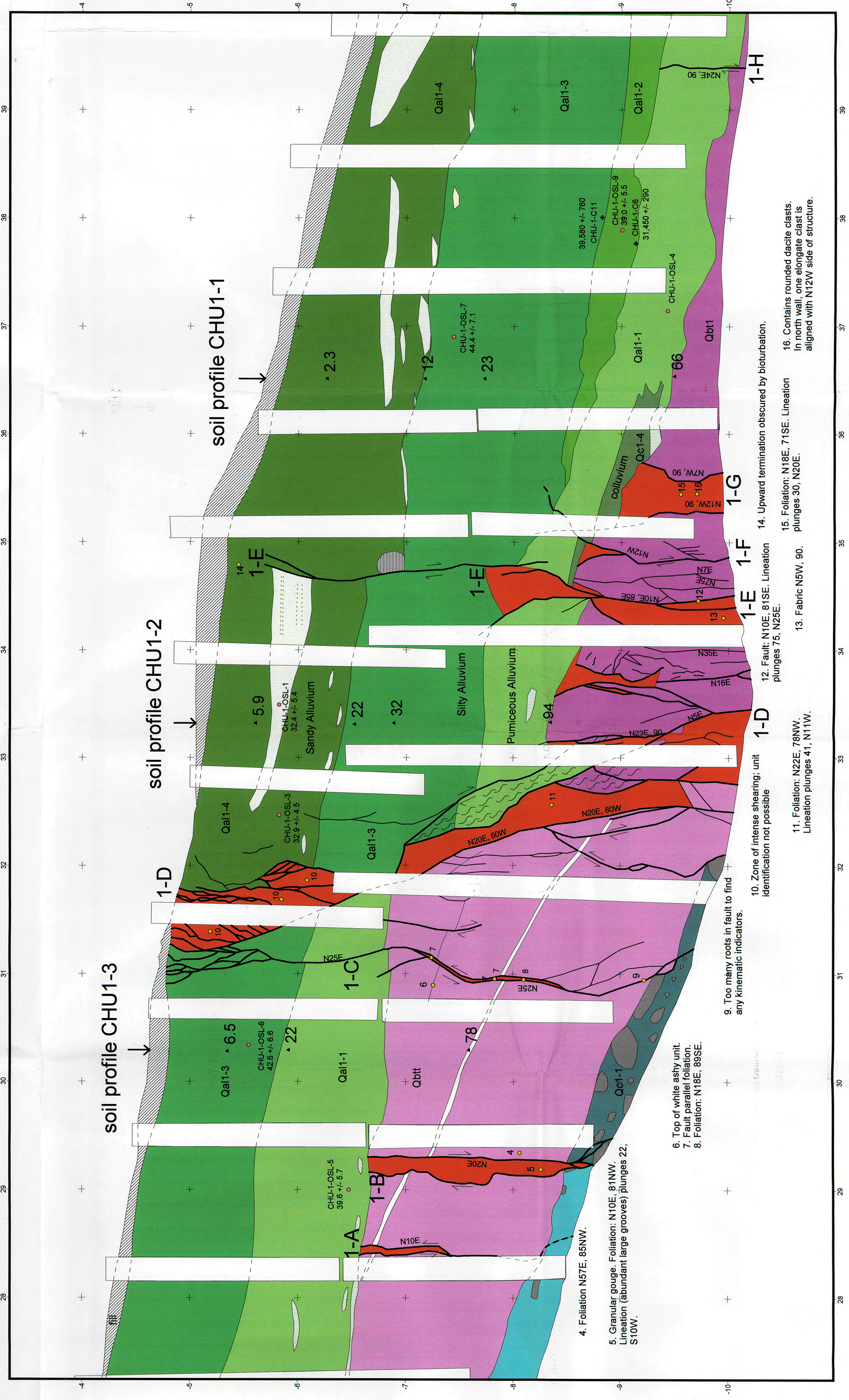
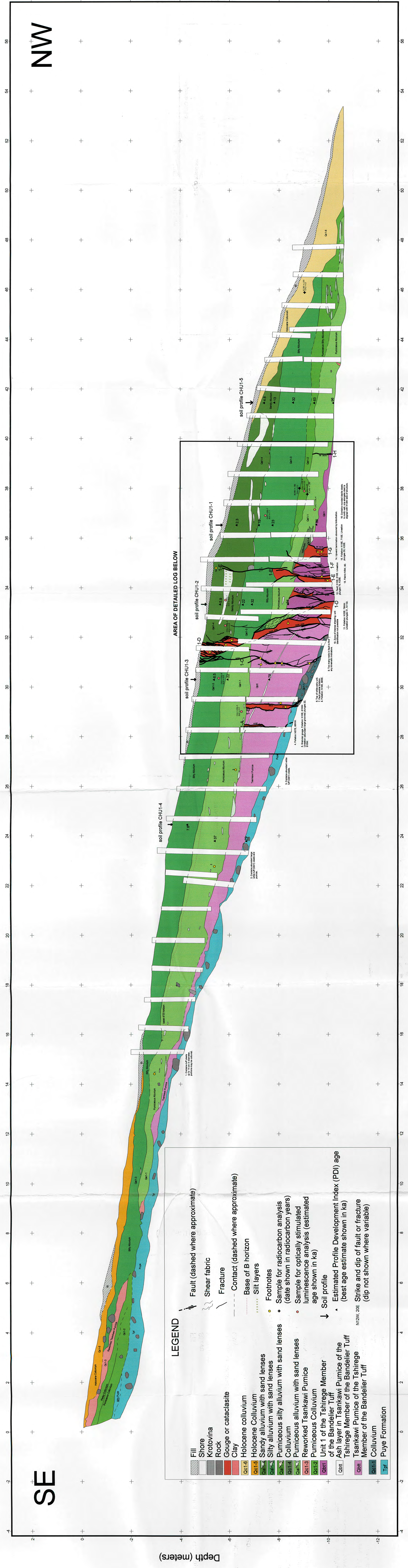


Plate 2-C: Detailed log of mid-trench strike slip zone on southwest wall of trench. View to northeast.

Plate 3. Log of Southwest Wall of Trench CHU-1 (trench trends N48W). View to southwest.



This report has been reproduced directly from the best available copy. It is available electronically on the Web (<http://www.doe.gov/bridge>).

Copies are available for sale to U.S. Department of Energy employees and contractors from:

Office of Scientific and Technical Information
P.O. Box 62
Oak Ridge, TN 37831
(865) 576-8401

Copies are available for sale to the public from:

National Technical Information Service
U.S. Department of Commerce
5285 Port Royal Road
Springfield, VA 22161
(800) 553-6847



Los Alamos NM 87545